




## PRIMARY RESEARCH ARTICLE

# Remodeling of Arctic char (*Salvelinus alpinus*) lipidome under a stimulated scenario of Arctic warming

Chao Wang<sup>1,2</sup>  | Yufeng Gong<sup>2</sup>  | Fuchang Deng<sup>1</sup> | Enmin Ding<sup>1</sup> | Jie Tang<sup>2,3</sup> | Garry Codling<sup>2,4</sup> | Jonathan K. Challis<sup>2</sup> | Derek Green<sup>2</sup> | Jing Wang<sup>5</sup> | Qiliang Chen<sup>2,6</sup> | Yuwei Xie<sup>2</sup> | Shu Su<sup>2</sup> | Zilin Yang<sup>2</sup> | Jason Raine<sup>2</sup> | Paul D. Jones<sup>2</sup> | Song Tang<sup>1,7</sup>  | John P. Giesy<sup>2,8,9,10</sup>

<sup>1</sup>China CDC Key Laboratory of Environment and Population Health, National Institute of Environmental Health, Chinese Center for Disease Control and Prevention, Beijing, China

<sup>2</sup>Toxicology Centre, University of Saskatchewan, Saskatoon, SK, Canada

<sup>3</sup>School of Resources and Environment, Anhui Agricultural University, Hefei, Anhui, China

<sup>4</sup>Research Centre for Contaminants in the Environment, Masaryk University, Brno, Czech Republic

<sup>5</sup>MOE Key Laboratory of Marine Genetics and Breeding, College of Marine Life Sciences, Ocean University of China, Qingdao, China

<sup>6</sup>College of Life Sciences, Chongqing Normal University, Chongqing, China

<sup>7</sup>Center for Global Health, School of Public Health, Nanjing Medical University, Nanjing, China

<sup>8</sup>Department of Veterinary Biomedical Sciences, University of Saskatchewan, Saskatoon, SK, Canada

<sup>9</sup>Department of Environmental Sciences, Baylor University, Waco, TX, USA

<sup>10</sup>State Key Laboratory of Pollution Control and Resource Reuse, School of the Environment, Nanjing University, Nanjing, China

## Correspondence

Yufeng Gong, Toxicology Centre,  
University of Saskatchewan, Saskatoon,  
SK, Canada.  
Email: yufeng.gong@usask.ca

## Funding information

Banting Postdoctoral Fellowship; Canada First Research Excellence Fund; Young Scholar Scientific Research Foundation of China CDC, Grant/Award Number: 2018A201; Oversea Research Training Program of NIEH, China CDC; NSERC Doctoral Scholarship Funding, Grant/Award Number: PGSD 3-504735-2017; European Union's Horizon 2020 Research and Innovation Programme under the Marie Skłodowska-Curie grant agreement, Grant/Award Number: 839243; Global Water Futures Program; Fisheries and Oceans Canada's National Contaminants Advisory Group

## Abstract

Arctic warming associated with global climate change poses a significant threat to populations of wildlife in the Arctic. Since lipids play a vital role in adaptation of organisms to variations in temperature, high-resolution mass-spectrometry-based lipidomics can provide insights into adaptive responses of organisms to a warmer environment in the Arctic and help to illustrate potential novel roles of lipids in the process of thermal adaption. In this study, we studied an ecologically and economically important species—Arctic char (*Salvelinus alpinus*)—with a detailed multi-tissue analysis of the lipidome in response to chronic shifts in temperature using a validated lipidomics workflow. In addition, dynamic alterations in the hepatic lipidome during the time course of shifts in temperature were also characterized. Our results showed that early life stages of Arctic char were more susceptible to variations in temperature. One-year-old Arctic char responded to chronic increases in temperature with coordinated regulation of lipids, including headgroup-specific remodeling of acyl chains in glycerophospholipids (GP) and extensive alterations in composition of lipids in membranes, such as less lyso-GPs, and more ether-GPs and sphingomyelin. Glycerolipids (e.g., triacylglycerol, TG) also participated in adaptive responses of the lipidome of Arctic char. Eight-week-old Arctic char exhibited rapid adaptive alterations of the hepatic lipidome to stepwise decreases in temperature while showing blunted responses to gradual increases in temperature, implying an inability to adapt rapidly to

warmer environments. Three common phosphatidylethanolamines (PEs) (PE 36:6|PE 16:1\_20:5, PE 38:7|PE 16:1\_22:6, and PE 40:7|PE 18:1\_22:6) were finally identified as candidate lipid biomarkers for temperature shifts via machine learning approach. Overall, this work provides additional information to a better understanding of underlying regulatory mechanisms of the lipidome of Arctic organisms in the face of near-future warming.

#### KEYWORDS

Arctic warming, chronic temperature shifts, dynamic alterations, glycerolipids, glycerophospholipids, lipidomics, machine learning

## 1 | INTRODUCTION

The Arctic, one of the regions that are most at risk from changes in climate (ACIA, 2005), is warming faster than the rest of the globe (Hoegh-Guldberg & Bruno, 2010). This is caused primarily by a phenomenon known as Arctic amplification, where the loss of reflective sea ice and replacement by darker ocean surfaces increases thermal absorption. Specifically, Arctic winters experienced extreme warm temperature anomalies of +6°C in 2016 and 2018, which are almost double those of previous record highs (Overland & Wang, 2016; Overland et al., 2019). Major results of arctic warming could include shifts in Arctic vegetation (Pearson et al., 2013), loss of sea ice (Ding et al., 2019), biodiversity redistribution (Pecl et al., 2017), changes in seafood nutrients (Koelmel et al., 2020), altered economic access and transportation patterns, and other direct and indirect effects. Some of these effects are on wild populations that are essential for the diet and economy of northern communities.

Temperature shapes physiologies of aquatic ectotherms. Results of previous studies have shown that water temperature can affect basic physiological processes of fish, such as growth, development, reproduction, immune response, and metabolism (Cheng et al., 2018; Dadras et al., 2017; Jonsson & Jonsson, 2009; Rountrey et al., 2014). Animals in the Arctic are adapted to cold extremes, so even subtle changes in mean annual temperatures might affect their basic physiology as well as timing of reproduction or use of food resources. However, as the majority of the Arctic's aquatic system is oceanic, the focus of research conducted on these effects thus far has paid less attention to freshwater organisms found within the Arctic Circle.

Arctic char (*Salvelinus alpinus*) is a cold-water salmonid with a circumpolar distribution. It has the most northern distribution of any freshwater fish. It spawns in freshwater, but populations are known to be lacustrine, riverine, or even anadromous. Arctic char is the apex predator in many Arctic freshwater food webs and an important species for commercial fisheries that provide food and a source of protein and income to communities in the north. Results of previous studies suggest that Arctic char is sensitive to minor environmental changes and can be vulnerable to Arctic warming (Elliott & Elliott, 2010). Therefore, any temperature-induced change in their abundance or physiology might have significant effects on

functioning of Arctic ecosystems and, in particular, commercially viable stocks of this ecologically and economically important species.

Lipids play an important role in resistance to physiological stress in response to alterations in thermal regimes. Ectotherms, such as fish, acclimatize to varying temperatures by modulation of the proportion of unsaturated fatty acids in membranes to maintain membrane order (Ernst et al., 2016). This adaptive response, known as homeoviscous adaptation (HVA; Hazel & Williams, 1990; Sinensky, 1974), has been widely observed in ectotherm, such as fishes (Tiku et al., 1996), phototrophic sponges (Bennett et al., 2018), microorganisms (Gao et al., 2019; Řezanka et al., 2016), and bivalves (Pernet et al., 2007). However, due to the tremendous number of structurally and functionally diverse lipids in organisms, roles of lipids in response to thermal stimuli have not yet been fully described or understood. Previous studies (especially for fish) have typically focused on modulation in fatty acid composition of cell membranes (Bennett et al., 2018; Fadhlaoui & Couture, 2016; Malekar et al., 2018), which might ignore vital changes in other structural or functional lipids. Moreover, the dynamic process of alterations of absolute and relative concentrations of lipids during the course of thermal acclimation is poorly understood. Advances in high-resolution mass spectrometry and chemometric algorithms have expanded the potential for mass-spectrometry-based lipidomics as an emerging tool for lipidome profiling (Han, 2016; Hu & Zhang, 2018; Rustam & Reid, 2018). Such techniques can be employed to obtain a better understanding of chronic responses to Arctic warming in fishes.

In the present study, lipidomic responses of Arctic char to chronic shifts in temperature (either warm or cold) were systematically measured at multitude tissue levels and at two different life stages. First, global changes in the lipidome among blood plasma, brain, liver, and muscle of 1-year-old Arctic char were measured using a validated lipidomics workflow developed in-house. Second, dynamics of hepatic lipidome remodeling during the time course of temperature shifts were determined in 8-week-old Arctic char. Lastly, machine learning approach was employed to identify lipid biomarkers of Arctic char in response to chronic temperature shifts. Our work provides an important resource for molecular characterization of the teleost lipidome in response to chronic shifts in temperature and describes underlying mechanisms of lipid adaption to increasing temperatures. To the best

of our knowledge, this is the first study integrating modern lipidomics and machine learning approaches to characterize dynamic lipid remodeling and to identify lipid biomarkers of an Arctic fish in response to chronic temperature shifts.

## 2 | MATERIALS AND METHODS

### 2.1 | Chemicals and reagents

Formic acid, ammonium formate, and all solvents were LC-MS grade and obtained from Fisher Scientific. Internal lipid standards were purchased from Avanti Polar Lipids and were used for method validation and data quality control (QC). Please refer to Supporting Information S1 for more details.

### 2.2 | Experimental design

#### 2.2.1 | Fish and maintenance

Experiments were conducted in the Aquatic Toxicology Research Facility (ATRF) in the Toxicology Centre, University of Saskatchewan. Animal usage for the study and euthanasia procedure were reviewed and approved by the University of Saskatchewan's Animal Research Ethics Board, and adhered to the Canadian Council on Animal Care guidelines for humane animal use (protocol #20170096).

Arctic char used in the experiment were obtained as gametes from Miracle Spring Inc. North Vancouver, B.C. Eggs were fertilized and then raised in the ATRF. Fish were maintained on a 12 h light, 12 h dark photoperiod in 450 L aquaria with flow-through, aerated, and pre-treated freshwater at 8°C. Fish were acclimated to these holding conditions for more than 3 weeks prior to the temperature shift experiment. During the experiment, fish were fed commercial fish feed pellets *ad libitum* three times a day. Food residuals and waste were cleaned daily. Water quality parameters including dissolved oxygen (>9 mg/L) and ammonia nitrogen (<0.15 mg/L) were monitored on a weekly basis. Water temperatures were controlled precisely and were monitored by a VWR® Traceable® High-Accuracy Thermometer (VWR International) in real time during the experiment.

#### 2.2.2 | Experiment I: Changes in lipidomes across various tissues of Arctic char in response to chronic temperature shifts

The object of Experiment I was to document changes in lipidomes of blood plasma, brain, liver, and muscle of Arctic char in response to a chronic shift in temperature. Eighteen 1-year-old Arctic char (juvenile fish stage, initial body mass  $75.00 \pm 22.77$  g; initial body length  $17.15 \pm 1.63$  cm) were numbered with tags for observations of individual growth rates, and randomly distributed across three

treatment groups ( $N = 6$  per group). These treatment groups included warm treatment group, cold treatment group, and control group. Duplicate treatments were conducted for each exposure group. Fish were allowed to recover for 21 days after tagging. To achieve the final exposure temperature of 14°C for warm treatment group or 2°C for cold treatment group from the initial temperature of 8°C, the water temperature was gradually altered through six temperature steps, each of which lasted 5 days. At each temperature step, temperature was either increased or decreased by 1°C within 4 h and was then held constant during the next 5 days. After the final water temperature of 14 or 2°C was reached, fish were maintained at the temperature for 28 days. Individual body mass and fork length were measured at the end of each temperature period as well as 28 days after the final 14 or 2°C was reached, that is, on days 0, 5, 10, 15, 20, 25, 30, 35, or 53 (Figure S1). Water temperature for the control group was maintained at 8°C throughout the experiment. After the 53-day treatment regimen, fish were anesthetized with 75 mg/L MS-222 (Sigma Aldrich). Blood was collected from the caudal vein with syringes pre-rinsed with sodium heparin and immediately transferred to 1.5 ml centrifuge tubes. Plasma was obtained by centrifugation at  $1000 \times g$  at 4°C for 10 min. Fish were then euthanized and dissected. Brain, liver, and dorsal muscle were collected, weighed, and snap-frozen in liquid nitrogen. All samples were stored at -80°C until further analysis. Fish were fasted for 24 h before sampling.

#### 2.2.3 | Experiment II: Dynamics of lipidome in the time course of thermal acclimation

The object of Experiment II was to resolve the dynamic changes of lipidome in Arctic char during the time course of thermal acclimation. A total of 240 eight-week-old Arctic char (swim up stage; initial body mass  $298.26 \pm 27.07$  mg; initial body length  $3.03 \pm 0.28$  cm) were employed. The thermal exposure scheme was in accordance with Experiment I (Figure S1). On days 0, 5, 10, 15, 20, 25, 30, and 53, 8 or 10 randomly selected fish were anesthetized using MS-222. Body mass and fork length were measured, and liver was collected, snap-frozen, and stored at -80°C for lipidomic analysis. Liver was chosen for lipidomic analysis because of its central role to lipid metabolism.

### 2.3 | Extraction of lipids

Lipids were extracted by using an IPA-based protein precipitation approach (Calderón et al., 2019; Sarafian et al., 2014) with minor modifications. Lysophosphatidylcholine (lysoPC [19:0]), phosphatidylcholine (PC [19:0/19:0]), phosphatidylethanolamine (PE [17:0/17:0]), ceramide (Cer [d18:1/17:0]), and triacylglycerol (TG [15:0/18:1(d7)/15:0]) were added to each sample before extraction to serve as internal standards. QC samples were prepared by pooling 10 µl of aliquots from each sample (additional details in Supporting Information S2).

## 2.4 | Instrumental analysis for lipidomics

Non-targeted lipidomic analyses were conducted by using a Dionex Ultimate 3000 RS UHPLC system coupled to a Q-Exactive Orbitrap mass spectrometer (Thermo Scientific). The elution gradient was performed according to Narváez-Rivas and Zhang (2016). Mass spectra were acquired in both positive and negative modes by a data-dependent top 10 analysis (ddMS<sup>2</sup>-top10) method with a resolution of 70,000 at m/z 200. Details are provided in SI 3. The electrospray ionization (ESI) source parameters were optimized to reduce possible formation of in-source fragments (Gathungu et al., 2018; Xu et al., 2018) during development of the methods. The mass spectrometer was externally calibrated every week using Pierce<sup>TM</sup> LTQ Velos ESI Positive/Negative Ion Calibration solutions. Moreover, an iterative exclusion (IE) strategy, where selected precursors using ddMS<sup>2</sup>-top10 analysis were excluded in sequential injections, was applied to increase coverage of the lipidome (Koelmel et al., 2017). A total of five sequential injections of QC samples were analyzed for each polarity by ddMS<sup>2</sup>-top10 with IE.

## 2.5 | Quality control and method validation

Quality control samples were injected for the purpose of system equilibration before analysis of real biological samples. All samples were injected randomly, and QC samples were included after every 10 samples. The peak shape, retention time, intensity, and mass accuracy of spiked internal standards were monitored during the run. Procedural blanks were also prepared and analyzed with each batch of samples. Linearity, recovery, and repeatability were determined using 11 deuterated lipid standards in the presence of biological matrix. Additional analytical details are provided in Supporting Information S4.

## 2.6 | Feature detection and lipid annotation

An open-source software, MS-Dial (version 4.10), was used for peak picking and lipid annotation (Tsugawa et al., 2020). The public LipidBlast library was used to annotate lipids (Kind et al., 2013). Accurate mass tolerance for MS1 and MS2 were set to 0.01 and 0.05 Da, respectively. Adducts of +H and +NH<sub>4</sub> were selected for positive mode searches, whereas -H and +HCOO were selected for negative mode searches. The generated peak picking and integration results were checked manually to ensure data quality. Annotated peaks that showed low repeatability (<30%), that is, relative standard deviation (RSD) in QC samples were removed.

## 2.7 | Statistical analyses

After assuring that the assumptions of normality (one sample Kolmogorov-Smirnov test) and variance homogeneity (Levene's test) had been met, parameters associated with growth of fish were evaluated

using one-way ANOVA followed by Fisher's LSD test. Differences were considered significant at  $p < 0.05$ . Data are reported as mean  $\pm$  SE. For lipidomic data, area under the curve of each annotated lipid peak was normalized to the sum of all annotated lipids (mTIC) in the sample and then log-transformed. Significantly altered lipids were determined by one-way ANOVA followed by Fisher's LSD test. Benjamini-Hochberg corrected  $p$  values (false discovery rate, FDR) below 0.05 were considered significant. Principal component analysis (PCA) was carried out using the online MetaboAnalyst platform (version 4.0; Chong et al., 2018). Upset plot and heatmap analyses were produced by "UpsetR" (Conway et al., 2017) and "Pheatmap" packages in R (version 4.0.1). Chemical similarity enrichment analysis (ChemRICH) was performed on the annotated lipidomics dataset (Barupal & Fiehn, 2017). Chemical clusters with FDR < 0.05 were considered significant. Cluster directions are determined by the median log<sub>2</sub>(fold change) relative to control of significantly altered lipids in each lipid cluster (Contrepois et al., 2020). In addition, an advanced, correlation-based network analysis, that is, weighted correlation network analysis (WGCNA), was applied to the lipidomics dataset by using the "WGCNA" R package (Langfelder & Horvath, 2008; Zhang & Horvath, 2005). While WGCNA was initially developed for gene network construction, other studies asserted that it is also equally powerful and illustrative for metabolomics (DiLeo et al., 2011; McCall et al., 2018) and lipidomics datasets (Forest et al., 2018). Circos connectograms were made using CIRCOS software (version 0.69-6). A machine learning algorithm was performed by the R package "random forest" (version 4.6.14) to identify lipid biomarker of the lipidome of Arctic char in response to chronic temperature shifts.

## 3 | RESULTS

### 3.1 | Effects of chronic temperature shifts on growth of Arctic char

During a 53-day temperature shift exposure (Figure S1), no mortality was observed, but there were changes in allometric parameters. Body mass, fork length, and condition factor of 1-year-old Arctic char (Experiment I) did not differ significantly between the three experimental groups throughout the study (Figure 1a). However, for 8-week-old Arctic char (Experiment II), there were significant differences in body size between temperature groups (Figure 1b). The warm treatment group exhibited the greatest mean values at each sampling point from day 15 onwards for body mass or from day 25 for fork length, respectively. Moreover, the warm treatment group showed a mean condition factor significantly greater than that of the cold treatment group from day 20 onwards.

### 3.2 | Validation of lipidomics method

To achieve a comprehensive analysis of the Arctic char lipidome, an optimized solvent extraction protocol and elaborate UHPLC-MS parameters were employed to improve recovery, reproducibility,

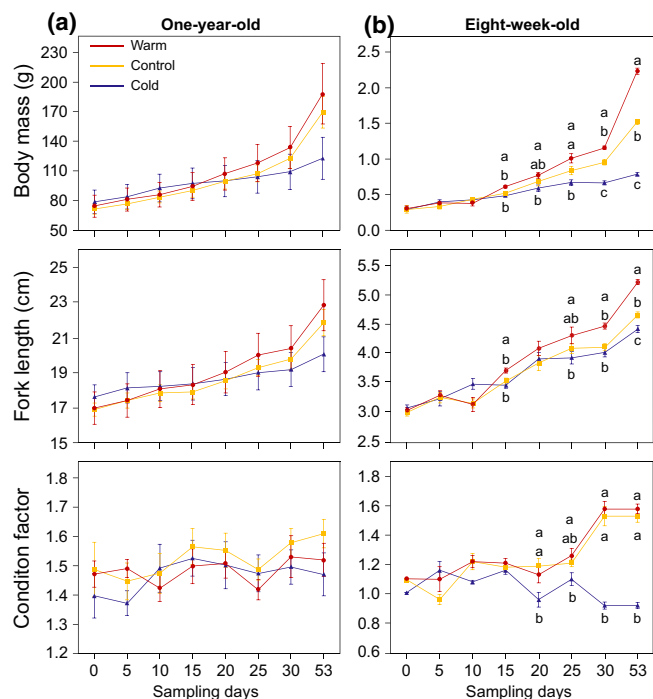


**FIGURE 1** Effects of chronic temperature shifts on growth of Arctic char. (a) Body mass, fork length, and condition factor of 1-year-old Arctic char. Values are means  $\pm$  SE;  $N = 6$ /group. (b) Body mass, fork length, and condition factor of 8-week-old Arctic char. Values are means  $\pm$  SE;  $N = 10$ /group. Different letters denote statistically significant differences among temperature groups for each sampling days ( $p < 0.05$ ) [Colour figure can be viewed at [wileyonlinelibrary.com](http://wileyonlinelibrary.com)]

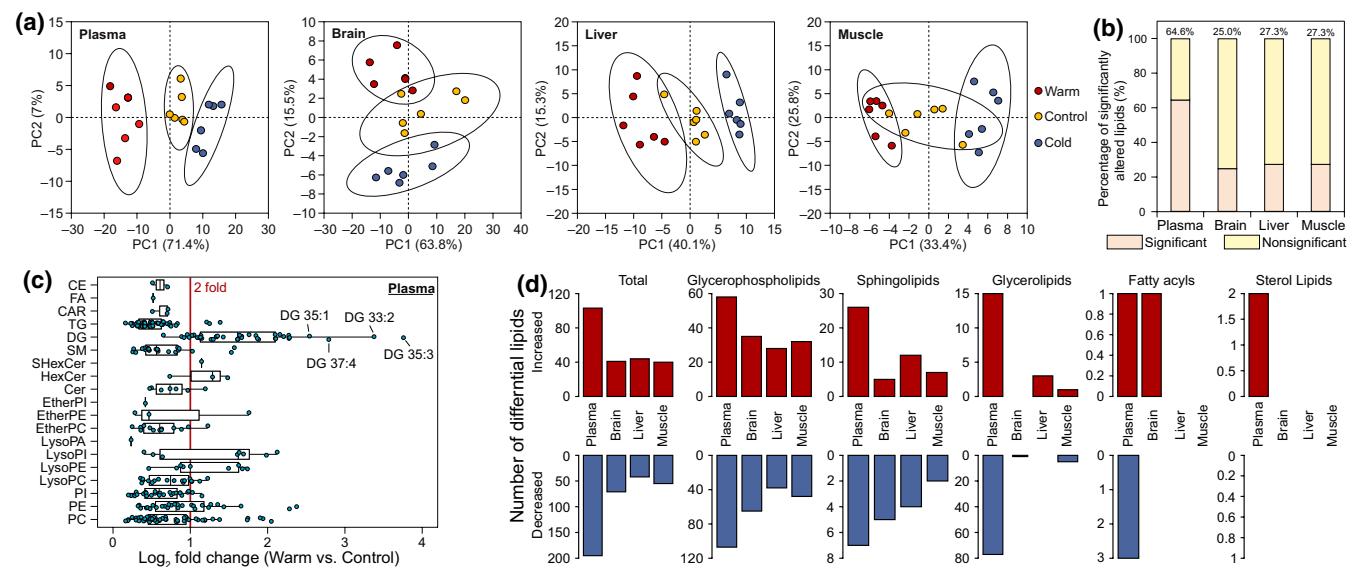


**FIGURE 2** Overall changes of the lipidome of 1-year-old Arctic char in response to temperature shifts. (a) Principal component analysis (PCA) of detected lipids in plasma, brain, liver, and muscle. The first two canonical axes are plotted. Data were log-transformed and auto-scaled prior to PCA analysis. (b) Proportion of changes in each tissue type of 1-year-old Arctic char. Pink bar indicates the proportion of lipids significantly altered in response to temperature shifts. (c) Variability of lipid species in plasma in response to warm treatment. Each data point represents the absolute value of  $\log_2$ (fold change) between warm treatment group and control group. Lipids are grouped by class. (d) Number of significantly altered lipids in warm treatment group relative to the control [Colour figure can be viewed at [wileyonlinelibrary.com](http://wileyonlinelibrary.com)]

and lipidome coverage. To validate the strength of the lipidomics method, 11 deuterated lipid standards representing major lipid subclasses were spiked into fish tissues before extraction and were subsequently processed through the whole lipidomics workflow. All lipid standards were correctly annotated based on fatty acyl constituents, indicating confidence in the lipid annotation of the method. Linear regression coefficients ( $R^2$ ) were better than 0.99 for all 11 lipid standards (Table S1). Recoveries of standards were in the range of 79.90–113.50%. To evaluate reproducibility, RSDs of peak areas for each detected lipid in QC samples were calculated and the distribution of RSDs is shown (Figure S2). Between 98.50% and 99.62% of detected lipids showed RSDs less than 15% in positive or negative ionization modes, respectively, which indicated a good reproducibility of the method for lipids in complex bio-matrices.

### 3.3 | Overall changes in lipidome of 1-year-old Arctic char by chronic temperature shifts

Total of 625, 565, 455, and 462 molecular lipid species among 31 lipid subclasses of five major lipid categories were confidently annotated and semi-quantified in plasma, brain, liver, and muscle of 1-year-old Arctic char, respectively (Figure S3). Lipid profiles from treatment groups were distinct in PCA plots of all tissue types (Figure 2a), which indicated significant changes in the lipidome of 1-year-old Arctic char after a 53-day exposure to various temperatures. Chronic temperature shifts caused extensive changes in 405, 141, 124, and 126 lipid molecules in plasma, brain, liver, and



muscle, respectively. Those significantly altered lipids accounted for 64.6%, 25.0%, 27.3%, and 27.3% of total detected lipids in plasma, brain, liver, and muscle, respectively (Figure 2b). Plasma was the tissue type with the greatest number of differences produced by temperature shifts. The significantly altered lipids span most of the major lipid categories, which implies widespread regulation of lipid metabolism by temperature shifts in Arctic char (Figure S4). Glycerophospholipids (GP) have the greatest number of significantly altered lipids in all analyzed tissue types. In addition, the Upset plot revealed a large proportion of overlap in significantly altered lipids between the warm and cold treatments (Figure S5), suggesting a similar regulatory mechanism for warm and cold adaptation. As shown in Figure 2c, diacylglycerol (DG) species in plasma showed the most significant response and greatest remodeling (in fold change) to the warm treatment. Compared to DG in plasma, other lipid classes were relatively invariant (Figures S6 and S7). Relative to that of the control, warm treatment significantly upregulated 103, 41, 44, and 40 lipid species while downregulating 195, 71, 42, and 55 lipid species in plasma, brain, liver, and muscle, respectively (Figure 2d).

### 3.4 | Identification of key lipid clusters in 1-year-old Arctic char in response to increased temperature

Chemical similarity enrichment analysis, which is based on chemical similarity and ontology mapping, was further applied to identify key lipid groups in response to increased temperature. Unlike canonical pathway enrichment, for example, KEGG pathway enrichment, ChemRICH enables study-specific and background-independent enrichment analysis of lipids, and thus is well suited for untargeted lipidomics datasets (Barupal & Fiehn, 2017; Contrepois et al., 2020). In this study, ChemRICH enrichment analysis identified several clusters of lipids that are associated with responses to increased temperature in 1-year-old Arctic char (Figure 3a), including increased saturated and monosaturated PC and PE, decreased polyunsaturated PE, decreased lysoPE and lysoPI, increased ether-linked GPs (except for PC in brain), decreased DG, and increased sphingomyelin (SM). Notably, warm treatment and cold treatment induced opposite effects on these lipid groups, implying that these identified lipid clusters are directly involved in regulation of thermal adaptation.

#### 3.4.1 | GP metabolism

A widespread remodeling of acyl chain profile was observed in major GP species after thermal treatment (Figure 3a). A close examination of fatty acid composition revealed that abundances of PE species with less unsaturation were significantly increased while that with greater unsaturation were significantly decreased during exposure to warmer temperature (Figure 3b; Figure S8). These data suggest that exposure to increased temperature downregulated degree of unsaturation of PE molecules in 1-year-old Arctic char. However,

for PC species, both degree of unsaturation and lengths of carbon chains were affected (Figure 3c; Figure S9). At warmer temperatures, PC molecules with lesser unsaturation and/or longer carbon chains tended to be accumulated and vice versa. Similarly, a lesser degree of unsaturation in fish exposed to the warmer temperature was also observed in plasma phosphatidylinositol (PI) and brain phosphatidylserine (PS; Figure 3d). As for PG species, the abundances of monoenes and polyenes were all significantly decreased in response to increased temperatures (Figure 3d).

In addition to regulation of acyl chain profile, extensive decreases in abundances of lysoPE and lysoPI were observed in 1-year-old Arctic char, when exposed to the warm temperature (Figure 3a; Figure S10). However, a mixed effect was observed for plasma lysoPC molecules. Abundances of several saturated lysoPCs were significantly greater while that of most unsaturated lysoPCs were significantly less in response to warm temperature (Figure S10a). Moreover, except for ether-linked PCs in brain, the abundances of most ether-linked GP molecules, as well as ether-linked TG species, were significantly increased by exposure to the warmer temperature (Figure 3a; Figure S11).

#### 3.4.2 | Sphingolipids metabolism

Lesser unsaturation was observed after exposure to warmer temperature in Cer, hexosylceramide (HexCer), and sulfatide (SHexCer) species (Figure S12). Additionally, clusters of SM were significantly enriched as shown by ChemRICH analysis in all analyzed tissue types of 1-year-old Arctic char (Figure 3a), and the abundances of almost all SM species were significantly increased in response to increased temperature (Figure S13).

#### 3.4.3 | Glycerolipid metabolism

Opposite regulations of the degree of unsaturation of TG molecules were observed in various tissues of 1-year-old Arctic char in response to temperature shifts. In plasma, exposure to warmer temperature resulted in greater abundances of highly unsaturated TG molecules (Figure 3e; Figure S14). However, in liver and muscle, abundances of TG molecules with less unsaturation were significantly increased by the warmer temperature while those with greater unsaturation were significantly decreased (Figure 3f). In addition, exposure to warmer temperature resulted in significantly lesser abundances of all DG species in plasma (Figure 3a; Figure S15).

### 3.5 | Coordinated regulation of lipid metabolism among tissues in response to temperature shifts

To better understand the interactions among lipids from various tissues in 1-year-old Arctic char, a WGCNA network analysis was performed. All annotated lipids from each tissue type were used

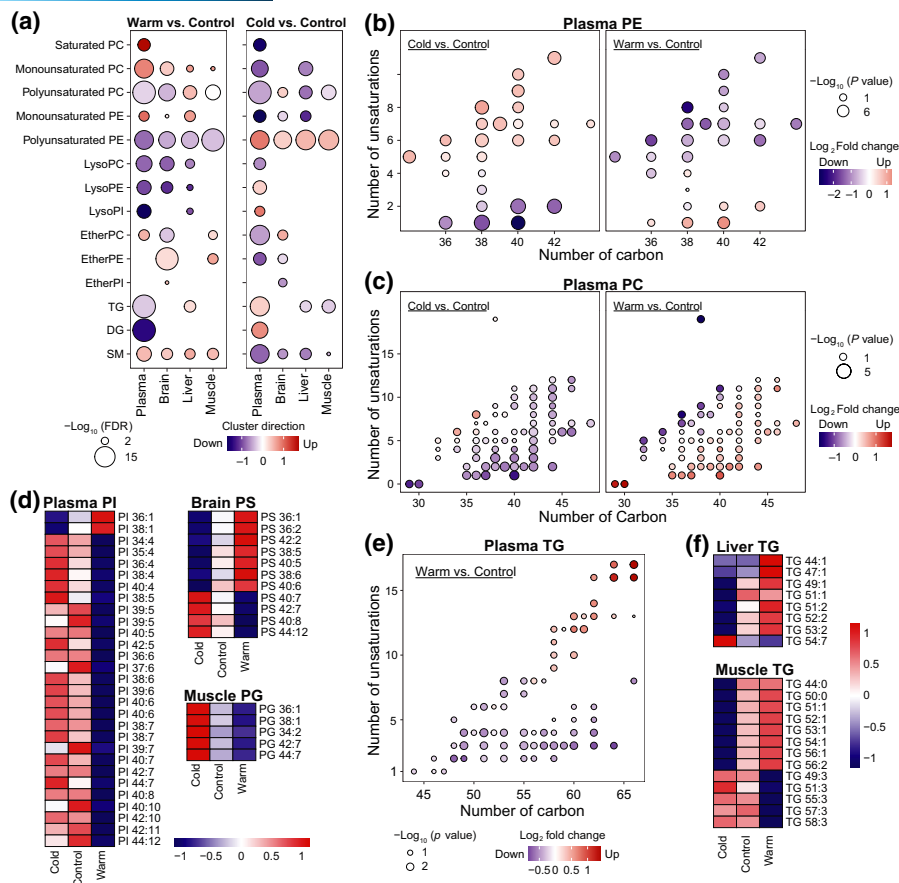


**FIGURE 3** Identification of key lipid clusters in 1-year-old Arctic char in response to increased temperature. (a) ChemRICH enrichment analysis of significantly altered lipid species identified in warm treatment group or cold treatment group. Cluster directions are the median  $\log_2$ (fold change) relative to control of significantly altered lipids in each lipid cluster (red, upregulated; blue, downregulated). The dot size indicates cluster significance (b) and (c) bubble plots illustrating altered fatty acid composition of PE and PC species in plasma. Dot color indicates the  $\log_2$ (fold change) relative to control. The dot size indicates the significance. (d) Heatmap plots of acyl chain profile in plasma PI, brain PS, and muscle PG. The average values of significantly altered lipids in each treatment group are presented. Data were log-transformed and Z-score scaled prior to data visualization. (e) Bubble plots illustrating altered fatty acid composition of TG species in plasma. Dot color indicates the  $\log_2$ (fold change) relative to control. The dot size indicates the significance. (f) Heatmap plots of acyl chain profile of TG species from liver and muscle. The average values of significantly altered lipids in each treatment group are presented. Data were log-transformed and Z-score scaled in prior to data visualization. DG, diacylglycerol; PC, phosphatidylcholine; PE, phosphatidylethanolamine; PG, phosphatidylglycerol; PI, phosphatidylinositol; PS, phosphatidylserine; SM, sphingomyelin; TG, triacylglycerol. [Colour figure can be viewed at [wileyonlinelibrary.com](http://wileyonlinelibrary.com)]

for construction of a network and assigned to modules (Figure S16). Then, thermal response modules were further identified by over-representation analysis of significantly altered lipids using a hypergeometric test with  $p < 0.05$  as cutoff. As a result, a total of two, two, four, and three thermal response modules were identified in plasma, brain, liver, and muscle, respectively. Significant overlaps were found between these thermal response modules by pairwise analysis (Figure 4a; Figure S17). These results suggested a coordinated regulation of lipid metabolism among tissues in response to changes in temperature. A lipid co-regulation network of the most significantly overlapped modules is visualized (Figure 4b). Lipid annotations are only shown for the top 20 hub lipids with greatest intra-modular connectivity. In brain, liver, and muscle, most of the hub lipids belonged to polyunsaturated PE or PC subclasses, while in plasma the majority of the top 20 hub lipids were DG lipids.

### 3.6 | Chronic temperature shifts-activated lipid dynamics in liver of 8-week-old Arctic char

For a comprehensive investigation of the lipid dynamics, a total of 520 lipid species (272 GPs, 53 SPs, 178 glycerolipids (GLs), 16 FAs, and 1 others) encompassing 30 major lipid subclasses were analyzed and semi-quantified in 228 liver samples collected serially from 8-week-old Arctic char over the course of thermal treatment. This large dataset coupled with time-series measurements enabled us to evaluate whether lipid remodeling occurs in a direction that would support the findings in 1-year-old Arctic char, and helped to detect novel transient patterns in 8-week-old fish during the course of chronic temperature shifts. Results of PCA analysis revealed that there were significant separations between the warm treatment group and the cold treatment group from day 20 onwards (Figure 5a;

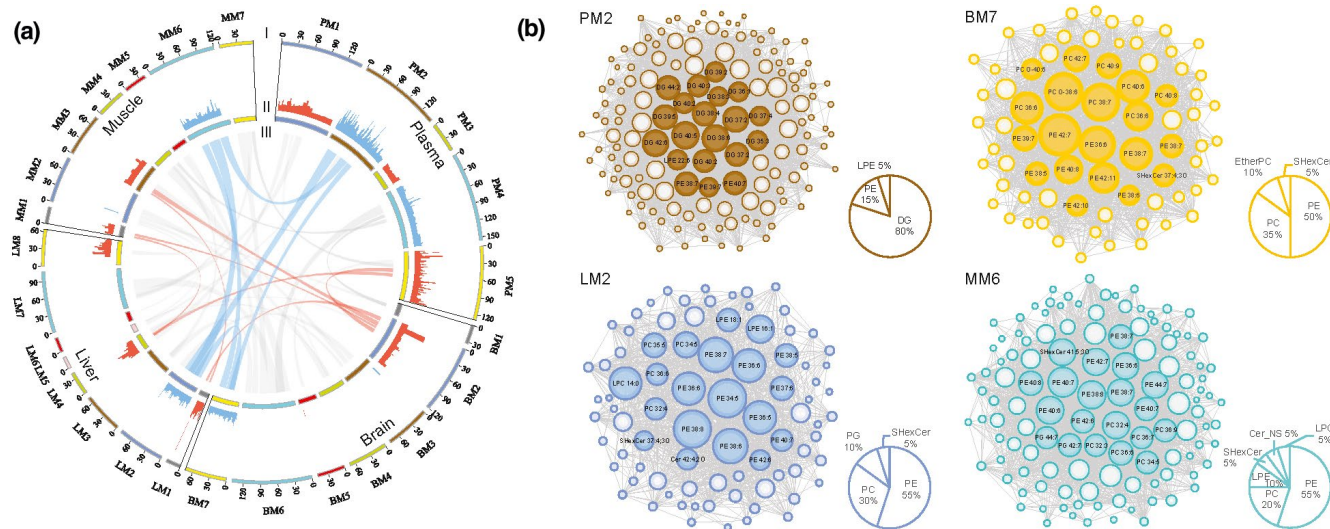


**FIGURE 4** Co-regulation of lipid species in different tissues of 1-year-old Arctic char in response to temperature shifts. (a) Circos connectogram depicting the association between significantly altered lipids from different types of tissue. From outer to inner circles: I. Modules identified in plasma, brain, liver, or muscle by weighted correlation network analysis (WGCNA). Arc length represents the number of lipids in each module (module size). II. Absolute  $\log_2$ (fold change) value of significantly altered lipids found in each module. Red color represents upregulation while blue color represents downregulation. III. Pairwise comparisons of modules. The number of overlapping lipids was enumerated, and the statistical significance of overlap was evaluated using the two-sided Fisher's exact test. Modules were considered as significantly overlapped if  $p < 0.01$ . The bundle width is proportional to the number of overlapping lipids in each bundle. Overlaps between thermal response modules are colored with red (between upregulated modules) or blue (between downregulated modules). (b) Visualized lipid co-regulation network of the most significantly overlapped modules. Lipid annotations are only shown for the top 20 hub lipids with highest intra-modular connectivity. Node size represents the intra-modular connectivity of a given lipid. Pie charts in the bottom right corner of each module represent the subclass composition of the top 20 hub lipids. BM, brain module; LM, liver module; MM, muscle module; PM, plasma module [Colour figure can be viewed at [wileyonlinelibrary.com](http://wileyonlinelibrary.com)]

Figure S18). Hierarchical clustering also showed that samples from the same treatment group clustered tightly after 20 days of treatment (Figure S19). The number of significantly altered lipids between the warm treatment group and the control group elevated gradually throughout the whole experiment, while that from cold treatment group in relative to the control increased to maximum at day 25 and then decreased (Figure 5b). Similar patterns were also observed for the significantly altered lipids in GP, GL, or sphingolipid (SP) categories (Figure S20). At all sampling points, GP species accounted for the largest proportion (>53.4%) of significantly altered lipids (Figure 5c).

Chemical similarity enrichment analysis enrichment using all significant altered lipids at each time point unveiled key lipid clusters involved in regulatory mechanisms of thermal adaption in the liver of 8-week-old Arctic char over the course of temperature shifts. Compared to the control, consistent and uniform patterns were observed in cold treatment group in response to stepwise temperature decreases (Figure 5d). Notably, a quick and significant lipid modulation, that is, increased abundance of polyunsaturated PEs, emerged just after a minor temperature drop of 1°C (day 5). On the contrary, during gradually increased temperatures, 8-week-old Arctic char showed poor consistency in regulation of liver lipidome during the early period of temperature shifts (Figure 5e, days 10–20). Then, from day 25 onwards, significantly altered lipids in the warm treatment group exhibited consistent but opposite changing patterns to that in the cold treatment group. The opposite changing

patterns imply that these identified lipid groups are directly involved in thermal adaption in Arctic char. In accordance with results from 1-year-old fish, downregulated unsaturation degrees were detected for PE and TG molecules in liver of 8-week-old Arctic char exposed to increased temperatures, as indicated by the accumulation of saturates and monoenes but depletions of polyenes. Close examinations of fatty acid composition further confirmed this trajectory (Figures S21 and S22). Moreover, decreased abundances of PG and lysoPE species from day 25 onwards and increased abundances of SMs from day 15 onwards were also seen. However, unexpected alterations in abundances of PC species were observed. The abundances of almost all PC species were increased in warm treatment group compared to the control during the course of warm treatment (Figure S23).

### 3.7 | Identification of lipid biomarkers of Arctic char lipidome in response to chronic temperature shifts

The above analysis showed that 1-year-old and 8-week-old Arctic char had similar patterns for the significantly altered lipids responding to chronic temperature shifts. Here, to identify lipid biomarkers of Arctic char lipidome in response to chronic temperature shifts, we built a random forest model using the intersection data



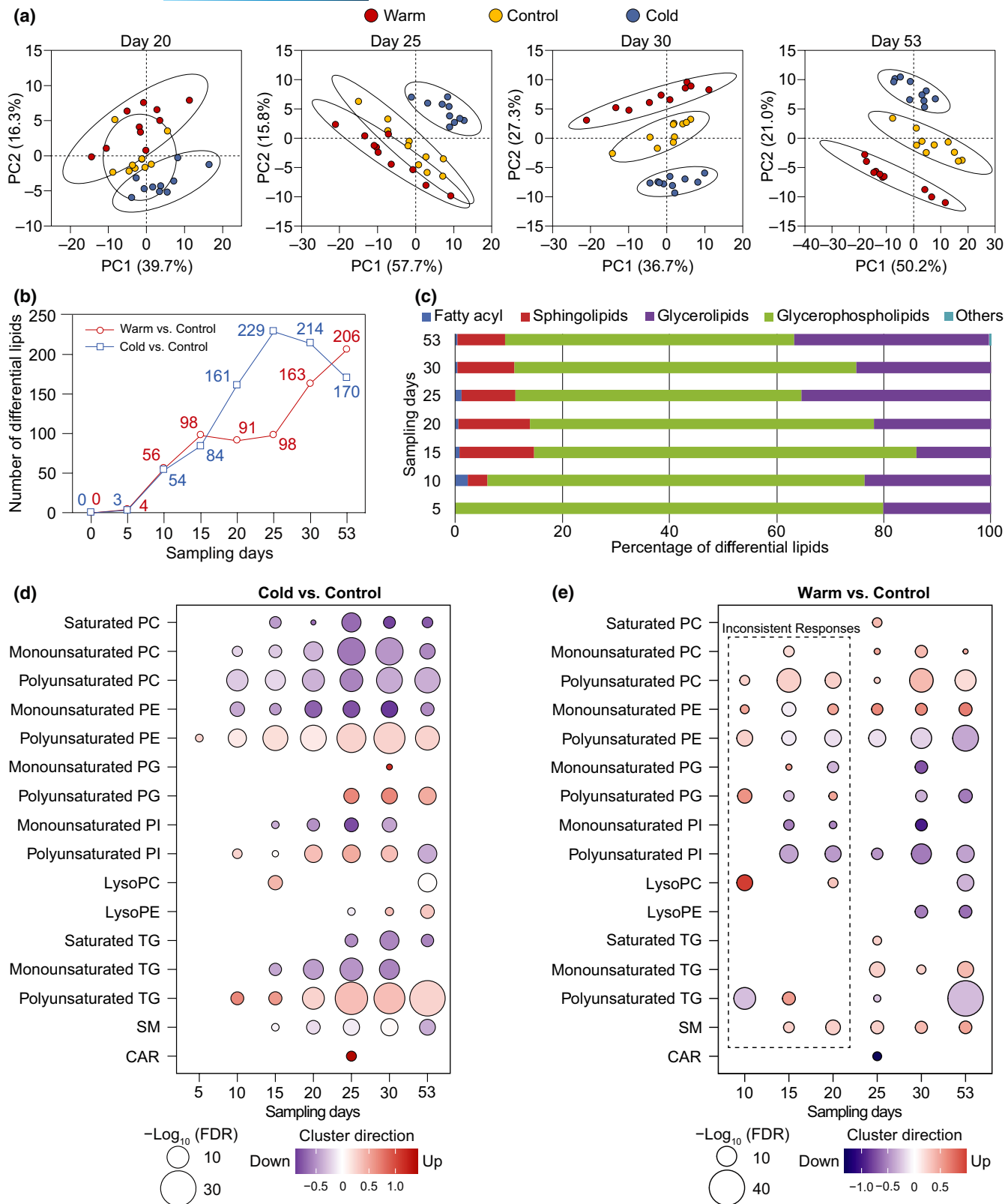


**FIGURE 5** Temporal changes of lipids in liver of 8-week-old Arctic char during the course of chronic temperature shifts. (a) Principal component analysis (PCA) of detected lipids at sampling days 20, 25, 30, and 53. The first two canonical axes are plotted. Data were log-transformed and auto-scaled prior to PCA analysis. (b) Numbers of significantly altered lipids. (c) Percentages of significantly altered lipids in each lipid category. (d, e) ChemRICH enrichment analysis of significantly altered lipid species identified in warm or cold treatment groups. Cluster directions are the median  $\log_2$ (fold change) relative to control of significantly altered lipids in each lipid cluster (red, upregulated; blue, downregulated). The dot size indicates cluster significance. CAR, acylcarnitine; PC, phosphatidylcholine; PE, phosphatidylethanolamine; PG, phosphatidylglycerol; PI, phosphatidylinositol; SM, sphingomyelin; TG, triacylglycerol [Colour figure can be viewed at [wileyonlinelibrary.com](http://wileyonlinelibrary.com)]

of plasma, liver, brain, and muscle samples from 1-year-old Arctic char as a discovery dataset (18 fish and 72 samples), which included training (7/10) and validation (3/10) sets. Key lipids were found after binary classification in cold, control, and warm groups compared with each other. Next, the lipids from 8-week-old Arctic char (30 fish and 30 samples) were employed as an independent test data (Figure 6a). Three common features (PE 36:6|PE 16:1\_20:5, PE 38:7|PE 16:1\_22:6, and PE 40:7|PE 18:1\_22:6) in all thermal treatment groups were finally extracted as a lipid biomarker panel for classifying warm versus control, cold versus control, and cold versus warm groups with 90%, 87%, and 94% accuracy, respectively (Figure 6b,c). The three PE species were confirmed by highly confident MS2 spectra matching (Figures S24–S26). Our results indicated

that the three PE species identified by machine learning, that is, PE 36:6|PE 16:1\_20:5, PE 38:7|PE 16:1\_22:6, and PE 40:7|PE 18:1\_22:6, are closely associated with thermal adaptation of Arctic char lipidome. Further work is required to confirm this association and, if confirmed, to elucidate the underlying mechanism.

## 4 | DISCUSSION

It has been predicted that both marine and freshwater temperatures will continue to rise due to global warming (Meredith, 2019). The global surface temperatures relative to the years 1850–1900 are projected to increase by 1.1–2.0°C under RCP2.6 (Representative

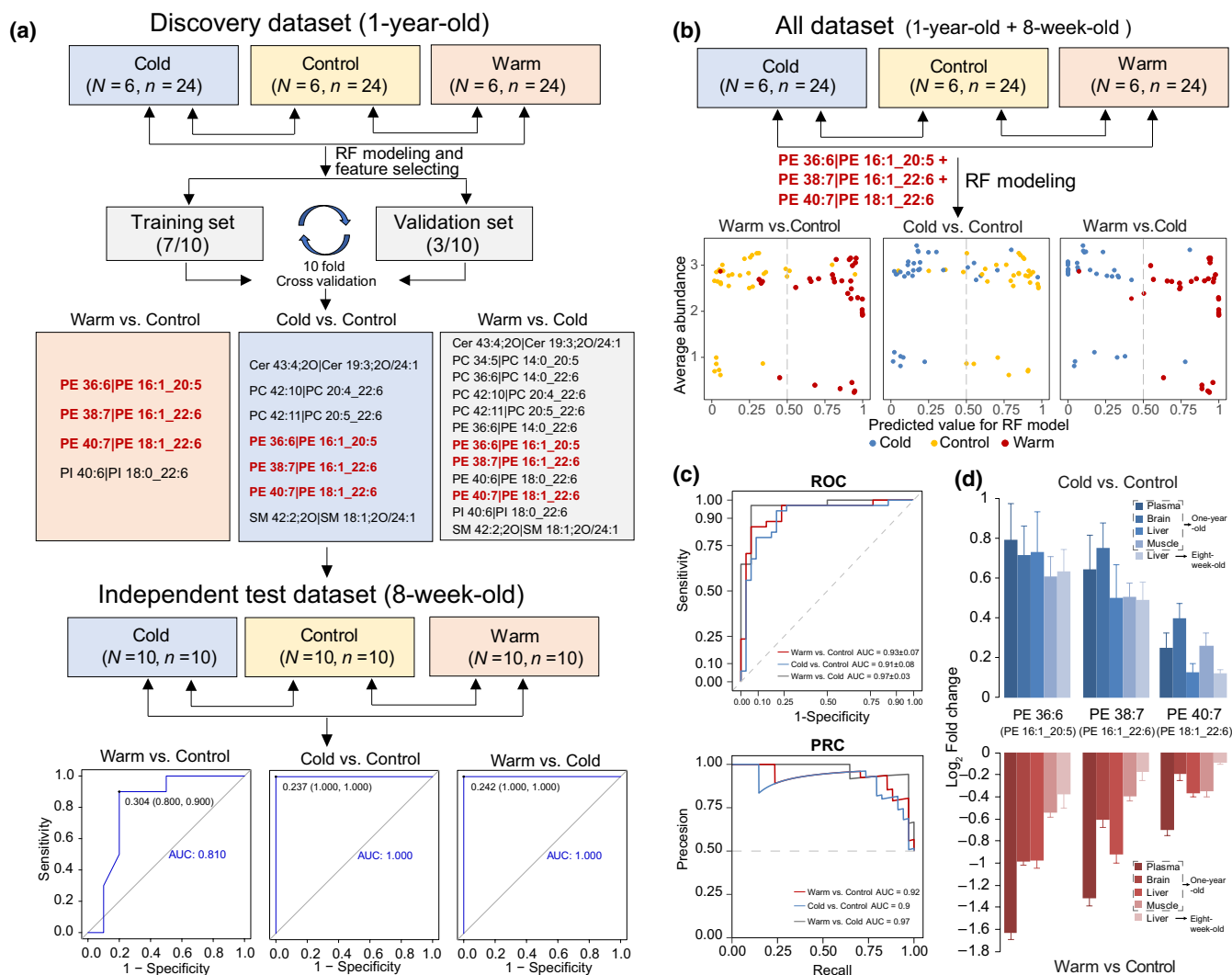


**FIGURE 6** Identification of key lipids species of Arctic char lipidome in response to chronic temperature shifts by machine learning algorithm. (a) Workflow for machine learning algorithm. (b) Performance of the model in all dataset including both 1-year-old and 8-week-old Arctic char. The plot matrix at the bottom shows the prediction accuracy of three common features selected in all temperature groups. The X-axis shows the predicted value for random forest model, and Y-axis shows the average abundance of all the samples. Blue, yellow, and red colors mean cold, control, and warm treatment, respectively. (c) Receiver-operator characteristic curve (ROC) and Precision-Recall Curve (PRC) of three common features selected in all temperature groups. (d) The  $\log_2$ (fold change) of PE 36:6|PE 16:1\_20:5, PE 38:7|PE 16:1\_22:6, and PE 40:7|PE 18:1\_22:6 between treatment and control. Data were log-transformed prior to data visualization [Colour figure can be viewed at [wileyonlinelibrary.com](http://wileyonlinelibrary.com)]

Concentration Pathways 2.6) scenario or 1.5–2.4°C under RCP8.5 scenario until 2050, with land, high latitudes, and winter warming faster or to a greater extent (Meredith, 2019). Arctic char prefer cold temperatures and are generally found in water with a temperature less than 10°C. Thus, the temperature range of 2–14°C employed in the study, results of which are presented here, could be regarded as a scenario of near-future Arctic warming.

Our results indicate that early life stages of Arctic char are more susceptible to temperature variation than older life stages. The growth of 8-week-old Arctic char was significantly influenced by ambient temperature, whereas no significant effects of temperature shifts on 1-year-old fish were observed. The preferred temperature of Arctic char is dependent on life stage, with younger fish having a narrower optimal range of temperature and preferring colder environments (Larsson, 2005). This discrepancy could be explained, in part, by the size buffering effect (Elliott, 1982). In addition, both 1-year-old and 8-week-old fish showed no physical signs of deleterious effects at the warmer temperature, which suggested that they have a strong capability to adjust to rising temperatures within the range of this study. A positive effect of an increased summer ice-free period on the condition of Arctic char has been suggested (Harwood et al., 2013). However, further investigation including fecundity and long-term exposure would be needed to observe whether the thermal adaptation has any negative effects on species fitness.

Lipids play crucial roles in structure and dynamics of membranes, energy homeostasis, and signal transduction (Shevchenko & Simons, 2010). In-depth analysis of alterations in the lipidome in response to increased temperature would be beneficial for a better understanding of acclimatization and adaptation potential of Arctic species in the face of warming of the Arctic. So far, previous work has predominantly focused on remodeling of fatty acid composition in membrane GPs (Bennett et al., 2018; Fadhloui & Couture, 2016; Malekar et al., 2018), ignoring the potential role of other vital lipid classes and the dynamics changes of lipidome. In the present study, significant alterations in the lipidome were observed in all tissues of 1-year-old Arctic char (Figure 2) and liver in 8-week-old fish over the course of temperature shifts (Figure 5). Furthermore, significantly altered lipids are not limited to GP lipids, but instead span most of the major classes of the lipidome, indicating the broad participation of various lipids in the adaptability of Arctic char in warming environments.

Biological membranes are complex and dynamic assemblies of various lipids and proteins and lipid composition crucially affect the properties of membranes, such as fluidity, curvature, lipid packing, surface charge, and subdomain architecture (Ballweg et al., 2020; Harayama & Riezman, 2018). GP lipids, especially for PC and PE, are major building blocks of membrane bilayers. Generally, GP lipids with saturated acyl chains form non-fluid and tightly packed gel phases while replacement with unsaturated acyl chains reduces membrane rigidity (Ernst et al., 2016). At an organism's adapted temperature, membrane lipids are in a relatively fluid liquid-crystalline phase while once above the optimal temperature range, membrane lipids become "hyperfluid" which can compromise vital cellular functions (Hazel, 1995). Ectothermic organisms counteract effects of

variations in temperature by modulating proportions of saturated and unsaturated acyl chains in membrane GPs (Martin et al., 2007; Muir et al., 2016; Saita et al., 2016; Sinensky, 1974). In the present study, widespread decreases in the degree of acyl chain unsaturation in bulk membrane constituents were observed in tissues of 1-year-old Arctic char (Figure 3; Figures S8 and S9), indicating an attempt to stabilize membranes at higher temperatures. The results of the study reported here are consistent with essential features of HVA theory. The compensatory changes in unsaturation rate of membrane lipids in response to warmer environment could further effect on Arctic char nutritional value (Koelmel et al., 2020). More importantly, the lipidomics data, down to the lipid species level, further suggest that remodeling of acyl chain profiles in GP lipids by increased temperatures is headgroup-specific. For instance, shifts in temperature affected both lengths of carbon chains and degree of unsaturation in PC lipids, but for other GP classes, only degrees of unsaturation were affected. In addition, all PI polyenes were decreased by warm treatment, whereas only more unsaturated polyenes (unsaturation >4) in PE class were decreased. Similarly, Chwastek et al., (2020) also reported that PC exhibited the greatest variability in both acyl chain length and unsaturation to changing environmental conditions among other lipid classes in the bacterium *Methylobacterium extorquens*. Headgroup-specific effects represent a mixed effect of headgroup and acyl chain profile on properties of membranes (Klose et al., 2013; Patton-Vogt & Kroon, 2020).

Another striking observation is that regulation of degree of unsaturation of TG in plasma (Figure 3e) was opposite of that observed for GP species (Figure 3b,d), as well as that of TG species in liver and muscle (Figure 3f). The reverse regulation suggests an exchange of fatty acids between plasma TG and membrane GP lipids. It was demonstrated that direct desaturation of fatty acids by desaturases works as a major adaptive mechanism to regulate the proportion of unsaturated fatty acids in membrane lipids, allowing fish to cope with fluctuations in temperature (Hsieh & Kuo, 2005; Tiku et al., 1996). Here, based on our data, it can be inferred that except for direct desaturation of fatty acids, unsaturated fatty acids can be originated from plasma TG species, and plasma TG serves as cache of fatty acids for membrane lipid remodeling during adaption to temperature. In the face of increased temperatures, TG molecules containing more saturated fatty acids in plasma could be incorporated into hepatocyte/myocyte and release saturated fatty acids (or fatty acid with less unsaturation) that would be reactivated to acyl-CoA and utilized for remodeling of GP acyl chain through the Lands' cycle process (Lands, 1960).

In addition to acyl chain remodeling, progressive modifications of GP composition were also observed in Arctic char during changes in temperature. In this study, abundances of most lysoPE, lysoPI, and lysoPC species were significantly decreased by warmer temperature, except for several saturated species (Figure 3a; Figure S10). Lyso-GPs are non-cylindrical amphipathic molecules and have an overall inverted conical shape (Arouri & Mouritsen, 2013). Their conical geometry disrupts tight packing of membrane lipids and thus incorporation of lyso-GPs leads to instabilities in the lipid bilayer

(Inoue & Kitagawa, 1974). Additionally, significantly increased abundances by warmer temperature were noted for ether-linked GP species (Figure 3a; Figure S11). Incorporation of ether-linkages and lack of carbonyl oxygen at the *sn*-1 position permit tighter packing of the membrane bilayer and result in decreased membrane fluidity and increased rigidity (Dean & Lodhi, 2018; Lohner, 1996). Thus, the extensively increased abundances of ether-linked lipids likely contribute to the ability of Arctic char to maintain membrane order and restore cellular function following thermal increase. In addition, although contradictory results exist (Broniec et al., 2017; Wang & Wang, 2010), several studies suggest that ether lipids could potentially protect membranes against oxidative stress by acting as sacrificial antioxidants (Dorninger et al., 2017). Thus, the increased abundances of ether lipids might also contribute to attenuation of oxidative stress, induced by the warmer temperature in this study (Cheng et al., 2018; Lushchak & Bagnyukova, 2006; Mueller et al., 2011). Decreased abundances of ether-linked PC species in fish brain (Figure 3a; Figure S11a) in response to increased temperature could result from increased utilization of these molecules as sacrificial antioxidants for scavenging reactive oxygen species due to the susceptibility of brain to oxidative damage (Bharath et al., 2002; Dringen et al., 2000).

Analysis of lipidomics also revealed involvement of SP lipids in the process of thermal adaptation. Consistent with GP lipids, a significantly greater proportion of saturation in acyl chains of Cer, HexCer, and SHexCer species was observed (Figure S12). Additionally, abundances of most of the SM species in tissues of 1-year-old Arctic char were significantly greater after exposure to warmer conditions (Figure 3a; Figure S13). These data demonstrate that the modification of GP lipids is not the only mechanism through which Arctic char can cope with exposure to higher temperatures. SM are the most abundant SP lipids and more than half of the cellular SM is confined to the plasma membrane (Koval & Pagano, 1991). Due to its acyl chain composition, SM is packed tightly and can increase packing density in membranes (Holthuis & Menon, 2014; van Meer et al., 2008). Thus, globally increased abundances of SM could offset the fluidizing effect induced by increased temperature and help to stabilize structures of membranes. Moreover, SM has a strong tendency to form transient, dynamic, and relatively ordered "lipid raft" microdomains with cholesterol and proteins on plasma membranes (Ando et al., 2015; Bieberich, 2018). These lipid rafts are thought to regulate protein trafficking and important signal transductions related to cell adhesion, migration, survival, and proliferation (Hanzal-Bayer & Hancock, 2007; Lingwood & Simons, 2010). The greater amounts of SM present in Arctic char might be a result of active formation of dynamic lipid raft structures due to upregulated intercellular interactions in response to temperature shifts. A similar finding of greater abundances of SM species has been reported in crucian carp (*Carassius carassius*) acclimated to warmer temperatures (Käkelä et al., 2008).

Weighted correlation network analysis clusters features into co-expressed modules, with features in the same module sharing the same expression pattern. By using unsupervised and

completely data-driven network analysis, thermal response modules in different tissues were identified individually and significant overlaps between these thermal response modules from different tissues were revealed (Figure 4a). The results of the WGCNA analysis demonstrate coordinated and co-regulated changes in the lipidome of various tissues and suggest that various cell types, including neurocytes, hepatocytes, and myocytes, share a conserved mechanism for lipid remodeling to cope with shifts in temperature. Hub lipids are lipids with greatest intra-modular connectivities and represent a disproportionate role in influencing changing patterns of other lipids in the network. In this study, most of the hub lipids in brain, liver, and muscle were PE and PC (Figure 4b), which highlights the central role of PE and PC lipids in regulation of membrane homeostasis in these tissues. However, in plasma, DG was identified as the hub lipid (Figure 4b) and at the same time the most responsive molecules (in fold change) in response to warm treatment (Figure 2c). DG lipids are key intermediates in lipid metabolism and important second messengers in cellular signaling processes (Carrasco & Mérida, 2007). DG could be used with either CDP—choline or CDP—ethanolamine for de novo PC or PE biosynthesis through the Kennedy pathway (Kennedy & Weiss, 1956), which might provide an additional pathway for membrane lipid remodeling caused by shifts in temperature. In addition, DG could also directly affect physical properties of membranes, although they are a minor component of membranes in quantitative terms. Due to their small headgroup, DGs tend to form inverted micellar structures and thus, increased DG concentration would introduce a disruption of the lamellar phase of lipid membranes and promote fusion and fission (Furt & Moreau, 2009; Gómez-Fernández & Corbalán-García, 2007). In this study, the decreased DG concentrations could help to stabilize membrane bilayer structure when exposed to the warmer temperature. Overall, these findings indicate the potential roles of plasma DG in Arctic char dealing with shifts in temperature.

Using time-series analysis, results of this study provide insights into dynamic regulation of global lipid metabolism during shifts in temperature. To date, studies monitoring dynamics of lipids in response to chronic temperature shifts are limited. In this study, lipids in liver of 8-week-old Arctic char exhibited rapid and consistent responses to stepwise decreases in temperature (Figure 5d). Particularly, polyunsaturated PE species responded quickly to a minor temperature drop of 1°C. Additionally, several major and significant alterations in the hepatic lipidome of Arctic char were observed to persist during the course of cold treatment, including increased degree of lipid unsaturation in PE and TG classes, increased abundances of lysoPE, and decreased abundances of unsaturated PG and SM molecules. These observations are consistent between 1-year-old and 8-week-old fish, indicating that these modulations are conserved during larval development in Arctic char. It is possible that lipid composition and the regulatory mechanisms of lipidome adaptation in Arctic char have evolved to be well suited for lower temperature environments. However, during the early period of warm treatment, 8-week-old Arctic char showed a delay and inconsistent regulation of the hepatic lipidome (Figure 5e). These

findings suggest an inability of Arctic char to adapt rapidly to increasing ambient temperatures and can partly explain the sensitivity of this species to high summer temperatures (Elliott & Elliott, 2010). Moreover, unlike older fishes, the abundances of almost all PC molecules were significantly greater during the warmer temperature, whereas opposite changes were seen in individuals at the colder temperature (Figure S23). It has been reported that PE are non-bilayer lipids and addition of unsaturated PE could destabilize membranes (Cullis & De Kruijff, 1979; de Kroon et al., 2013). Facilitated by its cylindrical shape, PC molecules self-assemble into closed bilayers and possess a stabilizing effect on the membrane bilayer architecture (Holthuis & Menon, 2014). Thus, the increased abundances of PC could counter the destabilizing effect induced by the increased proportion of unsaturated PE species in 8-week-old Arctic char. The apparent discrepancy in regulating PC profiles between 1-year-old and 8-week-old Arctic char may explain the observation that younger fish are more susceptible to temperature shifts than older fish.

In summary, a multi-tissue analysis of the Arctic char lipidome revealed several adaptive mechanisms of this ecologically and economically important species in response to shifts in temperature, which could be caused by near-future Arctic warming (Figure 7). This study is the first to elucidate hepatic lipid dynamics over the time course of temperature shifts by a large-scale lipidomics approach. Another strength of this study is the use of both warm and cold treatment to study the changes of lipidome in the face of temperature changes. The opposite effects induced by warm or cold

treatment further verified direct participation of the identified lipid groups in regulation of thermal adaption. The main findings include the following:

1. Early life stages of Arctic char are more susceptible to temperature variations.
2. Arctic char respond to increased temperatures with highly coordinated lipid regulations, including headgroup-specific remodeling of acyl chain profile in GP molecules and extensive alterations in membrane lipid composition, such as less lyso-GPs, and more ether-GPs and SMs.
3. Except for phospholipids, glycerolipids also participate in the adaptive regulations of Arctic char lipidome in response to temperature shifts. For instance, plasma TG can serve as cache of fatty acids for membrane lipids remodeling during the thermal adaption process.
4. Eight-week-old Arctic char exhibited rapid adaptive alterations in the hepatic lipidome in response to stepwise temperature decreases while showing blunted responses to gradual temperature increases, implying an inability to adapt rapidly to a warmer environment.

These findings demonstrate the central role of lipids in response to temperature changes and underscore the utility of lipidomics for studying the regulation and function of lipids. Our work provides a comprehensive source to better understand the regulatory mechanisms of Arctic organisms in the face of near-future Arctic warming.

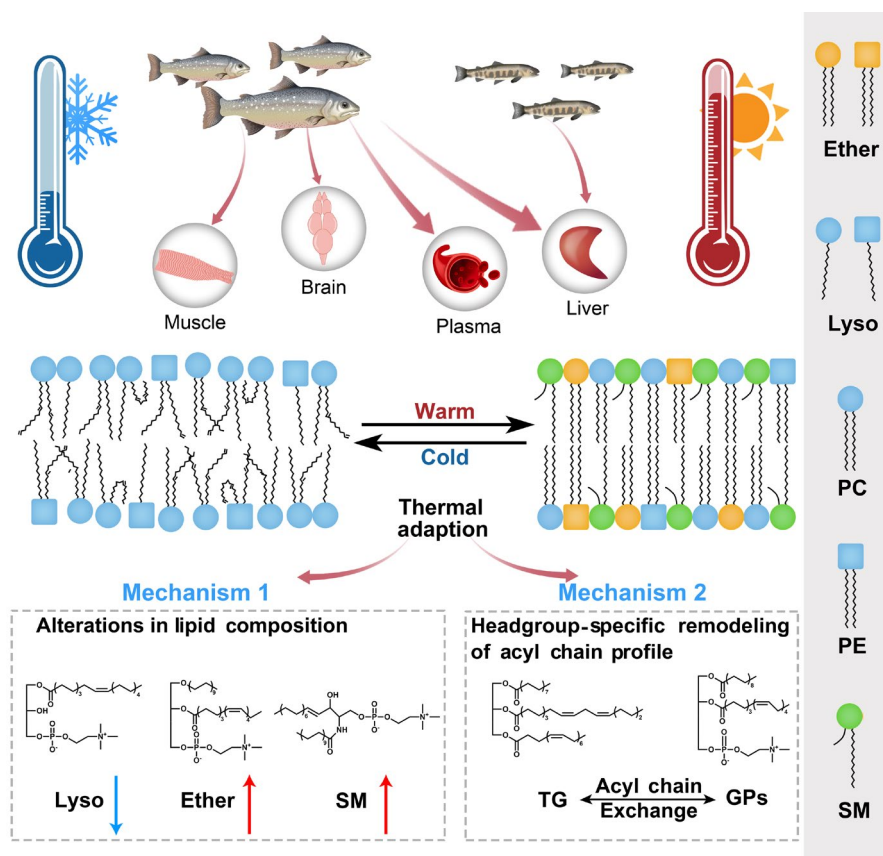


FIGURE 7 Two main regulatory mechanisms of Arctic char lipidome in response to chronic temperature shifts (warm or cold). GP, glycerophospholipid; PC, phosphatidylcholine; PE, phosphatidylethanolamine; PG, phosphatidylglycerol; PI, phosphatidylinositol; SM, sphingomyelin; TG, triacylglycerol [Colour figure can be viewed at [wileyonlinelibrary.com](http://wileyonlinelibrary.com)]



Further study will be needed to identify the metabolic cost of different lipid adaptations and whether fecundity is affected by thermal changes.

## ACKNOWLEDGEMENTS

Funding was provided by "Next generation solutions to ensure healthy water resources for future generations" funded by the Global Water Futures Program, Canada First Research Excellence Fund (no. 419205), and Fisheries and Oceans Canada's National Contaminants Advisory Group. Chao Wang was supported by the Oversea Research Training Program of NIEH, China CDC. Prof. Song Tang was supported by the Young Scholar Scientific Research Foundation of China CDC (no. 2018A201) from China CDC and the Start-up Funding from Oversea Research Training Program of NIEH, China CDC. Prof. Giesy was supported by the Canada Research Chairs Program of the NSERC Doctoral Scholarship Funding (no. PGSD 3-504735-2017). Dr. Codling was funded from the European Union's Horizon 2020 Research and Innovation Program under the Marie Skłodowska-Curie grant agreement no. 839243. This publication reflects only the authors' views, and the EU is not liable for any use that may be made of the information contained herein. Dr. Challis was supported by a Banting Postdoctoral Fellowship. D. Green was supported by NSERC Doctoral Scholarship funding (no. PGSD 3-504735-2017).

## CONFLICT OF INTEREST

The authors have no real or perceived competing financial interests to declare.

## DATA AVAILABILITY STATEMENT

The data that support the findings of this study are openly available in MetaboLights at <https://www.ebi.ac.uk/metabolights/>, reference number MTBLS2617.

## ORCID

Chao Wang  <https://orcid.org/0000-0002-5056-9903>

Yufeng Gong  <https://orcid.org/0000-0002-1396-527X>

Song Tang  <https://orcid.org/0000-0003-3219-1422>

## REFERENCES

- ACIA. (2005). *Arctic climate impact assessment. ACIA overview report*. Cambridge University Press, 1020 pp.
- Ando, J., Kinoshita, M., Cui, J., Yamakoshi, H., Dodo, K., Fujita, K., Murata, M., & Sodeoka, M. (2015). Sphingomyelin distribution in lipid rafts of artificial monolayer membranes visualized by Raman microscopy. *Proceedings of the National Academy of Sciences*, 112(15), 4558–4563. <https://doi.org/10.1073/pnas.1418088112>
- Aroui, A., & Mouritsen, O. G. (2013). Membrane-perturbing effect of fatty acids and lysolipids. *Progress in Lipid Research*, 52(1), 130–140. <https://doi.org/10.1016/j.plipres.2012.09.002>
- Ballweg, S., Sezgin, E., Doktorova, M., Covino, R., Reinhard, J., Wunnicke, D., Hänel, I., Levental, I., Hummer, G., & Ernst, R. (2020). Regulation of lipid saturation without sensing membrane fluidity. *Nature Communications*, 11(1). <https://doi.org/10.1038/s41467-020-14528-1>
- Barupal, D. K., & Fiehn, O. (2017). Chemical Similarity Enrichment Analysis (ChemRICH) as alternative to biochemical pathway mapping for metabolomic datasets. *Scientific Reports*, 7(1), 14567. <https://doi.org/10.1038/s41598-017-15231-w>
- Bennett, H., Bell, J. J., Davy, S. K., Webster, N. S., & Francis, D. S. (2018). Elucidating the sponge stress response; lipids and fatty acids can facilitate survival under future climate scenarios. *Global Change Biology*, 24(7), 3130–3144. <https://doi.org/10.1111/gcb.14116>
- Bharath, S., Hsu, M., Kaur, D., Rajagopalan, S., & Andersen, J. K. (2002). Glutathione, iron and Parkinson's disease. *Biochemical Pharmacology*, 64(5–6), 1037–1048. [https://doi.org/10.1016/s0006-2952\(02\)01174-7](https://doi.org/10.1016/s0006-2952(02)01174-7)
- Bieberich, E. (2018). Sphingolipids and lipid rafts: Novel concepts and methods of analysis. *Chemistry and Physics of Lipids*, 216, 114–131. <https://doi.org/10.1016/j.chemphyslip.2018.08.003>
- Broniec, A., Źądło, A., Pawlak, A., Fuchs, B., Kłosiński, R., Thompson, D., & Sarna, T. (2017). Interaction of plasmamethylcholine with free radicals in selected model systems. *Free Radical Biology and Medicine*, 106, 368–378. <https://doi.org/10.1016/j.freeradbiomed.2017.02.029>
- Calderón, C., Sanwald, C., Schlotterbeck, J., Drotleff, B., & Lämmerhofer, M. (2019). Comparison of simple monophasic versus classical biphasic extraction protocols for comprehensive UHPLC-MS/MS lipidomic analysis of HeLa cells. *Analytica Chimica Acta*, 1048, 66–74. <https://doi.org/10.1016/j.aca.2018.10.035>
- Carrasco, S., & Mérida, I. (2007). Diacylglycerol, when simplicity becomes complex. *Trends in Biochemical Sciences*, 32(1), 27–36. <https://doi.org/10.1016/j.tibs.2006.11.004>
- Cheng, C. H., Guo, Z. X., Luo, S. W., & Wang, A. L. (2018). Effects of high temperature on biochemical parameters, oxidative stress, DNA damage and apoptosis of pufferfish (*Takifugu obscurus*). *Ecotoxicology and Environmental Safety*, 150, 190–198. <https://doi.org/10.1016/j.ecoenv.2017.12.045>
- Chong, J., Soufan, O., Li, C., Caraus, I., Li, S., Bourque, G., Wishart, D. S., & Xia, J. (2018). MetaboAnalyst 4.0: Towards more transparent and integrative metabolomics analysis. *Nucleic Acids Research*, 46(W1), W486–W494. <https://doi.org/10.1093/nar/gky310>
- Chwastek, G., Surma, M. A., Rizk, S., Grosser, D., Lavrynenko, O., Rucińska, M., Jambor, H., & Sáenz, J. (2020). Principles of membrane adaptation revealed through environmentally induced bacterial lipidome remodeling. *Cell Reports*, 32(12), 108165. <https://doi.org/10.1016/j.celrep.2020.108165>
- Contrepois, K., Wu, S. I., Moneghetti, K. J., Hornburg, D., Ahadi, S., Tsai, M.-S., Metwally, A. A., Wei, E., Lee-McMullen, B., Quijada, J. V., Chen, S., Christle, J. W., Ellenberger, M., Balliu, B., Taylor, S., Durrant, M. G., Knowles, D. A., Choudhry, H., Ashland, M., ... Snyder, M. P. (2020). Molecular choreography of acute exercise. *Cell*, 181(5), 1112–1130.e16. <https://doi.org/10.1016/j.cell.2020.04.043>
- Conway, J. R., Lex, A., & Gehlenborg, N. (2017). UpSetR: An R package for the visualization of intersecting sets and their properties. *Bioinformatics*, 33(18), 2938–2940. <https://doi.org/10.1093/bioinformatics/btx364>
- Cullis, P. R., & De Kruijff, B. (1979). Lipid polymorphism and the functional roles of lipids in biological membranes. *Biochimica et Biophysica Acta (BBA) - Reviews on Biomembranes*, 559(4), 399–420. [https://doi.org/10.1016/0304-4157\(79\)90012-1](https://doi.org/10.1016/0304-4157(79)90012-1)
- Dadras, H., Dzyuba, B., Cosson, J., Golpour, A., Siddique, M. A. M., & Linhart, O. (2017). Effect of water temperature on the physiology of fish spermatozoon function: A brief review. *Aquaculture Research*, 48(3), 729–740. <https://doi.org/10.1111/are.13049>
- de Kroon, A. I. P. M., Rijken, P. J., & De Smet, C. H. (2013). Checks and balances in membrane phospholipid class and acyl chain homeostasis, the yeast perspective. *Progress in Lipid Research*, 52(4), 374–394. <https://doi.org/10.1016/j.plipres.2013.04.006>

- Dean, J. M., & Lodhi, I. J. (2018). Structural and functional roles of ether lipids. *Protein & Cell*, 9(2), 196–206. <https://doi.org/10.1007/s13238-017-0423-5>
- DiLeo, M. V., Strahan, G. D., den Bakker, M., & Hoekenga, O. A. (2011). Weighted correlation network analysis (WGCNA) applied to the tomato fruit metabolome. *PLoS One*, 6(10), e26683. <https://doi.org/10.1371/journal.pone.0026683>
- Ding, Q., Schweiger, A., L'Heureux, M., Steig, E. J., Battisti, D. S., Johnson, N. C., Blanchard-Wrigglesworth, E., Po-Chedley, S., Zhang, Q., Harnos, K., Bushuk, M., Markle, B., & Baxter, I. (2019). Fingerprints of internal drivers of Arctic sea ice loss in observations and model simulations. *Nature Geoscience*, 12, 28–33. <https://doi.org/10.1038/s41561-018-0256-8>
- Dorninger, F., Forss-Petter, S., & Berger, J. (2017). From peroxisomal disorders to common neurodegenerative diseases – The role of ether phospholipids in the nervous system. *FEBS Letters*, 591(18), 2761–2788. <https://doi.org/10.1002/1873-3468.12788>
- Dringen, R., Gutterer, J. M., & Hirrlinger, J. (2000). Glutathione metabolism in brain. *European Journal of Biochemistry*, 267(16), 4912–4916. <https://doi.org/10.1046/j.1432-1327.2000.01597.x>
- Elliott, J. M. (1982). The effects of temperature and ration size on the growth and energetics of salmonids in captivity. *Comparative Biochemistry and Physiology Part B: Comparative Biochemistry*, 73, 81–91. [https://doi.org/10.1016/0305-0491\(82\)90202-4](https://doi.org/10.1016/0305-0491(82)90202-4)
- Elliott, J. M., & Elliott, J. A. (2010). Temperature requirements of Atlantic salmon *Salmo salar*, brown trout *Salmo trutta* and Arctic charr *Salvelinus alpinus*: Predicting the effects of climate change. *Journal of Fish Biology*, 77(8), 1793–1817. <https://doi.org/10.1111/j.1095-8649.2010.02762.x>
- Ernst, R., Ejsing, C. S., & Antonny, B. (2016). Homeoviscous adaptation and the regulation of membrane lipids. *Journal of Molecular Biology*, 428, 4776–4791. <https://doi.org/10.1016/j.jmb.2016.08.013>
- Fadhlaoui, M., & Couture, P. (2016). Combined effects of temperature and metal exposure on the fatty acid composition of cell membranes, antioxidant enzyme activities and lipid peroxidation in yellow perch (*Perca flavescens*). *Aquatic Toxicology*, 180, 45–55. <https://doi.org/10.1016/j.aquatox.2016.09.005>
- Forest, A., Ruiz, M., Bouchard, B., Boucher, G., Gingras, O., Daneault, C., Robillard Frayne, I., Rhinds, D., iGenoMed Consortium, NIDDK IBD Genetics Consortium, Tardif, J.-C., Rioux, J. D., & Des Rosiers, C. (2018). Comprehensive and reproducible untargeted lipidomic workflow using LC-QTOF validated for human plasma analysis. *Journal of Proteome Research*, 17(11), 3657–3670. <https://doi.org/10.1021/acs.jproteome.8b00270>
- Furt, F., & Moreau, P. (2009). Importance of lipid metabolism for intracellular and mitochondrial membrane fusion/fission processes. *The International Journal of Biochemistry & Cell Biology*, 41(10), 1828–1836. <https://doi.org/10.1016/j.biocel.2009.02.005>
- Gao, X., Liu, W., Mei, J., & Xie, J. (2019). Quantitative analysis of cold stress inducing lipidomic changes in *Shewanella putrefaciens* using UHPLC-ESI-MS/MS. *Molecules*, 24(24), 4609. <https://doi.org/10.3390/molecules24244609>
- Gathungu, R. M., Larrea, P., Sniatynski, M. J., Marur, V. R., Bowden, J. A., Koelmel, J. P., Starke-Reed, P., Hubbard, V. S., & Kristal, B. S. (2018). Optimization of electrospray ionization source parameters for lipidomics to reduce misannotation of in-source fragments as precursor ions. *Analytical Chemistry*, 90(22), 13523–13532. <https://doi.org/10.1021/acs.analchem.8b03436>
- Gómez-Fernández, J. C., & Corbalán-García, S. (2007). Diacylglycerols, multivalent membrane modulators. *Chemistry and Physics of Lipids*, 148(1), 1–25. <https://doi.org/10.1016/j.chemphyslip.2007.04.003>
- Han, X. (2016). Lipidomics for studying metabolism. *Nature Reviews Endocrinology*, 12(11), 668–679. <https://doi.org/10.1038/nrendo.2016.98>
- Hanzal-Bayer, M. F., & Hancock, J. F. (2007). Lipid rafts and membrane traffic. *FEBS Letters*, 581(11), 2098–2104. <https://doi.org/10.1016/j.febslet.2007.03.019>
- Harayama, T., & Riezman, H. (2018). Understanding the diversity of membrane lipid composition. *Nature Reviews Molecular Cell Biology*, 19(5), 281–296. <https://doi.org/10.1038/nrm.2017.138>
- Harwood, L. A., Sandstrom, S. J., Papst, M. H., & Melling, H. (2013). Kuujua River Arctic Char: monitoring stock trends using catches from an under-ice subsistence fishery, Victoria Island, Northwest Territories, Canada, 1991–2009. *Arctic*, 66(3). <https://doi.org/10.14430/arctic4308>
- Hazel, J. R. (1995). Thermal adaptation in biological membranes: Is homeoviscous adaptation the explanation? *Annual Review of Physiology*, 57, 19–42. <https://doi.org/10.1146/annurev.ph.57.030195.000315>
- Hazel, J. R., & Williams, E. E. (1990). The role of alterations in membrane lipid composition in enabling physiological adaptation of organisms to their physical environment. *Progress in Lipid Research*, 29(3), 167–227. [https://doi.org/10.1016/0163-7827\(90\)90002-3](https://doi.org/10.1016/0163-7827(90)90002-3)
- Hoegh-Guldberg, O., & Bruno, J. F. (2010). The impact of climate change on the world's marine ecosystems. *Science*, 328(5985), 1523–1528. <https://doi.org/10.1126/science.1189930>
- Holthuis, J. C., & Menon, A. K. (2014). Lipid landscapes and pipelines in membrane homeostasis. *Nature*, 510(7503), 48–57. <https://doi.org/10.1038/nature13474>
- Hsieh, S. L., & Kuo, C. M. (2005). Stearoyl-CoA desaturase expression and fatty acid composition in milkfish (*Chanos chanos*) and grass carp (*Ctenopharyngodon idella*) during cold acclimation. *Comparative Biochemistry and Physiology Part B: Biochemistry and Molecular Biology*, 141(1), 95–101. <https://doi.org/10.1016/j.cbpc.2005.02.001>
- Hu, T., & Zhang, J. L. (2018). Mass-spectrometry-based lipidomics. *Journal of Separation Science*, 41(1), 351–372. <https://doi.org/10.1002/jssc.201700709>
- Inoue, K., & Kitagawa, T. (1974). Effect of exogenous lysolecithin on liposomal membranes its relation to membrane fluidity. *Biochimica et Biophysica Acta (BBA) - Biomembranes*, 363(3), 361–372. [https://doi.org/10.1016/0005-2736\(74\)90075-3](https://doi.org/10.1016/0005-2736(74)90075-3)
- Jonsson, B., & Jonsson, N. (2009). A review of the likely effects of climate change on anadromous Atlantic salmon *Salmo salar* and brown trout *Salmo trutta*, with particular reference to water temperature and flow. *Journal of Fish Biology*, 75(10), 2381–2447. <https://doi.org/10.1111/j.1095-8649.2009.02380.x>
- Käkelä, R., Mattila, M., Hermansson, M., Haimi, P., Uphoff, A., Paajanen, V., Somerharju, P., & Vornanen, M. (2008). Seasonal acclimatization of brain lipidome in a eurythermal fish (*Carassius carassius*) is mainly determined by temperature. *American Journal of Physiology-Regulatory, Integrative and Comparative Physiology*, 294(5), R1716–R1728. <https://doi.org/10.1152/ajpregu.00883.2007>
- Kennedy, E. P., & Weiss, S. B. (1956). The function of cytidine coenzymes in the biosynthesis of phospholipides. *The Journal of Biological Chemistry*, 222(1), 193–214.
- Kind, T., Liu, K. H., Lee, D. Y., DeFelice, B., Meissen, J. K., & Fiehn, O. (2013). LipidBlast *in silico* tandem mass spectrometry database for lipid identification. *Nature Methods*, 10(8), 755–758. <https://doi.org/10.1038/nmeth.2551>
- Klose, C., Surma, M. A., & Simons, K. (2013). Organellar lipidomics—background and perspectives. *Current Opinion in Cell Biology*, 25(4), 406–413. <https://doi.org/10.1016/j.ceb.2013.03.005>
- Koelmel, J. P., Kroeger, N. M., Gill, E. L., Ulmer, C. Z., Bowden, J. A., Patterson, R. E., Yost, R. A., & Garrett, T. J. (2017). Expanding lipidome coverage using LC-MS/MS data-dependent acquisition with automated exclusion list generation. *Journal of the American Society for Mass Spectrometry*, 28(5), 908–917. <https://doi.org/10.1007/s13361-017-1608-0>
- Koelmel, J. P., Napolitano, M. P., Ulmer, C. Z., Vasiliou, V., Garrett, T. J., Yost, R. A., Prasad, M., Godri Pollitt, K. J., & Bowden, J. A. (2020).

- Environmental lipidomics: Understanding the response of organisms and ecosystems to a changing world. *Metabolomics*, 16(5). <https://doi.org/10.1007/s11306-020-01665-3>
- Koval, M., & Pagano, R. E. (1991). Intracellular transport and metabolism of sphingomyelin. *Biochimica et Biophysica Acta (BBA) – Lipids and Lipid Metabolism*, 1082(2), 113–125. [https://doi.org/10.1016/0005-2760\(91\)90184-j](https://doi.org/10.1016/0005-2760(91)90184-j)
- Lands, W. E. (1960). Metabolism of glycerolipids: II. The enzymatic acylation of lysolecithin. *The Journal of Biological Chemistry*, 235, 2233–2237.
- Langfelder, P., & Horvath, S. (2008). WGCNA: An R package for weighted correlation network analysis. *BMC Bioinformatics*, 9(1). <https://doi.org/10.1186/1471-2105-9-559>
- Larsson, S. (2005). Thermal preference of Arctic charr, *Salvelinus alpinus*, and brown trout, *Salmo trutta* – Implications for their niche segregation. *Environmental Biology of Fishes*, 73(1), 89–96. <https://doi.org/10.1007/s10641-004-5353-4>
- Lingwood, D., & Simons, K. (2010). Lipid rafts as a membrane-organizing principle. *Science*, 327(5961), 46–50. <https://doi.org/10.1126/science.1174621>
- Lohner, K. (1996). Is the high propensity of ethanolamine plasmalogens to form non-lamellar lipid structures manifested in the properties of biomembranes? *Chemistry and Physics of Lipids*, 81(2), 167–184. [https://doi.org/10.1016/0009-3084\(96\)02580-7](https://doi.org/10.1016/0009-3084(96)02580-7)
- Lushchak, V. I., & Bagnyukova, T. V. (2006). Temperature increase results in oxidative stress in goldfish tissues. 1. Indices of oxidative stress. *Comparative Biochemistry and Physiology Part C: Toxicology & Pharmacology*, 143(1), 30–35. <https://doi.org/10.1016/j.cbpc.2005.11.017>
- Malekar, V. C., Morton, J. D., Hider, R. N., Cruickshank, R. H., Hodge, S., & Metcalf, V. J. (2018). Effect of elevated temperature on membrane lipid saturation in Antarctic notothenioid fish. *PeerJ*, 6, e4765. <https://doi.org/10.7717/peerj.4765>
- Martin, C. E., Oh, C. S., & Jiang, Y. (2007). Regulation of long chain unsaturated fatty acid synthesis in yeast. *Biochimica et Biophysica Acta (BBA) – Molecular and Cell Biology of Lipids*, 1771(3), 271–285. <https://doi.org/10.1016/j.bbalip.2006.06.010>
- McCall, L. I., Tripathi, A., Vargas, F., Knight, R., Dorrestein, P. C., & Siqueira-Neto, J. L. (2018). Experimental Chagas disease-induced perturbations of the fecal microbiome and metabolome. *PLoS Neglected Tropical Diseases*, 12(3), e0006344. <https://doi.org/10.1371/journal.pntd.0006344>
- Meredith, M. (2019). *IPCC special report on the ocean and cryosphere in a changing climate* (H.-O. Pörtner, D. C. Roberts, V. Masson-Delmotte, P. Zhai, M. Tignor, E. Poloczanska, K. Mintenbeck, M. Nicolai, A. Okem, J. Petzold, B. Rama, N. Weyer, Eds.). Ch. 3. Cambridge University Press.
- Mueller, I. A., Grim, J. M., Beers, J. M., Crockett, E. L., & O'Brien, K. M. (2011). Inter-relationship between mitochondrial function and susceptibility to oxidative stress in red- and white-blooded Antarctic notothenioid fishes. *The Journal of Experimental Biology*, 214(22), 3732–3741. <https://doi.org/10.1242/jeb.062042>
- Muir, A. P., Nunes, F. L. D., Dubois, S. F., & Pernet, F. (2016). Lipid remodeling in the reef-building honeycomb worm, *Sabellaria alveolata*, reflects acclimation and local adaptation to temperature. *Scientific Reports*, 6(1). <https://doi.org/10.1038/srep35669>
- Narváez-Rivas, M., & Zhang, Q. (2016). Comprehensive untargeted lipidomic analysis using core-shell C30 particle column and high field orbitrap mass spectrometer. *Journal of Chromatography A*, 1440, 123–134. <https://doi.org/10.1016/j.chroma.2016.02.054>
- Overland, J., Dunlea, E., Box, J. E., Corell, R., Forsius, M., Kattsov, V., Olsen, M. S., Pawlak, J., Reiersen, L. O., & Wang, M. (2019). The urgency of Arctic change. *Polar Science*, 21, 6–13. <https://doi.org/10.1016/j.polar.2018.11.008>
- Overland, J. E., & Wang, M. (2016). Recent extreme arctic temperatures are due to a split polar vortex. *Journal of Climate*, 29(15), 5609–5616. <https://doi.org/10.1175/JCLI-D-16-0320.1>
- Patton-Vogt, J., & de Kroon, A. I. P. M. (2020). Phospholipid turnover and acyl chain remodeling in the yeast ER. *Biochimica et Biophysica Acta (BBA) – Molecular and Cell Biology of Lipids*, 1865(1), 158462. <https://doi.org/10.1016/j.bbalip.2019.05.006>
- Pearson, R. G., Phillips, S. J., Loranty, M. M., Beck, P. S. A., Damoulas, T., Knight, S. J., & Goetz, S. J. (2013). Shifts in Arctic vegetation and associated feedbacks under climate change. *Nature Climate Change*, 3(7), 673–677. <https://doi.org/10.1038/nclimate1858>
- Pecl, G. T., Araujo, M. B., Bell, J. D., Blanchard, J., Bonebrake, T. C., Chen, I.-C., Clark, T. D., Colwell, R. K., Danielsen, F., Evengård, B., Falconi, L., Ferrier, S., Frusher, S., Garcia, R. A., Griffis, R. B., Hobday, A. J., Janion-Scheepers, C., Jarzyna, M. A., Jennings, S., ... Williams, S. E. (2017). Biodiversity redistribution under climate change: Impacts on ecosystems and human well-being. *Science*, 355(6332), eaai9214. <https://doi.org/10.1126/science.aai9214>
- Pernet, F., Tremblay, R., Comeau, L., & Guderley, H. (2007). Temperature adaptation in two bivalve species from different thermal habitats: Energetics and remodelling of membrane lipids. *Journal of Experimental Biology*, 210(17), 2999–3014. <https://doi.org/10.1242/jeb.006007>
- Řezanka, T., Kolouchová, I., & Sigler, K. (2016). Lipidomic analysis of psychrophilic yeasts cultivated at different temperatures. *Biochimica et Biophysica Acta (BBA) – Molecular and Cell Biology of Lipids*, 1861(11), 1634–1642. <https://doi.org/10.1016/j.bbalip.2016.07.005>
- Rountrey, A. N., Coulson, P. G., Meeuwig, J. J., & Meekan, M. (2014). Water temperature and fish growth: Otoliths predict growth patterns of a marine fish in a changing climate. *Global Change Biology*, 20(8), 2450–2458. <https://doi.org/10.1111/gcb.12617>
- Rustam, Y. H., & Reid, G. E. (2018). Analytical challenges and recent advances in mass spectrometry based lipidomics. *Analytical Chemistry*, 90(1), 374–397. <https://doi.org/10.1021/acs.analchem.7b04836>
- Saita, E., Albanesi, D., & de Mendoza, D. (2016). Sensing membrane thickness: Lessons learned from cold stress. *Biochimica et Biophysica Acta (BBA) – Molecular and Cell Biology of Lipids*, 1861(8), 837–846. <https://doi.org/10.1016/j.bbalip.2016.01.003>
- Sarafian, M. H., Gaudin, M., Lewis, M. R., Martin, F. P., Holmes, E., Nicholson, J. K., & Dumas, M. E. (2014). Objective set of criteria for optimization of sample preparation procedures for ultra-high throughput untargeted blood plasma lipid profiling by ultra performance liquid chromatography–mass spectrometry. *Analytical Chemistry*, 86(12), 5766–5774. <https://doi.org/10.1021/ac500317c>
- Shevchenko, A., & Simons, K. (2010). Lipidomics: Coming to grips with lipid diversity. *Nature Reviews Molecular Cell Biology*, 11(8), 593–598. <https://doi.org/10.1038/nrm2934>
- Sinensky, M. (1974). Homeoviscous adaptation—A homeostatic process that regulates the viscosity of membrane lipids in *Escherichia coli*. *Proceedings of the National Academy of Sciences of the United States of America*, 71(2), 522–525. <https://doi.org/10.1073/pnas.71.2.522>
- Tiku, P. E., Gracey, A. Y., Macartney, A. I., Beynon, R. J., & Cossins, A. R. (1996). Cold-induced expression of delta 9-desaturase in carp by transcriptional and posttranslational mechanisms. *Science*, 271(5250), 815–818. <https://doi.org/10.1126/science.271.5250.815>
- Tsugawa, H., Ikeda, K., Takahashi, M., Satoh, A., Mori, Y., Uchino, H., Okahashi, N., Yamada, Y., Tada, I., Bonini, P., Higashi, Y., Okazaki, Y., Zhou, Z., Zhu, Z. J., Koelmel, J., Cajka, T., Fiehn, O., Saito, K., Arita, M., & Arita, M. (2020). A lipidome atlas in MS-DIAL 4. *Nature Biotechnology*, 38(10), 1159–1163. <https://doi.org/10.1038/s41587-020-0531-2>
- van Meer, G., Voelker, D. R., & Feigenson, G. W. (2008). Membrane lipids: Where they are and how they behave. *Nature Reviews Molecular Cell Biology*, 9(2), 112–124. <https://doi.org/10.1038/nrm2330>

- Wang, G., & Wang, T. (2010). The role of plasmalogen in the oxidative stability of neutral lipids and phospholipids. *Journal of Agricultural and Food Chemistry*, 58(4), 2554–2561. <https://doi.org/10.1021/jf903906e>
- Xu, L., Wang, X., Jiao, Y., & Liu, X. (2018). Assessment of potential false positives via orbitrap-based untargeted lipidomics from rat tissues. *Talanta*, 178, 287–293. <https://doi.org/10.1016/j.talanta.2017.09.046>
- Zhang, B., & Horvath, S. (2005). A general framework for weighted gene co-expression network analysis. *Statistical Applications in Genetics and Molecular Biology*, 4, <https://doi.org/10.2202/1544-6115.1128>

## SUPPORTING INFORMATION

Additional supporting information may be found online in the Supporting Information section.

**How to cite this article:** Wang C, Gong Y, Deng F, et al. Remodeling of Arctic char (*Salvelinus alpinus*) lipidome under a stimulated scenario of Arctic warming. *Glob Change Biol.* 2021;27:3282–3298. <https://doi.org/10.1111/gcb.15638>

1 ***Supporting Information***

2  
3 **Remodeling of Arctic char (*Salvelinus alpinus*) lipidome under a stimulated scenario of**  
4 **Arctic warming**

5  
6 Chao Wang<sup>1,2</sup>, Yufeng Gong<sup>2,\*</sup>, Fuchang Deng<sup>1</sup>, Enmin Ding<sup>1</sup>, Jie Tang<sup>2,3</sup>, Garry Codling<sup>2,4</sup>,  
7 Jonathan K. Challis<sup>2</sup>, Derek Green<sup>2</sup>, Jing Wang<sup>5</sup>, Qiliang Chen<sup>2,6</sup>, Yuwei Xie<sup>2</sup>, Shu Su<sup>2</sup>, Zilin  
8 Yang<sup>2</sup>, Jason Raine<sup>2</sup>, Paul D. Jones<sup>2</sup>, Song Tang<sup>1,7</sup>, John P. Giesy<sup>2,8,9,10</sup>

9  
10 <sup>1</sup>China CDC Key Laboratory of Environment and Population Health, National Institute of  
11 Environmental Health, Chinese Center for Disease Control and Prevention, Beijing, China

12 <sup>2</sup>Toxicology Centre, University of Saskatchewan, Saskatoon, SK, Canada

13 <sup>3</sup>School of Resources and Environment, Anhui Agricultural University, Hefei, Anhui, China

14 <sup>4</sup>Research Centre for Contaminants in the Environment, Pavilion 29 Masaryk University, Brno,  
15 Czech Republic

16 <sup>5</sup>MOE Key Laboratory of Marine Genetics and Breeding, College of Marine Life Sciences,  
17 Ocean University of China, Qingdao, China

18 <sup>6</sup>College of Life Sciences, Chongqing Normal University, Chongqing, China

19 <sup>7</sup>Center for Global Health, School of Public Health, Nanjing Medical University, Nanjing, China

20 <sup>8</sup>Department of Veterinary Biomedical Sciences, University of Saskatchewan, Saskatoon, SK,  
21 Canada

22 <sup>9</sup>Department of Environmental Sciences, Baylor University, Waco, Texas, USA

23 <sup>10</sup>State Key Laboratory of Pollution Control and Resource Reuse, School of the Environment,  
24 Nanjing University, Nanjing, People's Republic of China

25  
26 \*Corresponding author

27 Toxicology Centre, University of Saskatchewan, Saskatoon, SK, Canada

28 *Email:* [yufeng.gong@usask.ca](mailto:yufeng.gong@usask.ca) (Yufeng Gong)

29  
30 ***Numbers of pages: 36    Numbers of figures: 26    Numbers of tables: 1***



## Contents

32	
33	
34	<b>Materials and Methods</b>
35	1. Lipid standards
36	2. Lipid extraction method
37	3. Lipidomics method using UHPLC Q-Exactive Orbitrap MS platform
38	4. Validation of the untargeted lipidomics method
39	5. Weighted correlation network analysis (WGCNA)
40	
41	<b>Figures</b>
42	<b>Fig. S1.</b> Experimental design for the collection of samples.
43	<b>Fig. S2.</b> Reproducibility of untargeted lipidomics method for pooled QC in positive and negative
44	modes.
45	<b>Fig. S3.</b> Number of detected lipid species in plasma, brain, liver, and muscle in one-year-old
46	Arctic char.
47	<b>Fig. S4.</b> Composition of significantly altered lipids in different tissue types of one-year-old
48	Arctic char.
49	<b>Fig. S5.</b> Upset plot showing the overlaps of significantly altered lipids in different tissue types of
50	one-year-old Arctic char.
51	<b>Fig. S6.</b> Variability of lipid species in response to warm treatment.
52	<b>Fig. S7.</b> Variability of lipid species in response to cold treatment.
53	<b>Fig. S8.</b> Bubble plots illustrating altered fatty acid composition of PE species in brain, liver, and
54	muscle of one-year-old Arctic char.
55	<b>Fig. S9.</b> Bubble plots illustrating altered fatty acid composition of PC species in brain, liver, and
56	muscle of one-year-old Arctic char.
57	<b>Fig. S10.</b> Heatmap plots showing altered abundances of lysoglycerophospholipid (lysoGP) lipids
58	in one-year-old Arctic char by temperature shifts.
59	<b>Fig. S11.</b> Heatmap plots showing significantly altered abundances of ether-linked lipids in one-
60	year-old Arctic char by temperature shifts.
61	<b>Fig. S12.</b> Changes in acyl chain profile of ceramide (Cer), hexosylceramide (HexCer), and
62	sulfatide (SHexCer) molecules in one-year-old Arctic char by temperature shifts.

63 **Fig. S13.** Heatmap plot showing significantly altered abundances of sphingomyelin (SM) species  
64 in one-year-old Arctic char in response to thermal treatment.

65 **Fig. S14.** Bubble plots illustrating altered fatty acid composition of TG species in plasma after  
66 exposure to cold treatment.

67 **Fig. S15.** Heatmap plot showing significantly altered abundances of diacylglycerol (DG)  
68 molecules in plasma of one-year-old Arctic char in response to temperature shifts.

69 **Fig. S16.** Correlation networks and modules for the Arctic char plasma, brain, liver, and muscle  
70 after exposure to temperature shifts.

71 **Fig. S17.** Pairwise comparisons between modules constructed by WGCNA.

72 **Fig. S18.** Principal component analysis (PCA) of detected lipids in liver of eight-week-old fish  
73 on sampling day 0, 5, 10, and 15.

74 **Fig. S19.** Heatmap plot and hierarchical clustering (Euclidean distance and Ward procedure) of  
75 all identified lipids in liver of eight-week-old Arctic char.

76 **Fig. S20.** Number of significantly altered glycerophospholipid, glycerolipid or sphingolipid  
77 species in liver of eight-week-old Arctic char by temperature shifts.

78 **Fig. S21.** Changes in fatty acid composition of PE and TG species in liver of eight-week-old  
79 Arctic char during the course of stepwise temperature decreases.

80 **Fig. S22.** Changes in fatty acid composition of PE and TG species in liver of eight-week-old  
81 Arctic char during the course of stepwise temperature increases.

82 **Fig. S23.** Changes in fatty acid composition of PC species in liver of eight-week-old Arctic char  
83 during temperature shifts.

84 **Fig. S24.** Confirmation of PE 36:6|PE 16:1\_20:5 by MS2 matching.

85 **Fig. S25.** Confirmation of PE 38:7|PE 16:1\_22:6 by MS2 matching.

86 **Fig. S26.** Confirmation of PE 40:7|PE 18:1\_22:6 by MS2 matching.

87

## 88 **Tables**

89 **Table S1.** Analytical characteristics of the untargeted lipidomics method.

90

## 91 **Materials and Methods**

### 92 **1. Lipid standards**

93 For method validation, eleven deuterated lipid standards were employed. These lipid  
94 standards include phosphatidylcholine [PC (15:0/18:1(d7))], lysophosphatidylcholine [lysoPC  
95 (18:1(d7))], phosphatidylethanolamine [PE (15:0/18:1(d7))], lysophosphatidylethanolamine  
96 [lysoPE (18:1(d7))], phosphatidylglycerol [PG (15:0/18:1(d7))] (Na Salt), triacylglycerol [TG  
97 (15:0/18:1(d7)/15:0)], diacylglycerol [DG (15:0/18:1(d7))], monoacylglycerol [MG (18:1(d7))],  
98 cholesteryl ester [CE (18:1(d7))], sphingomyelin [SM (d18:1/18:1(d9))], and ceramide [Cer  
99 (d18:1(d7)/15:0)]. They were obtained from Avanti Polar Lipids (Alabaster, AL, USA) and have  
100 a purity > 99%.

101 Moreover, individual standards PC (19:0/19:0), lysoPC (19:0), PE (17:0/17:0), Cer  
102 (d18:1/17:0), and TG (15:0/18:1(d7)/15:0) were also obtained from Avanti Polar Lipids. These  
103 standards were spiked to each sample before lipid extraction and used as internal standards.

104 All standards were dissolved in chloroform/methanol solution (2:1, v/v).

105

### 106 **2. Lipid extraction method**

107 Lipid extraction was carried out using an isopropanol (IPA) based protein precipitation  
108 approach (Calderón et al., 2019; Sarafian et al., 2014) with minor modifications. For plasma, 400  
109  $\mu\text{L}$  of cold IPA/ $\text{H}_2\text{O}$  mixture (9:1, v/v) was added to 100  $\mu\text{L}$  of plasma. For tissues, 750  $\mu\text{L}$  of  
110 cold IPA/ $\text{H}_2\text{O}$  mixture (9:1, v/v) was added to 10 mg tissue and then finely homogenized using a  
111 TissueLyzer bead mill (Qiagen, Hilden, German) at 30 Hz for 1 min in a 2.0 mL microcentrifuge  
112 tube (Fisherbrand, Catalog# 02-682-558). Samples were vortex mixed and sonicated for 1 min.  
113 After incubation at room temperature for 10 min, samples were stored at  $-20\text{ }^\circ\text{C}$  overnight.  
114 Samples were next centrifuged for 20 min at 12,000 g and  $4\text{ }^\circ\text{C}$ . Finally, the supernatant was  
115 filtered through a  $0.2\text{ }\mu\text{m}$  Titan3<sup>TM</sup> hydrophobic filter (Thermo Scientific, San Jose, CA, USA)  
116 before LC-MS analysis. Lysophosphatidylcholine [lysoPC (19:0)], phosphatidylcholine [PC  
117 (19:0/19:0)], phosphatidylethanolamine [PE (17:0/17:0)], ceramide [Cer (d18:1/17:0)], and  
118 triacylglycerol [TG (15:0/18:1(d7)/15:0)] were added to each sample before extraction to serve as  
119 internal standards. Quality control (QC) samples were prepared by pooling 10  $\mu\text{L}$  of aliquots  
120 from each sample.

121

### 122 **3. Lipidomics method based on UHPLC Q-Exactive Orbitrap MS platform**

123 A Dionex Ultimate 3000 RS UHPLC system coupled online with a Q-Exactive Orbitrap  
124 mass spectrometer (Thermo Scientific, San Jose, CA, USA) was used for nontargeted lipidomics  
125 analysis. An Accucore™ C30 column (2.6 μm, 2.1 mm × 250 mm, Thermo Scientific, San Jose,  
126 CA, USA) was used for chromatographic separation of lipids. Mobile phase A was  
127 acetonitrile/water (60: 40, v/v) and mobile phase B was isopropanol/acetonitrile (90: 10, v/v),  
128 both containing 0.1% formic acid and 10 mM ammonium formate. The column was maintained  
129 at 40 °C and the flow rate was 0.35 mL/min. The elution gradient was performed as follows: 0–3  
130 min, isocratic flow with 30% B; 3–8 min, 30–43% B; 8–8.1 min, 43–50% B; 8.1–17 min, 50–70%  
131 B; 17.1–24 min, 70–99% B; 24–27 min, maintained with 99% B; 27–27.1 min, 99–30% B; 27.1–  
132 31 min, 30% B for column equilibration.

133 Mass spectrum was acquired in both positive and negative modes. The electrospray  
134 ionization (ESI) source parameters were optimized to reduce any possible in-source fragments  
135 (ISF). The spray voltage was set at 3.2 or 2.8 kV and capillary temperature was maintained at 285  
136 or 320 °C for positive or negative mode respectively. Sheath gas, aux gas, S-lens RF level, and  
137 probe heater were set at 35, 10, 50, and 370 °C for all ionization modes. The Orbitrap mass  
138 analyzer operated at a resolving power of 70,000 in full scan mode (scan range: 150–1200 m/z;  
139 AGC target: 1e<sup>6</sup>) and of 17,500 in the Top10 data-dependent MS<sup>2</sup> mode (HCD fragmentation  
140 with stepped normalized collision energy: 25 and 35 in positive mode, and 20, 30, and 40 in  
141 negative mode; Injection time: 50 ms; Isolation window: 1.2 m/z; AGC target: 1e<sup>5</sup>) with dynamic  
142 exclusion of 8 s. The mass spectrometer was externally calibrated every week using the Pierce™  
143 LTQ Velos ESI Positive/Negative Ion Calibration solutions. Moreover, an iterative exclusion (IE)  
144 strategy, where selected precursors using ddMS<sup>2</sup>-top10 analysis were excluded in sequential  
145 injections, was applied to increase lipidome coverage in the current study. In total of 5 sequential  
146 injections of QC samples were analyzed for each polarity by ddMS<sup>2</sup>-top10 with IE. A 100 ppm  
147 exclusion tolerance was used.

148

### 149 **4. Validation of the untargeted lipidomics method**

150 Validation of the lipidomics method was performed in the presence of fish tissue matrix.  
151 Linearity, recovery, and repeatability were assessed according to (Food and Drug Administration,  
152 2001).

#### 153 4.1 Linearity

154 Linearity was determined by eleven deuterated lipid standards covering the major lipid  
155 subclasses, i.e., PC (15:0/18:1(d7)), lysoPC (18:1(d7)), PE (15:0/18:1(d7)), lysoPE (18:1(d7)),  
156 PG (15:0/18:1(d7)) (Na Salt), TG (15:0/18:1(d7)/15:0), DG (15:0/18:1(d7)), MG (18:1(d7)), CE  
157 (18:1(d7)), SM (d18:1/18:1(d9)), and Cer (d18:1(d7)/15:0). All standards were spiked to fish  
158 tissue samples at 9 different concentrations (Table S1) before lipid extraction. The mean peak  
159 area of duplicate measurements at each concentration level was calculated, and the calibration  
160 curve for each lipid standards was constructed based on the mean peak area vs its corresponding  
161 concentration.

#### 162 4.2 Recovery

163 The recoveries were calculated for each lipid standard as the ratio of the peak area of that  
164 lipid in the sample spiked prior to extraction and that in the sample spiked after sample extraction.

#### 165 4.3 Repeatability

166 Repeatability was evaluated by % RSD of peak area of the detected lipids obtained from  
167 quality control (QC) samples. QC sample was prepared by pooling 10  $\mu$ L of aliquots from each  
168 sample. QC samples were inserted after every 10 samples throughout the analysis sequence.

169

### 170 5. Weighted correlation network analysis (WGCNA)

171 The weighted correlation network analysis (WGCNA) was constructed using the R package  
172 WGCNA (Langfelder et al., 2008). All the annotated lipids of each tissue type were used for  
173 network construction and assigned into modules. The intramodular connectivity ( $K_{within}$ )  
174 represents the hubness of a lipid in one module, i.e., the higher  $K_{within}$  value would indicate the  
175 stronger connection of one lipid to the other lipids in the specified module. To identify the  
176 thermal treatment related modules, over-representation analysis of significantly altered lipids  
177 were performed for each module using a hypergeometric test with  $P$ -values adjusted by the  
178 Benjamini-Hochberg method for multiple-test correction (Langfelder et al., 2008; Benjamini et  
179 al., 1995). Cytoscape was used for visualization of the co-expression networks (Shannon et al.,  
180 2003). Parameters used for network construction are as follows:

181 **Plasma:** with the parameters of softPower = 11, minimum module size = 15, and cutting height =  
182 0.995. All the 625 lipids that were confidently annotated by our lipidomics workflow were used  
183 for network construction and were assigned into 5 modules.

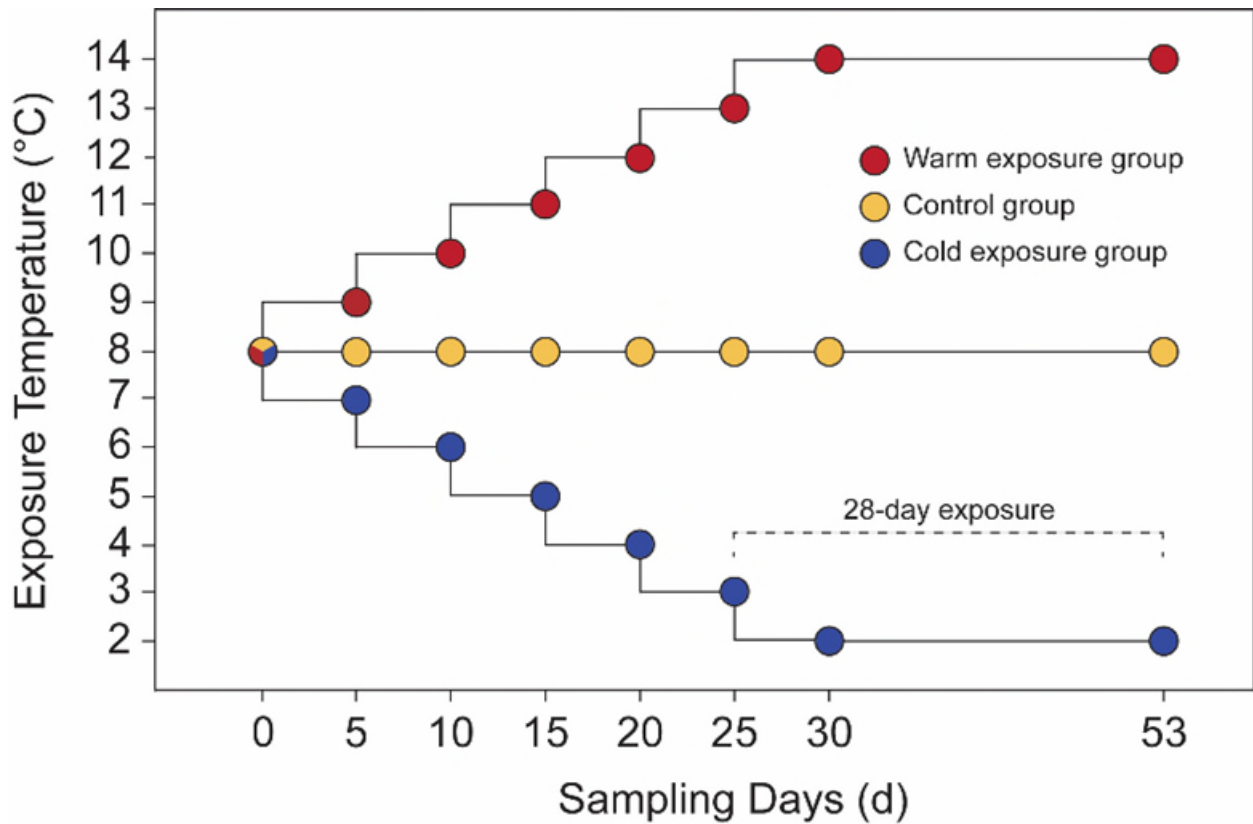


184 **Brain:** with the parameters of softPower = 14, minimum module size = 20 and cutting height =  
185 0.997. All the 565 lipids that were confidently annotated by our lipidomics workflow were used  
186 for network construction and were assigned into 7 modules.

187 **Liver:** with the parameters of softPower = 13, minimum module size = 20 and cutting height =  
188 0.995. All the 455 lipids that were confidently annotated by our lipidomics workflow were used  
189 for network construction and were assigned into 8 modules.

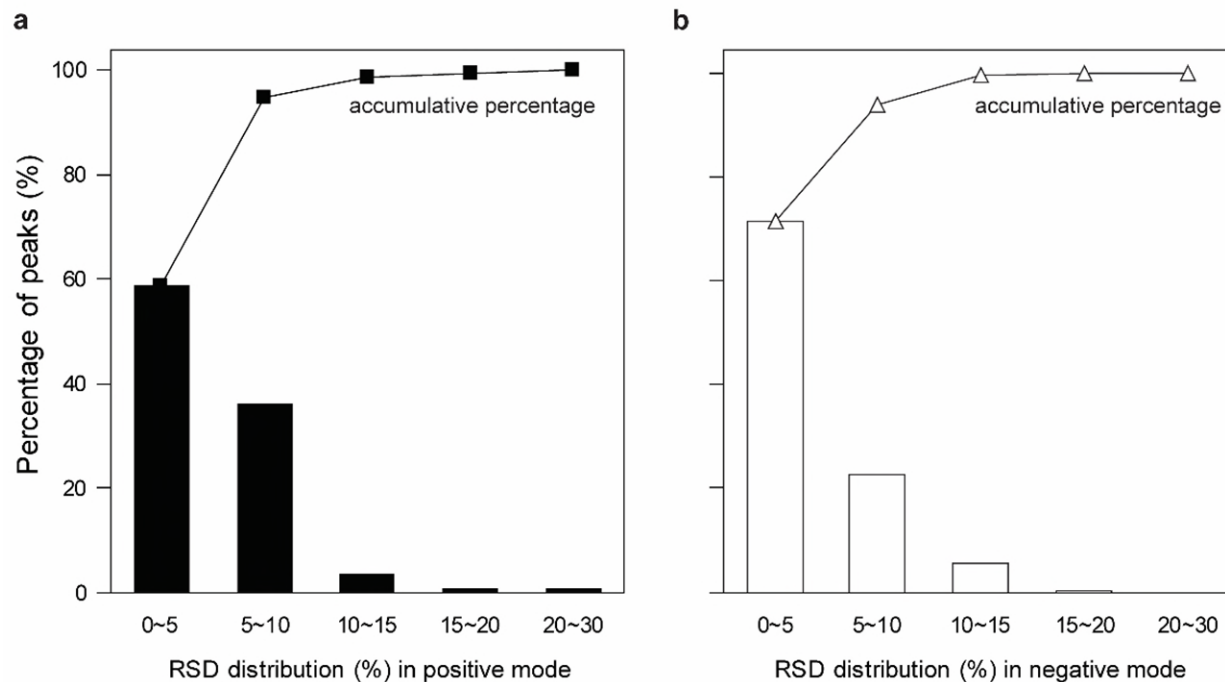
190 **Muscle:** with the parameters of softPower = 11, minimum module size = 20 and cutting height =  
191 0.995. All the 462 lipids that were confidently annotated by our lipidomics workflow were used  
192 for network construction and were assigned into 7 gene modules.

193

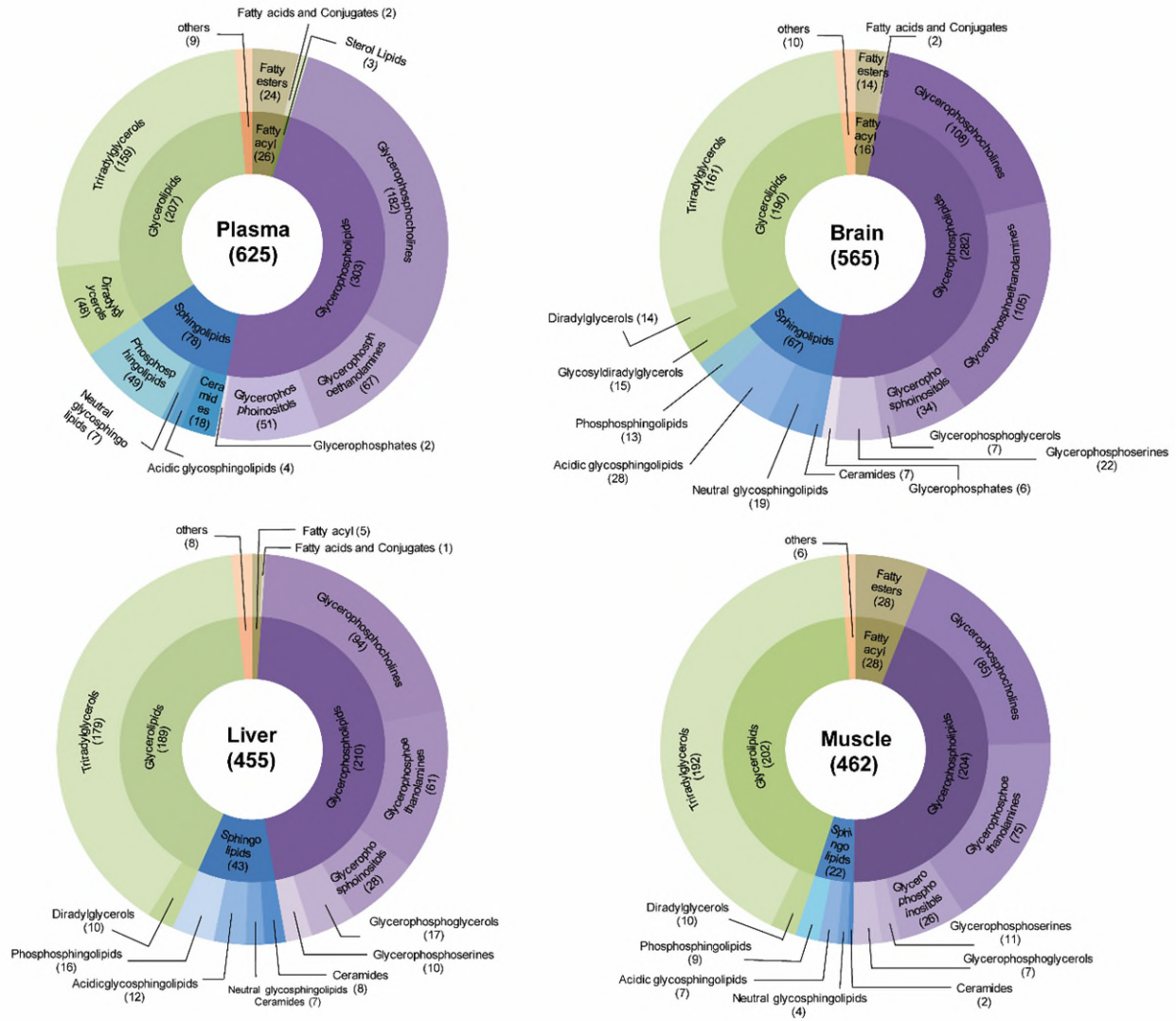


194

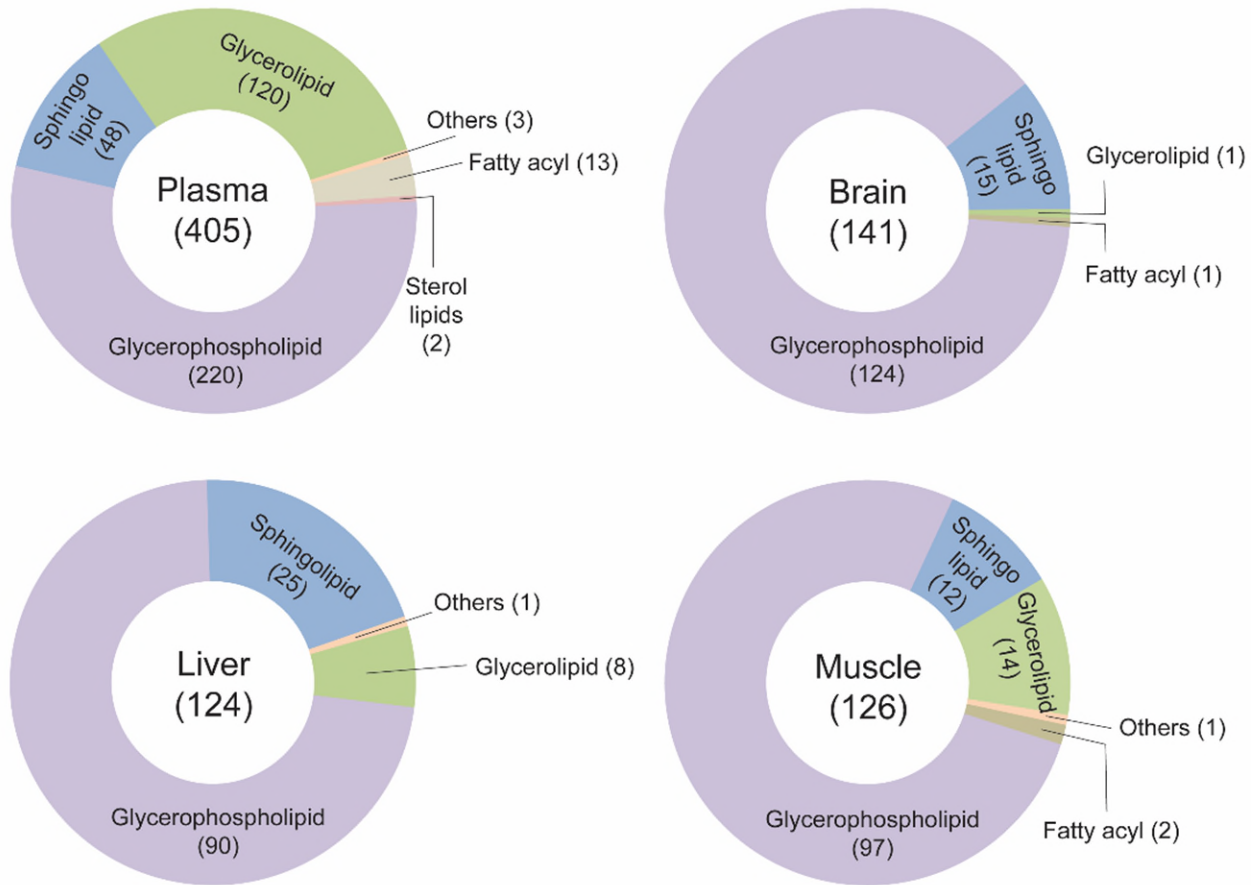
195 **Fig. S1.** Experimental design for the collection of samples. Circles indicate dates of sampling.  
 196 For one-year-old fish, individual body mass and fork length were measured on each sampling day  
 197 (circles), and on day-53 all fish were anesthetized and blood plasma, brain, liver, and muscle  
 198 tissues were taken for lipidomics analysis. For eight-week-old fish, 8 or 10 randomly selected  
 199 fish were anesthetized on each sampling day, and body mass and fork length were measured.  
 200 Meanwhile, liver tissues were collected humanely for lipidomics analysis.  
 201



202  
 203 **Fig. S2.** Reproducibility of untargeted lipidomics method for pooled QC samples in positive (**a**)  
 204 and negative (**b**) modes.  
 205



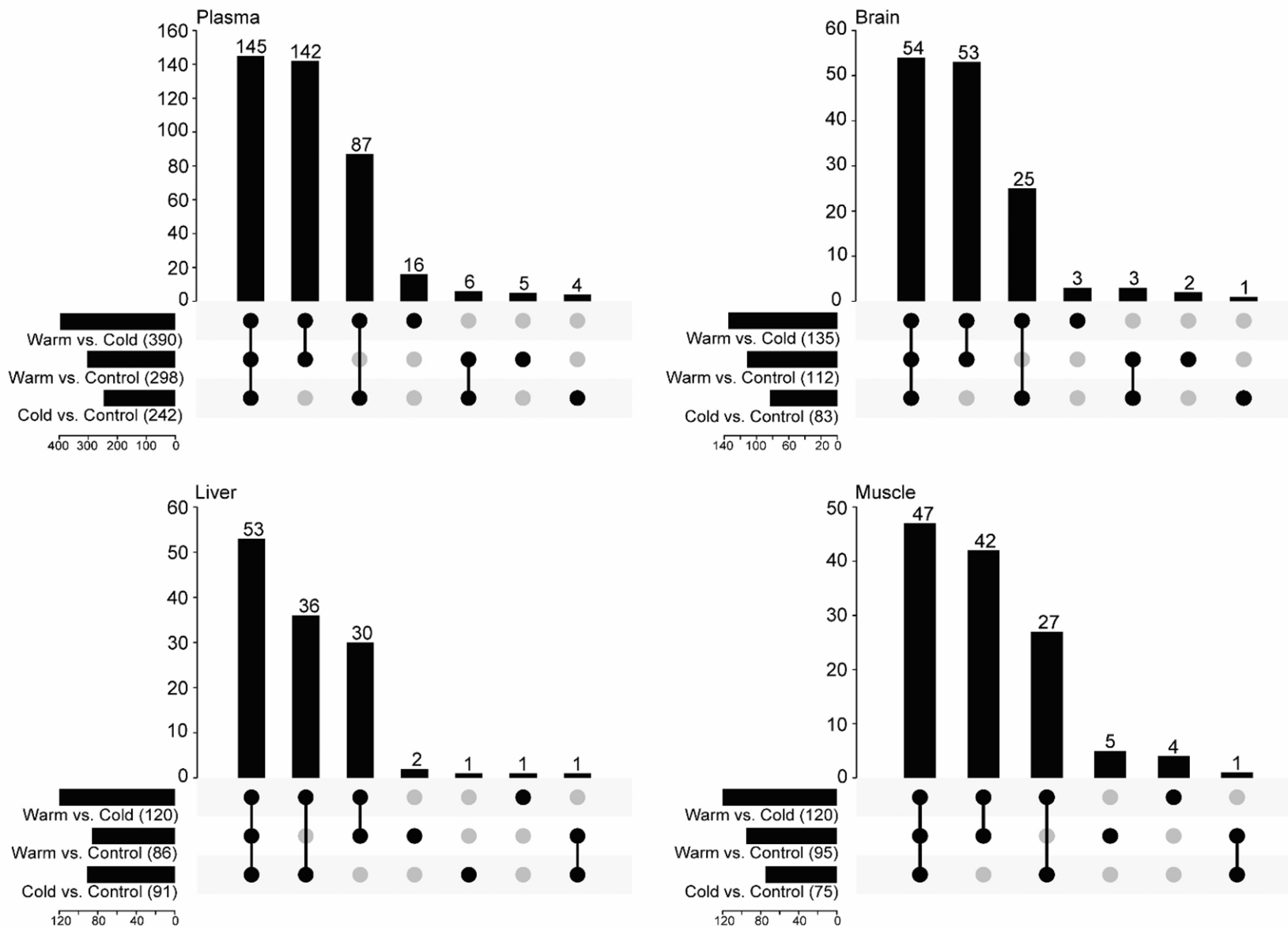
206  
 207 **Fig S3.** Number of detected lipid species in plasma, brain, liver, and muscle in one-year-old  
 208 Arctic char.  
 209



210

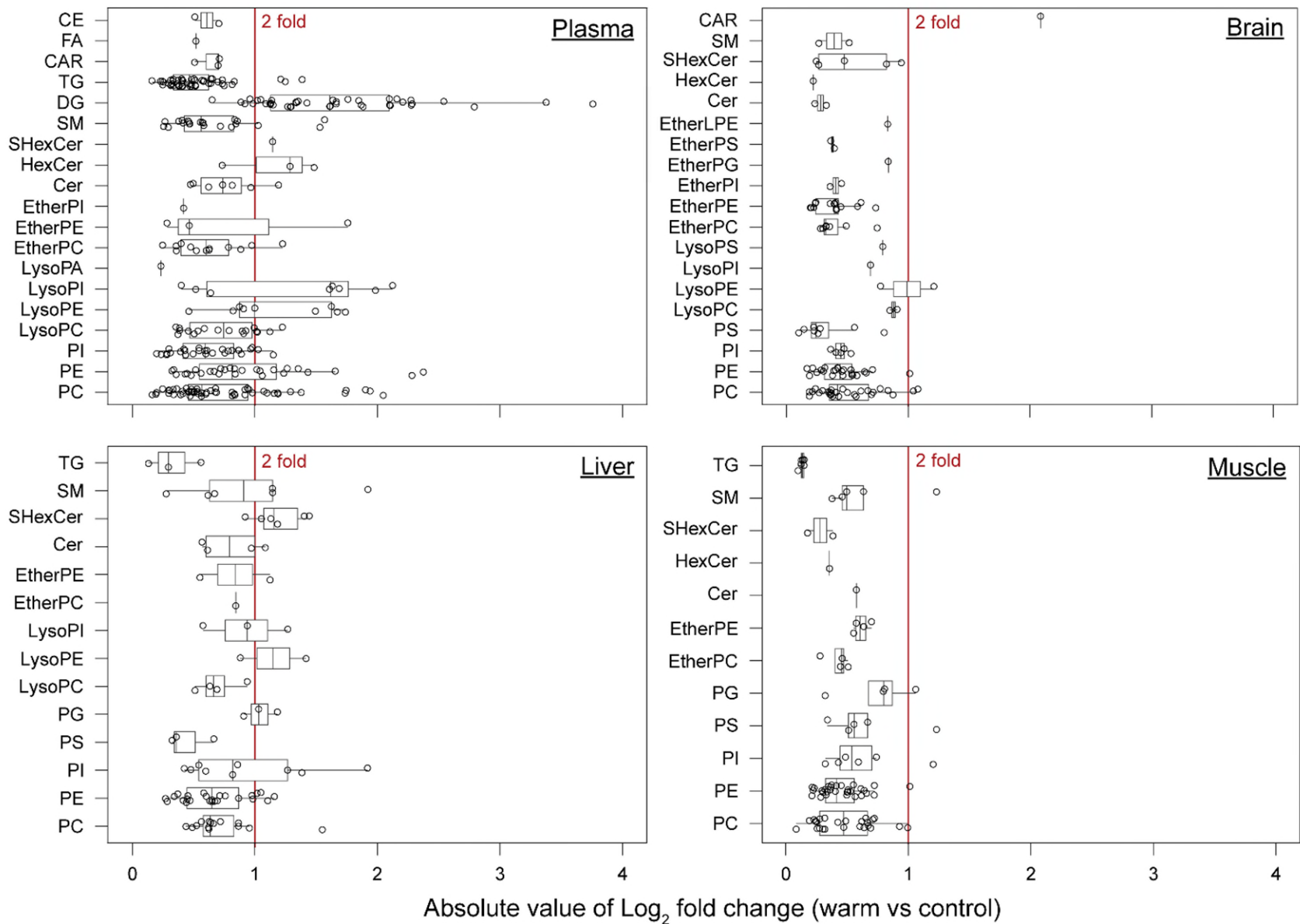
211 **Fig. S4.** Composition of significantly altered lipids in different tissue types of one-year-old  
 212 Arctic char. Benjamini-Hochberg corrected  $P$  value (FDR) < 0.05 by one-way ANOVA were  
 213 adopted as criteria for the determination of significantly altered lipids.  
 214





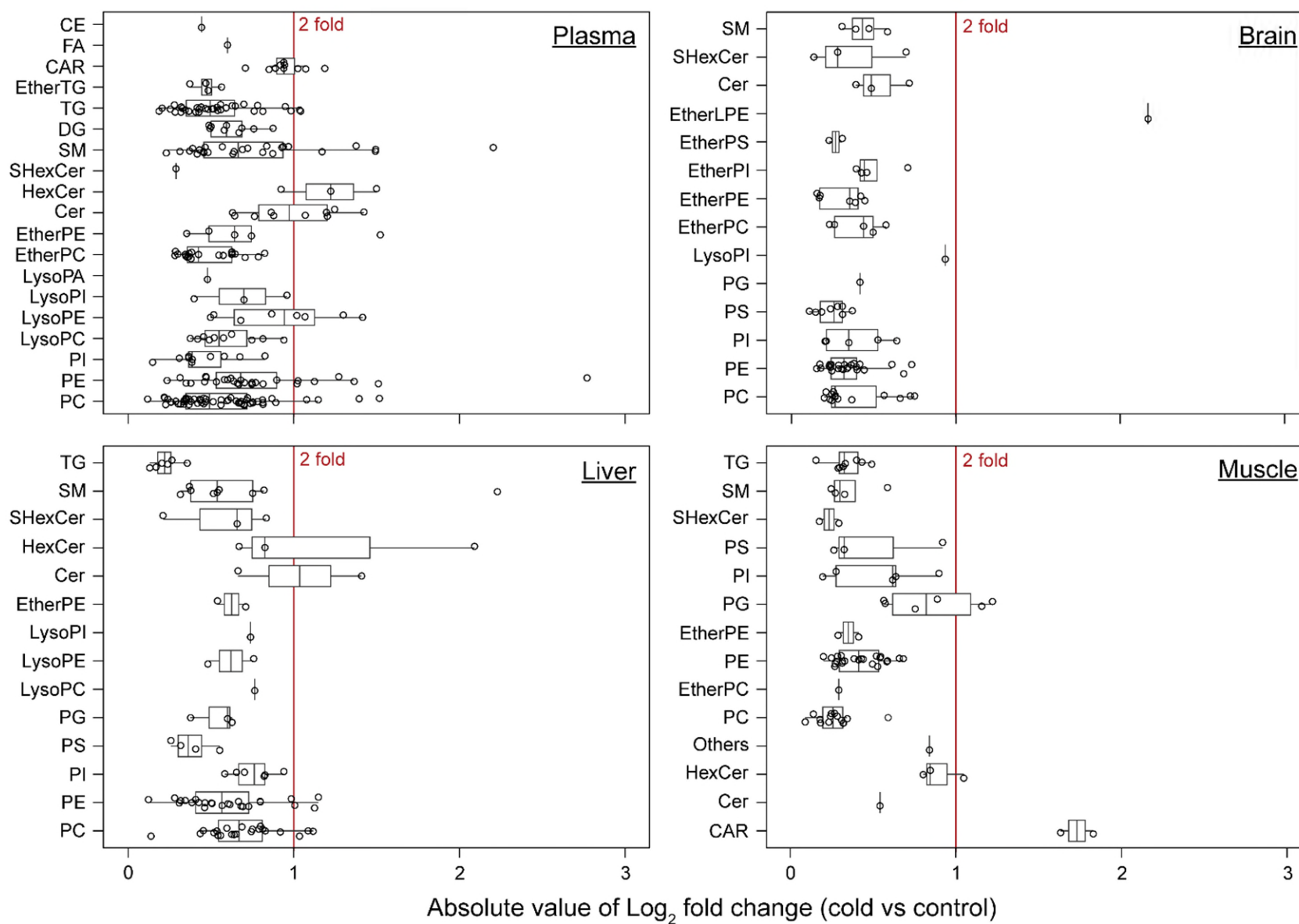
215

216 **Fig. S5.** Upset plot showing the overlaps of significantly altered lipids in different tissue types of one-year-old Arctic char. The plot  
 217 was produced by *UpsetR* package.



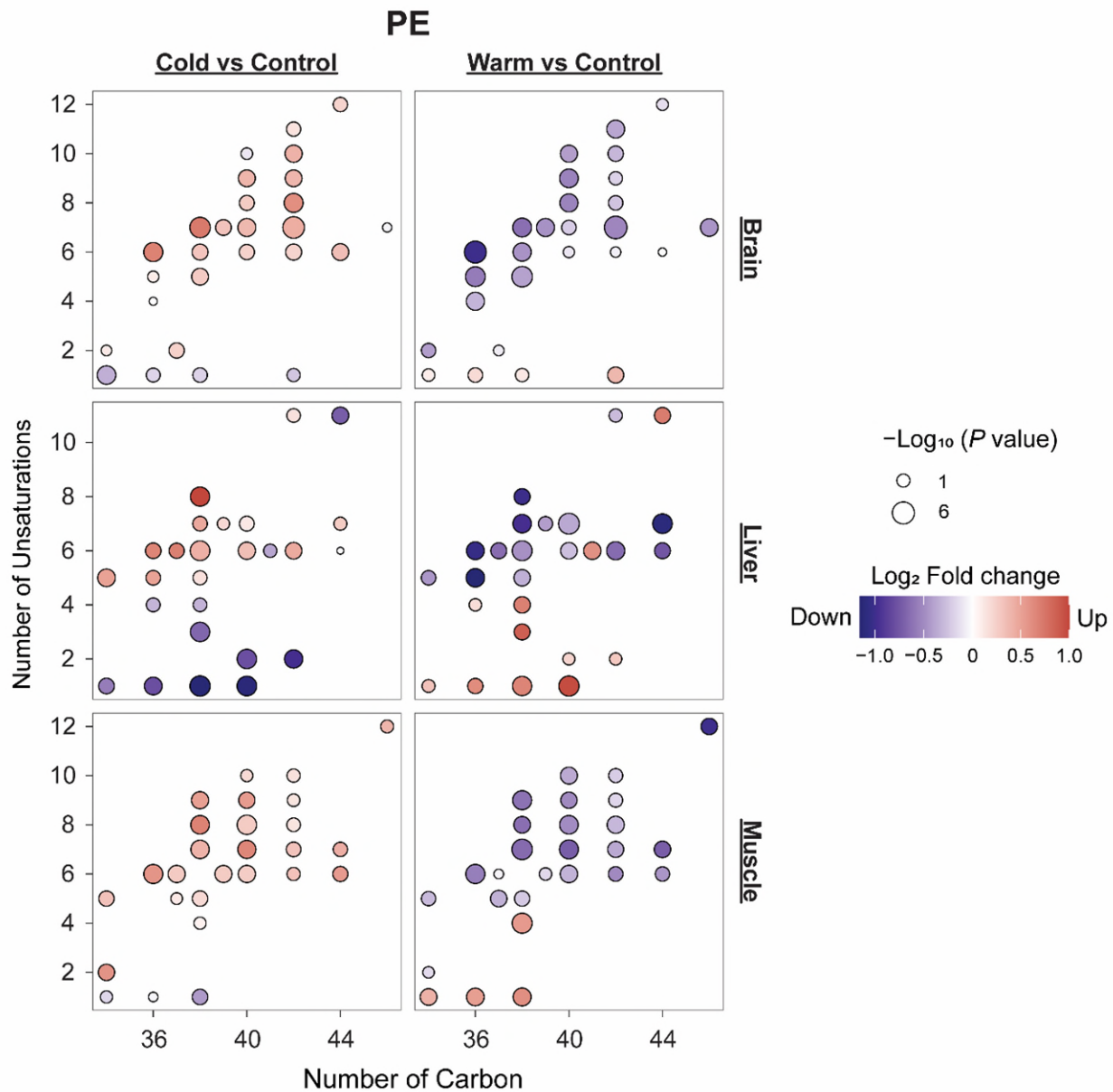
218

219 **Fig. S6.** Variability of lipid species in response to warm treatment. Each data point represents the absolute value of  $\log_2$ (fold change)  
 220 between warm treatment group and control group. Lipids are grouped by class.



221

222 **Fig. S7.** Variability of lipid species in response to cold treatment. Each data point represents the absolute value of  $\log_2$ (fold change)  
 223 between cold treatment group and control group. Lipids are grouped by class.

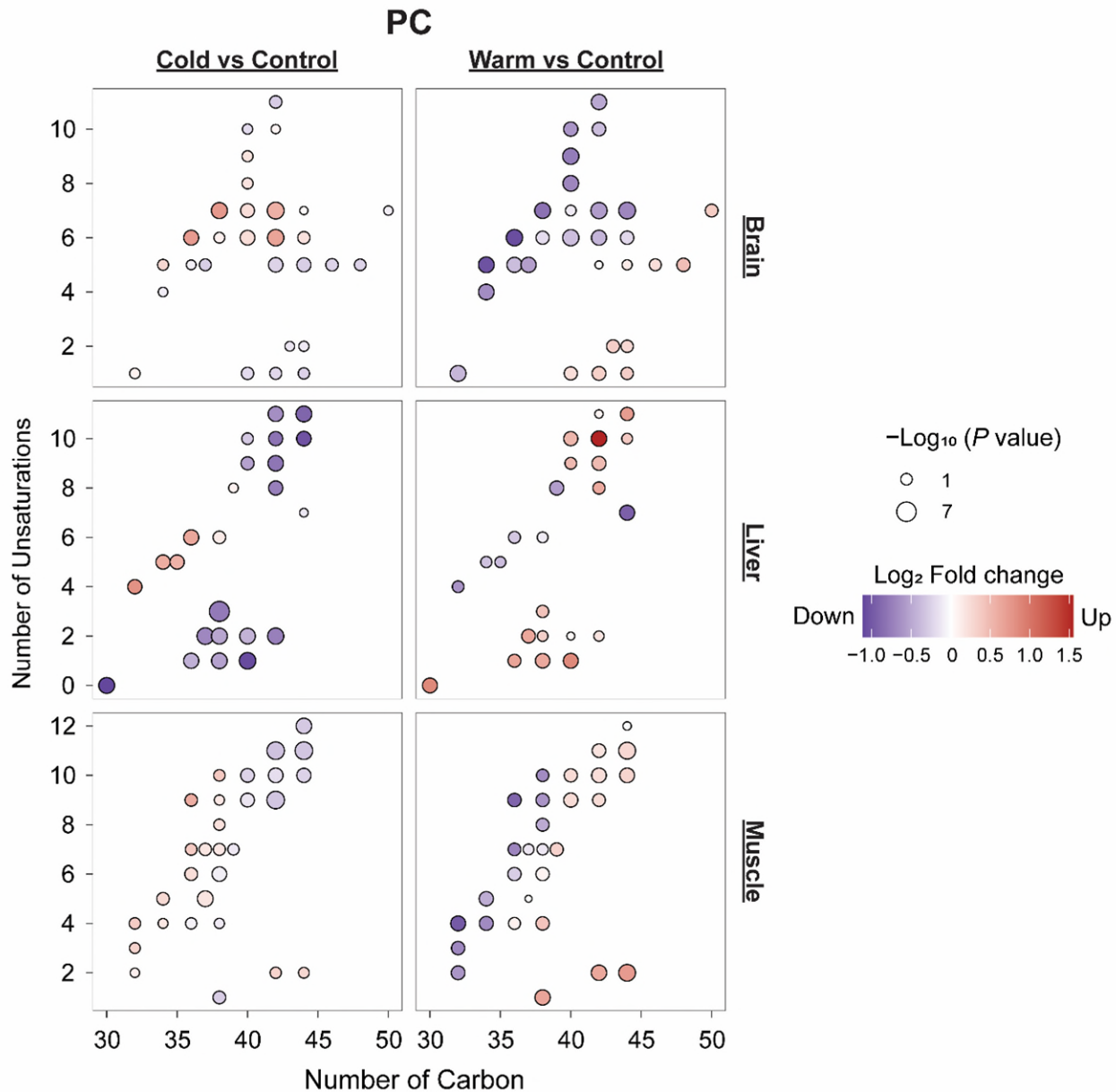


224

225 **Fig. S8.** Bubble plots illustrating altered fatty acid composition of PE species in brain, liver, and

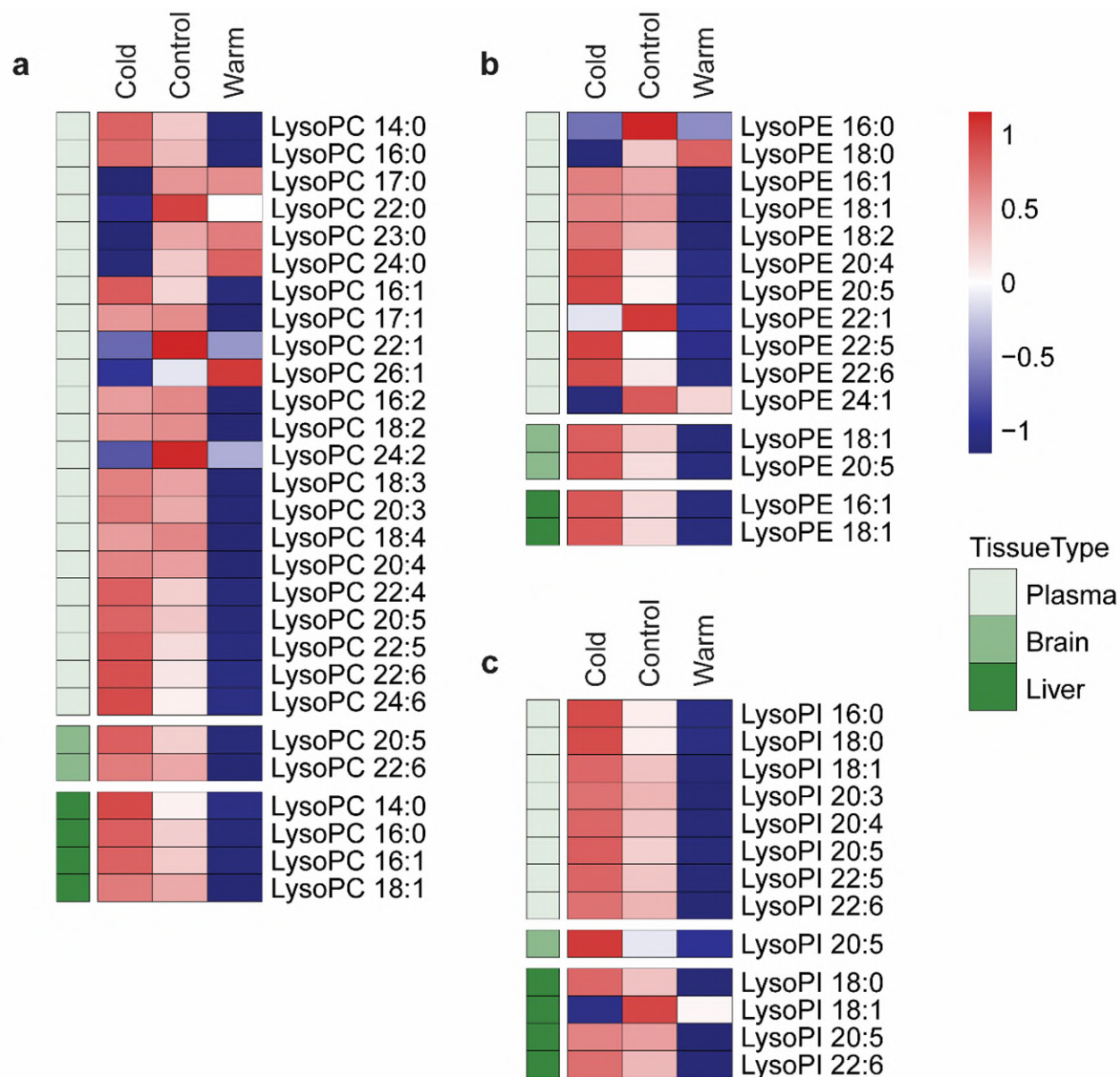
226 muscle of one-year-old Arctic char. Dot color indicates the log<sub>2</sub>(fold change) relative to control.

227 The dot size indicates the significance.



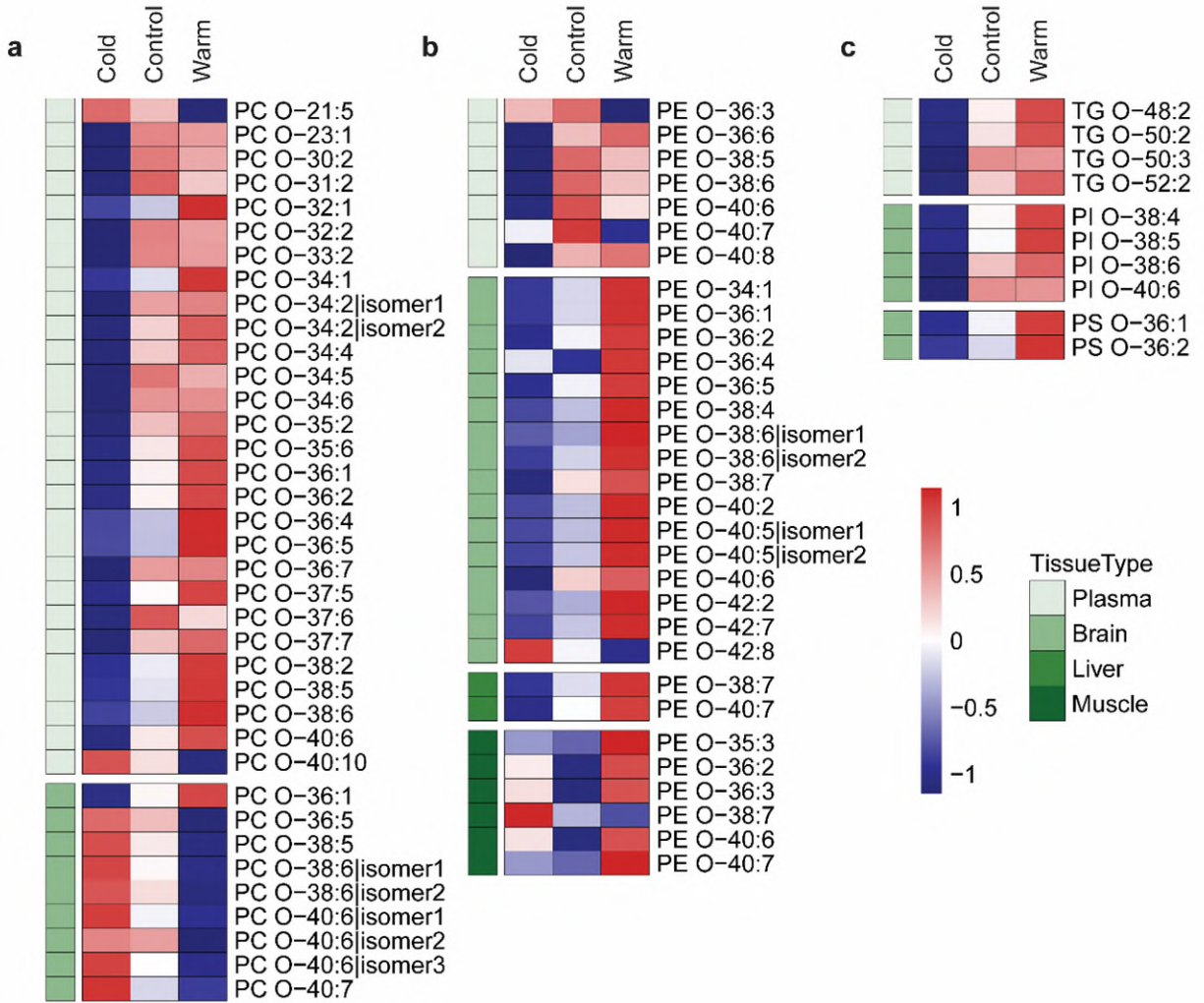
228

229 **Fig. S9.** Bubble plots illustrating altered fatty acid composition of PC species in brain, liver, and  
 230 muscle of one-year-old Arctic char. Dot color indicates the  $\text{log}_2(\text{fold change})$  relative to control.  
 231 The dot size indicates the significance.



232  
 233 **Fig. S10.** Heatmap plots showing altered abundances of lysoglycerophospholipid (lysoGP) lipids  
 234 in one-year-old Arctic char by temperature shifts. The average values of significantly altered  
 235 lipids in each treatment group were presented. Data were log-transformed and Z-score scaled in  
 236 prior to data visualization.  
 237

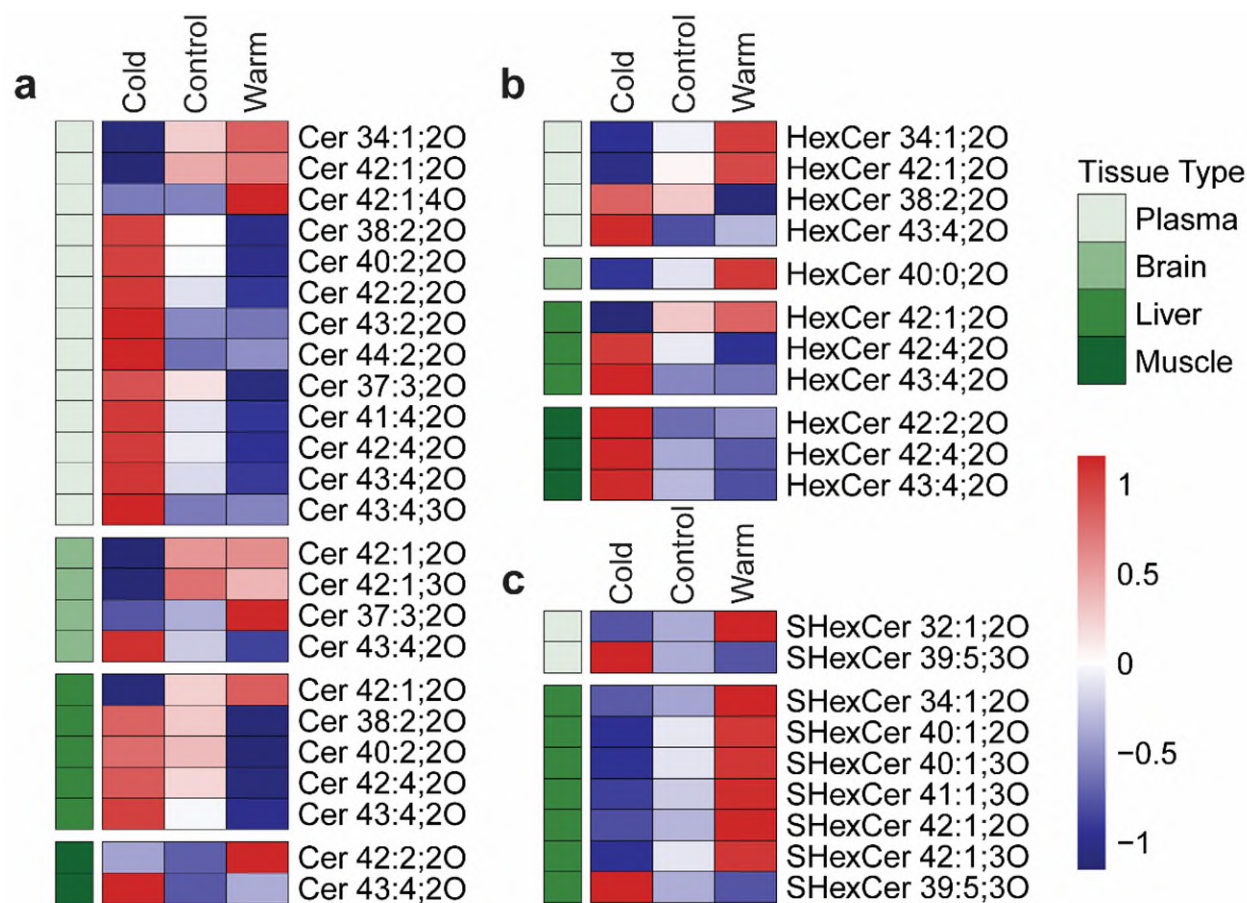




238

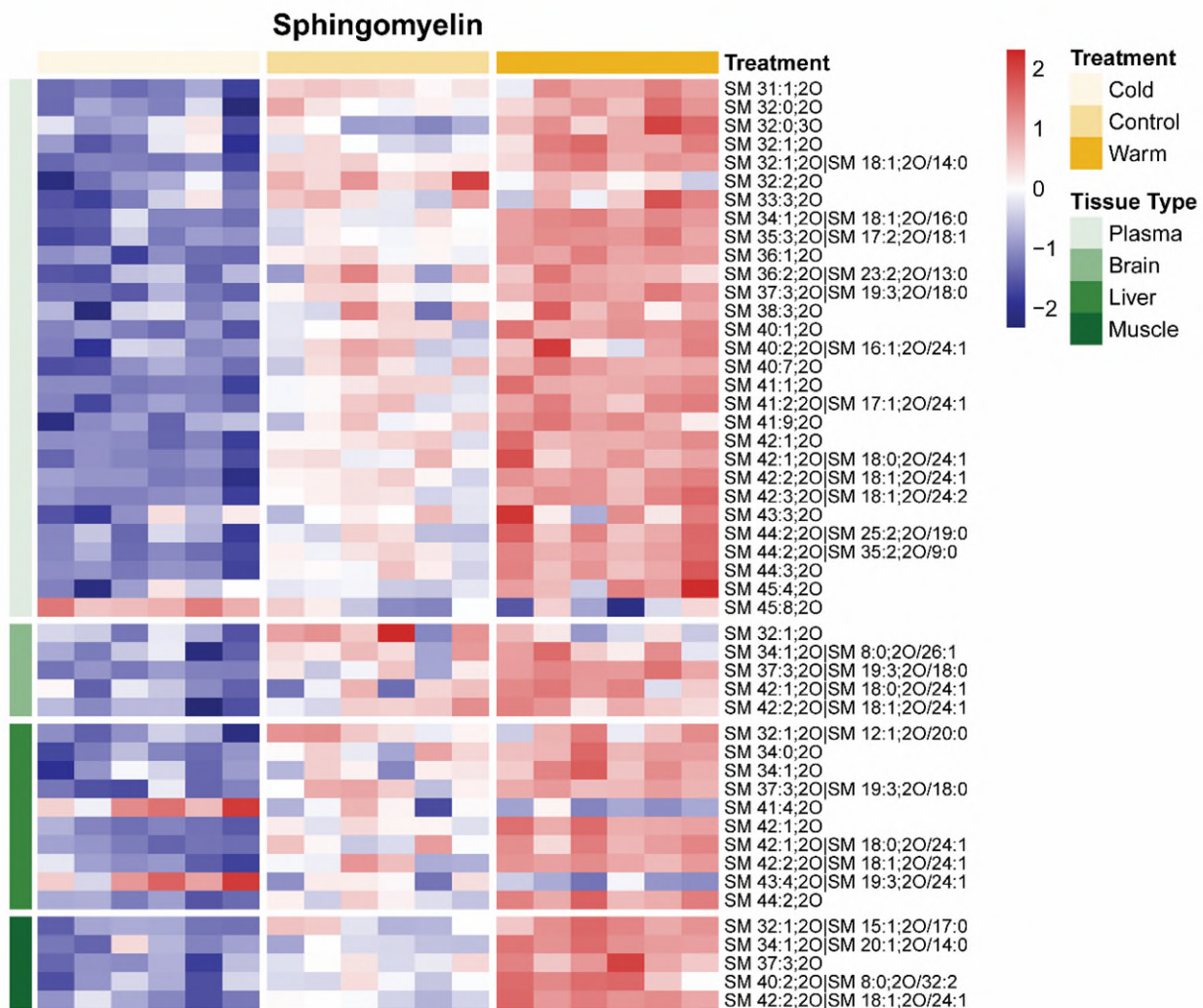
239 **Fig. S11.** Heatmap plots showing significantly altered abundances of ether-linked lipids in one-  
 240 year-old Arctic char by temperature shifts. The average values of significantly altered lipids in  
 241 each treatment group were presented. Data were log-transformed and Z-score scaled in prior to  
 242 data visualization.



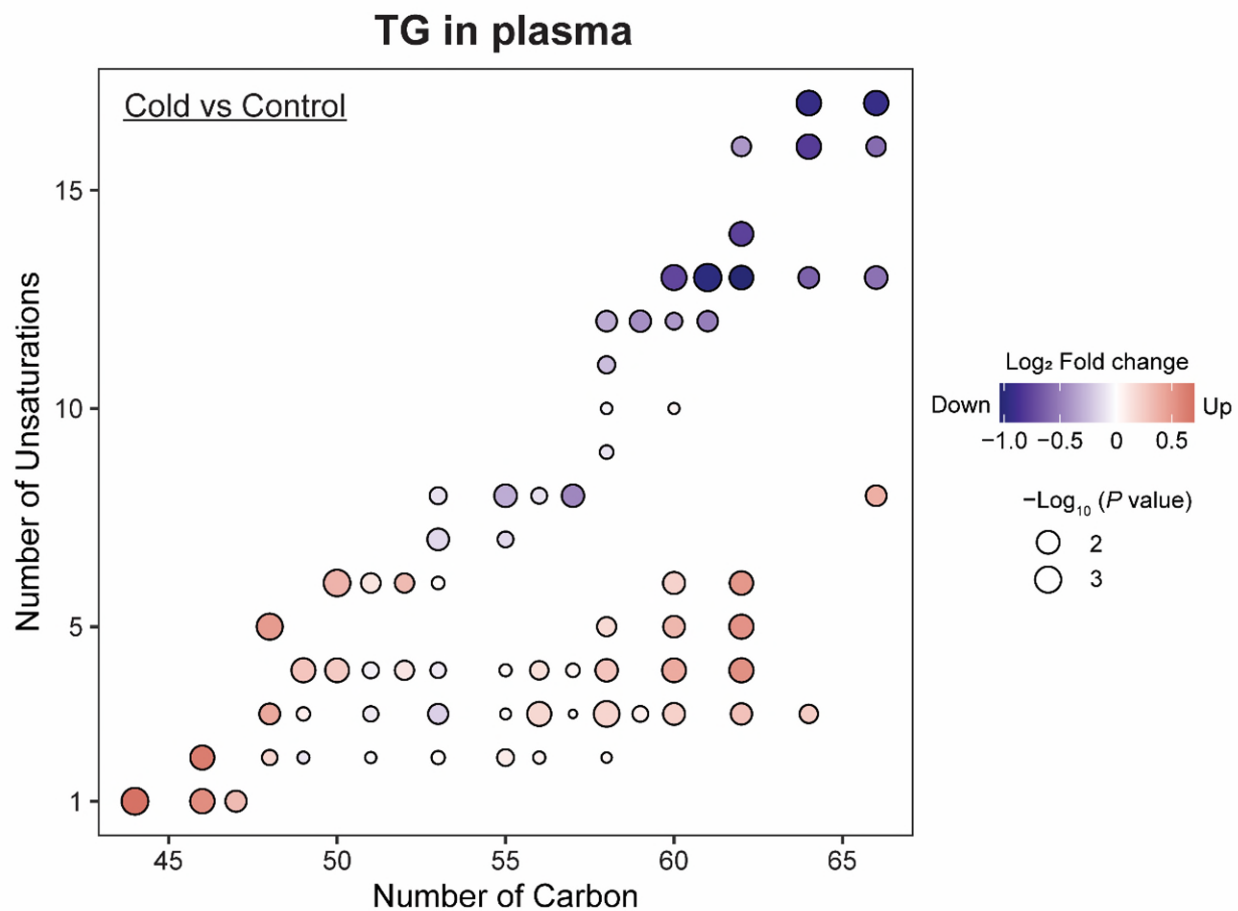


243

244 **Fig. S12.** Changes in acyl chain profile of ceramide (Cer), hexosylceramide (HexCer), and  
 245 sulfatide (SHexCer) molecules in one-year-old Arctic char by temperature shifts. The average  
 246 values of significantly altered lipids in each treatment group were presented. Data were log-  
 247 transformed and Z-score scaled in prior to data visualization. The lipids within each tissue type  
 248 are sorted first by the increasing total number of double bonds and then by the total number of  
 249 carbons in the hydrocarbon chains.

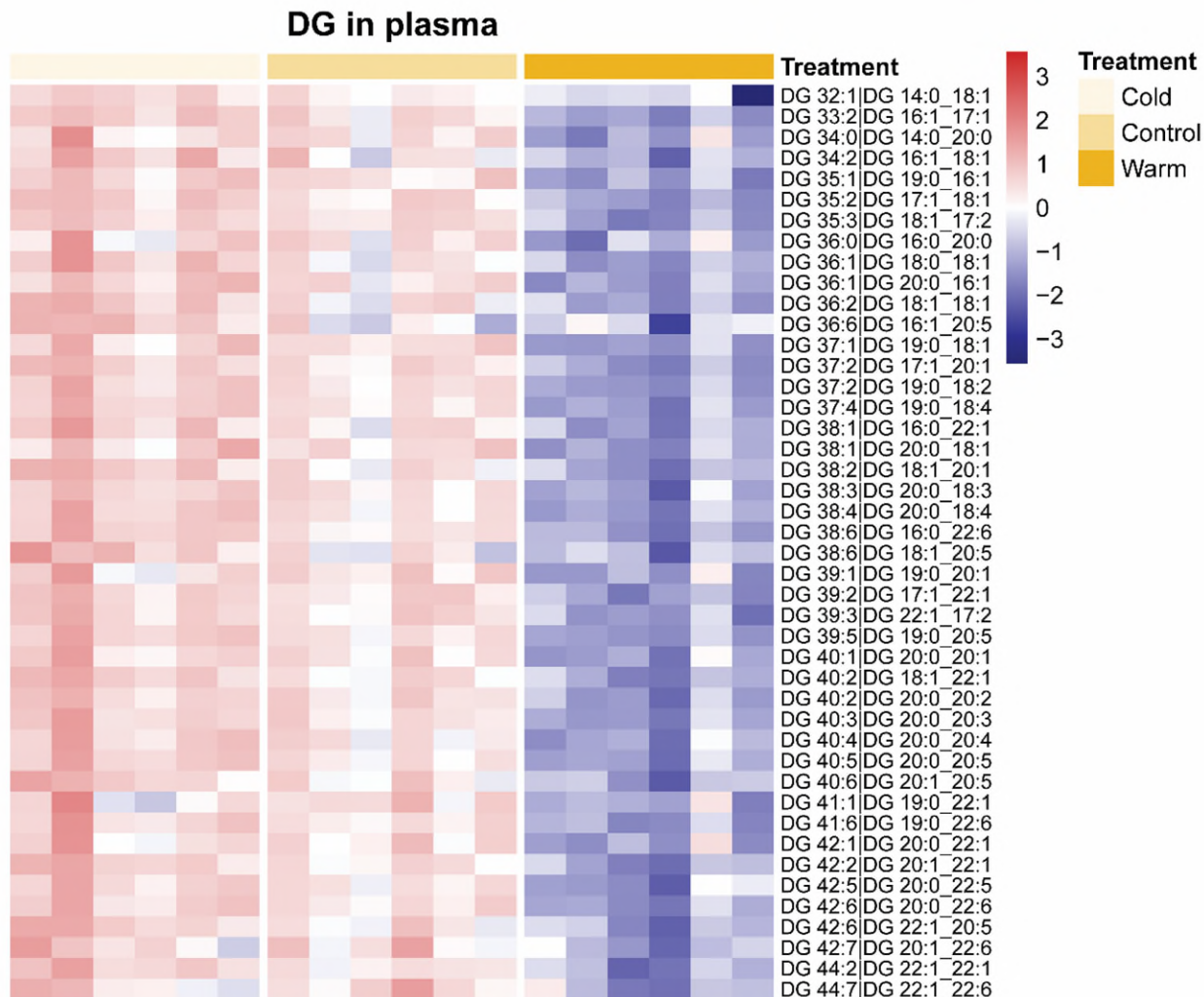


250  
251 **Fig. S13.** Heatmap plot showing significantly altered abundances of sphingomyelin (SM) species  
252 in one-year-old Arctic char in response to thermal treatment. All data were log-transformed and  
253 Z-score scaled in prior to heatmap analysis.  
254



255

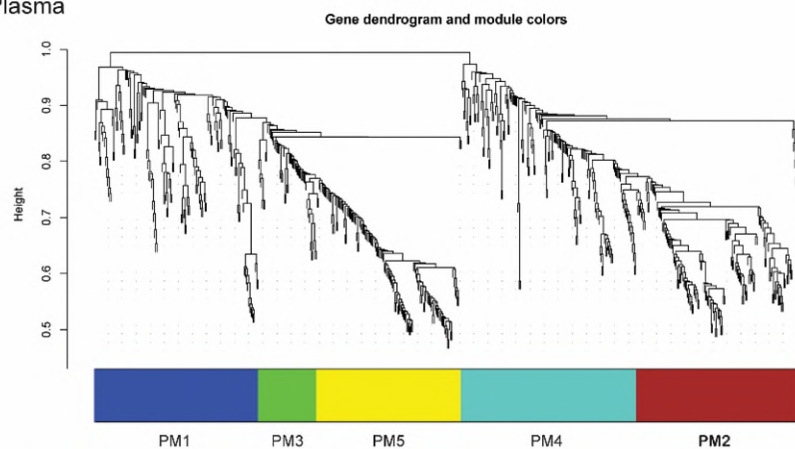
256 **Fig. S14.** Bubble plots illustrating altered fatty acid composition of TG species in plasma after  
 257 exposure to cold treatment. Dot color indicates the  $\log_2$  fold change relative to control. The dot  
 258 size indicates the significance.  
 259



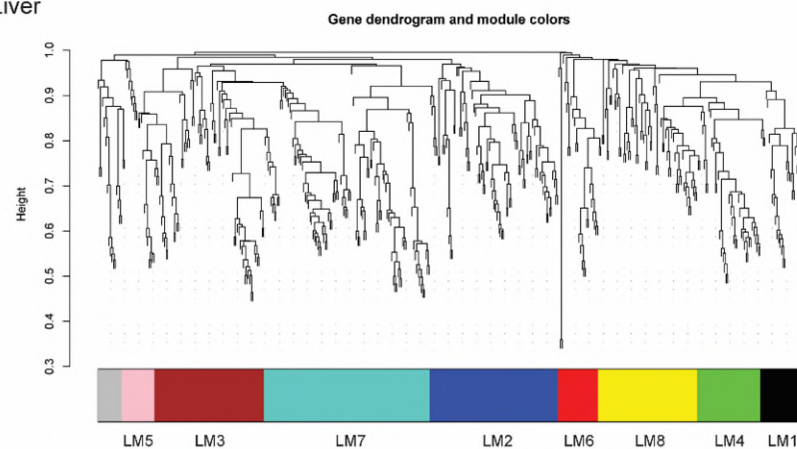
260  
261 **Fig. S15.** Heatmap plot showing significantly altered abundances of diacylglycerol (DG)  
262 molecules in plasma of one-year-old Arctic char in response to temperature shifts. All data were  
263 log-transformed and Z-score scaled in prior to heatmap analysis.  
264



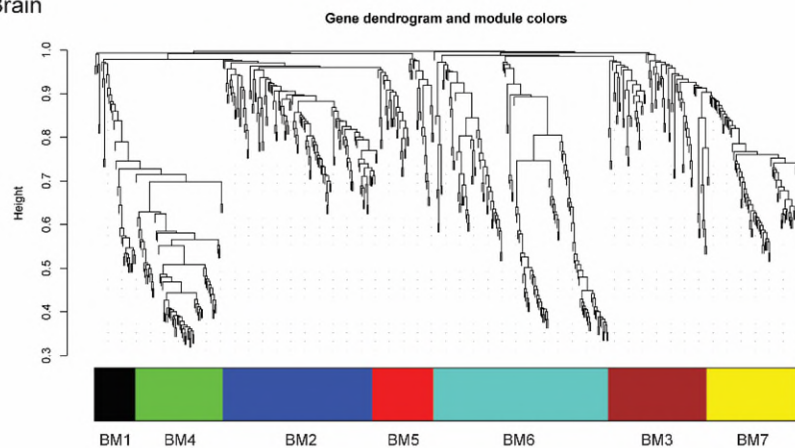
a Plasma



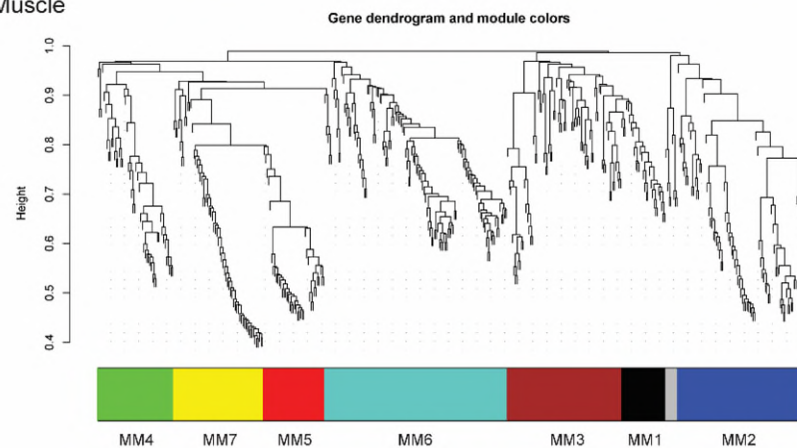
c Liver



b Brain

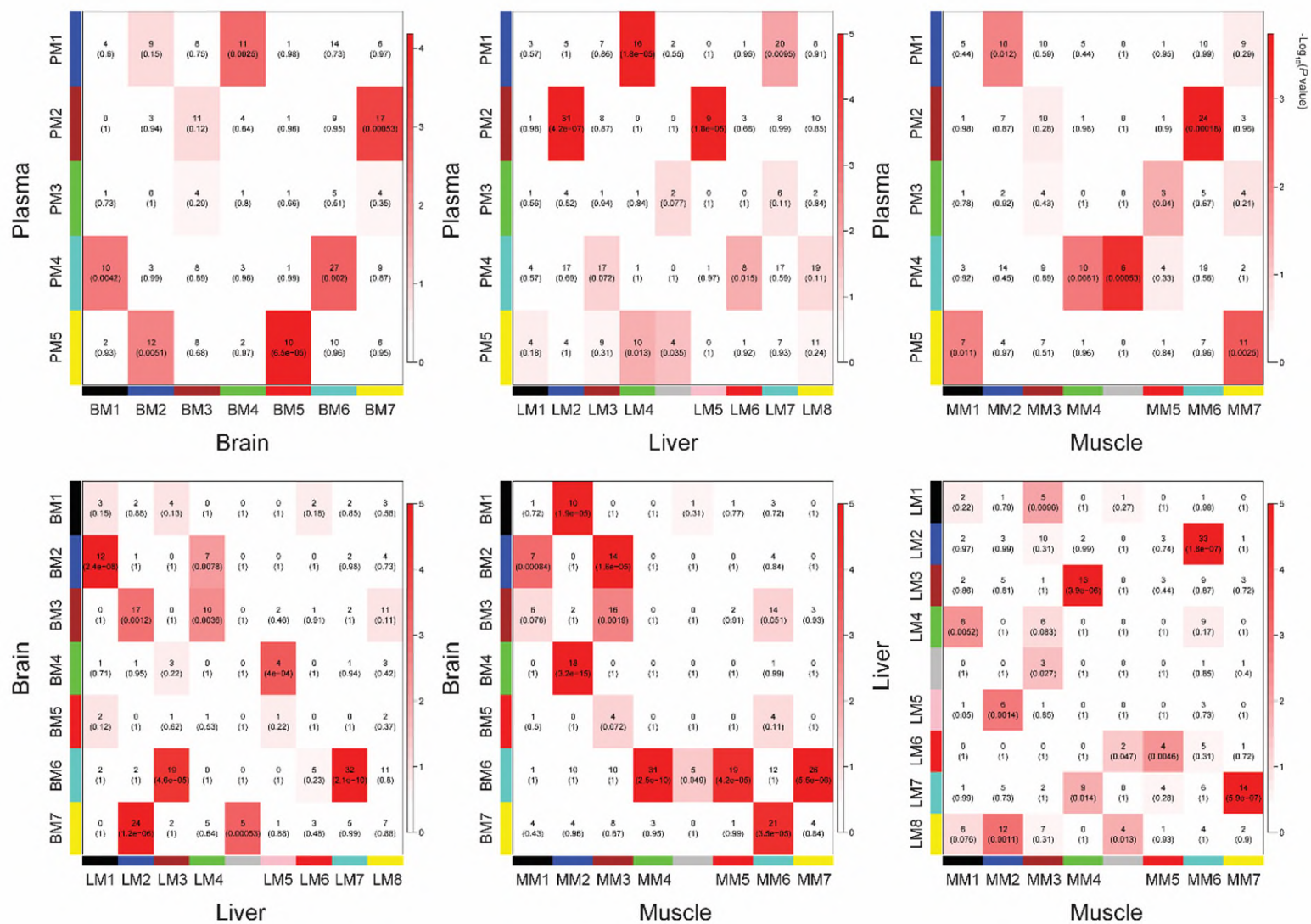


d Muscle



265

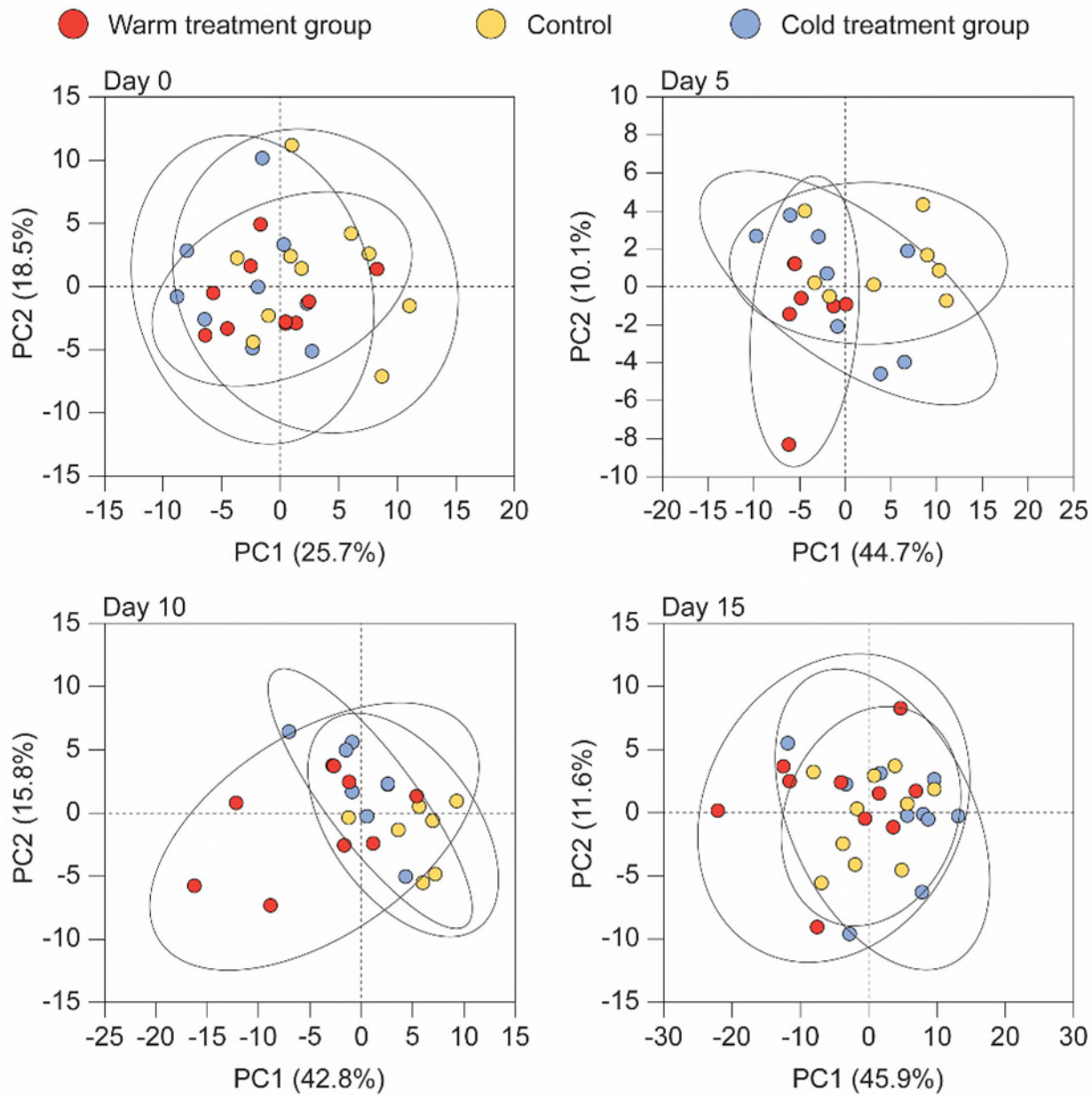
266 **Fig. S16.** Correlation networks and modules for the Arctic char plasma (a), brain (b), liver (c), and muscle (d) after exposure to  
267 temperature shifts. Dendrograms were produced by average linkage hierarchical clustering of lipids on the basis of a topological  
268 overlap. Horizontal color bars represent different modules of correlated lipids. Unassigned lipids are indicated in grey. PM, plasma  
269 module; BM, brain module; LM, liver module; MM, muscle module.



270

271 **Fig. S17.** Pairwise comparisons between modules constructed by WGCNA. Significance of the most highly overlapping modules for  
 272 each pairwise comparison is given alongside the number of overlapping lipids per module. The shading in the tables illustrates the  
 273 significance of overlapping as  $\log_{10}(P \text{ value})$ . Abbreviated names of each module were assigned for simplicity. PM, plasma module;  
 274 BM, brain module; LM, liver module; MM, muscle module.

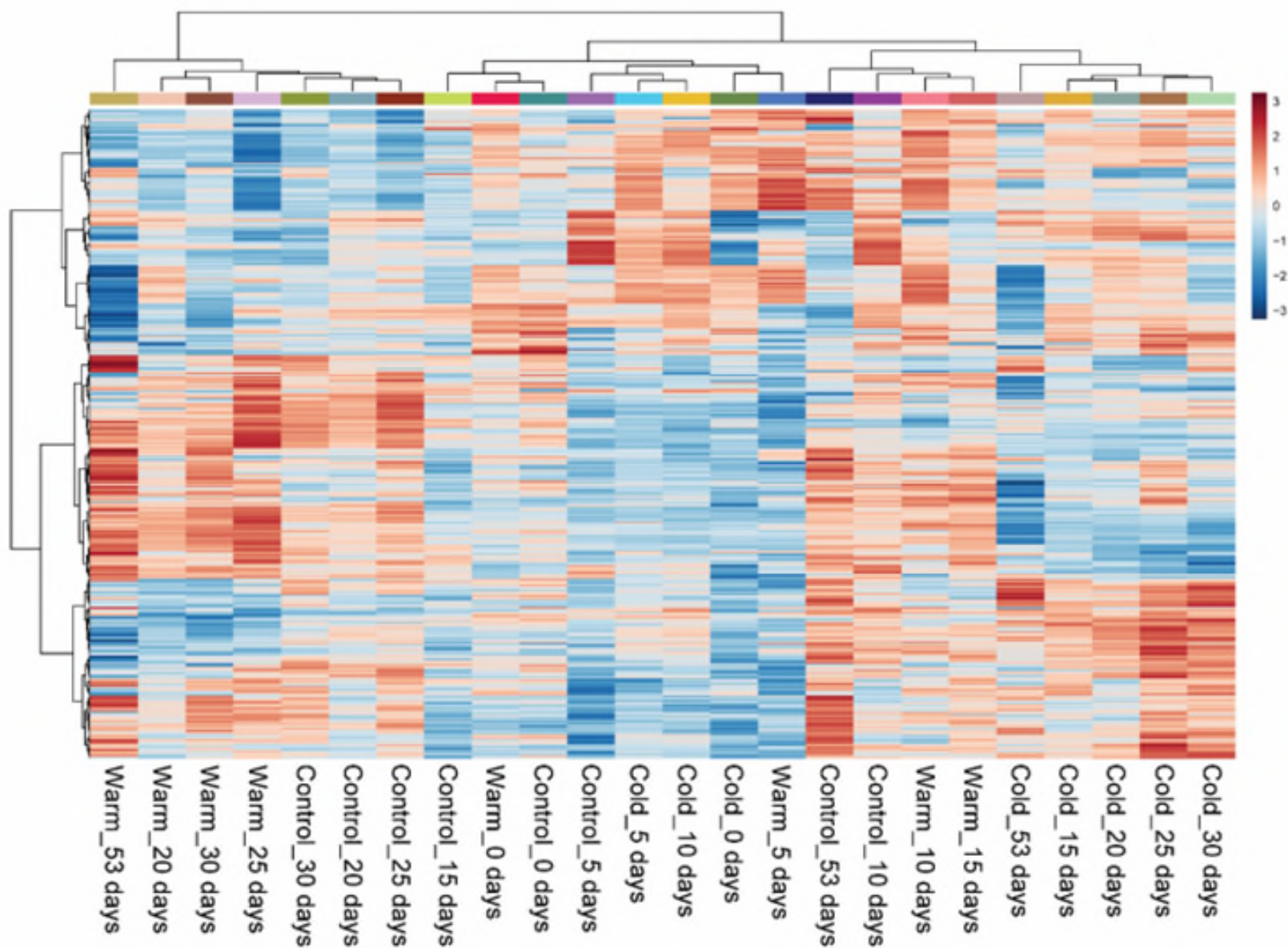




275

276 **Fig. S18.** Principal component analysis (PCA) of detected lipids in liver of eight-week-old fish  
 277 on sampling day 0, 5, 10, and 15. The first two canonical axes are plotted. Data were log-  
 278 transformed and auto-scaled in prior to PCA analysis.

279

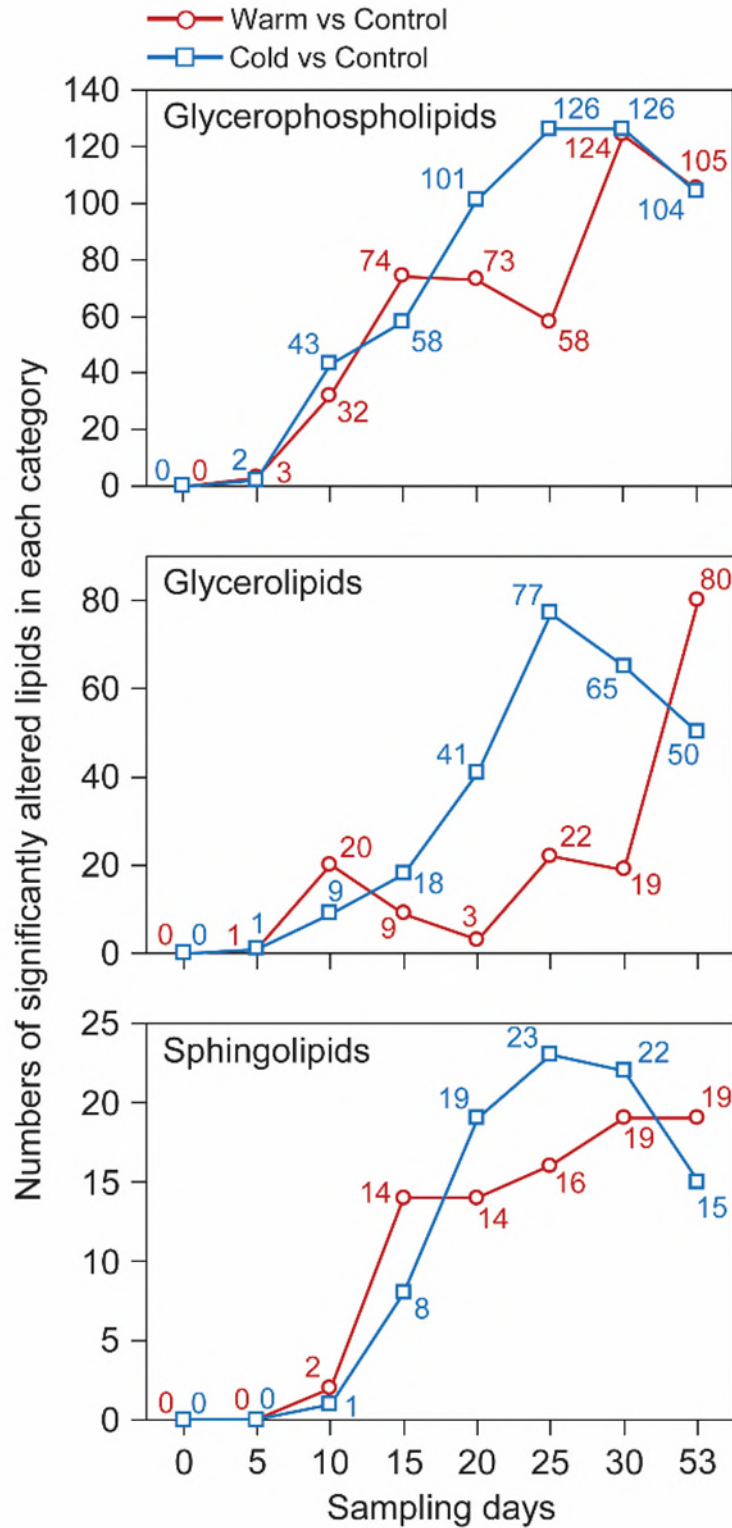


280

281

282

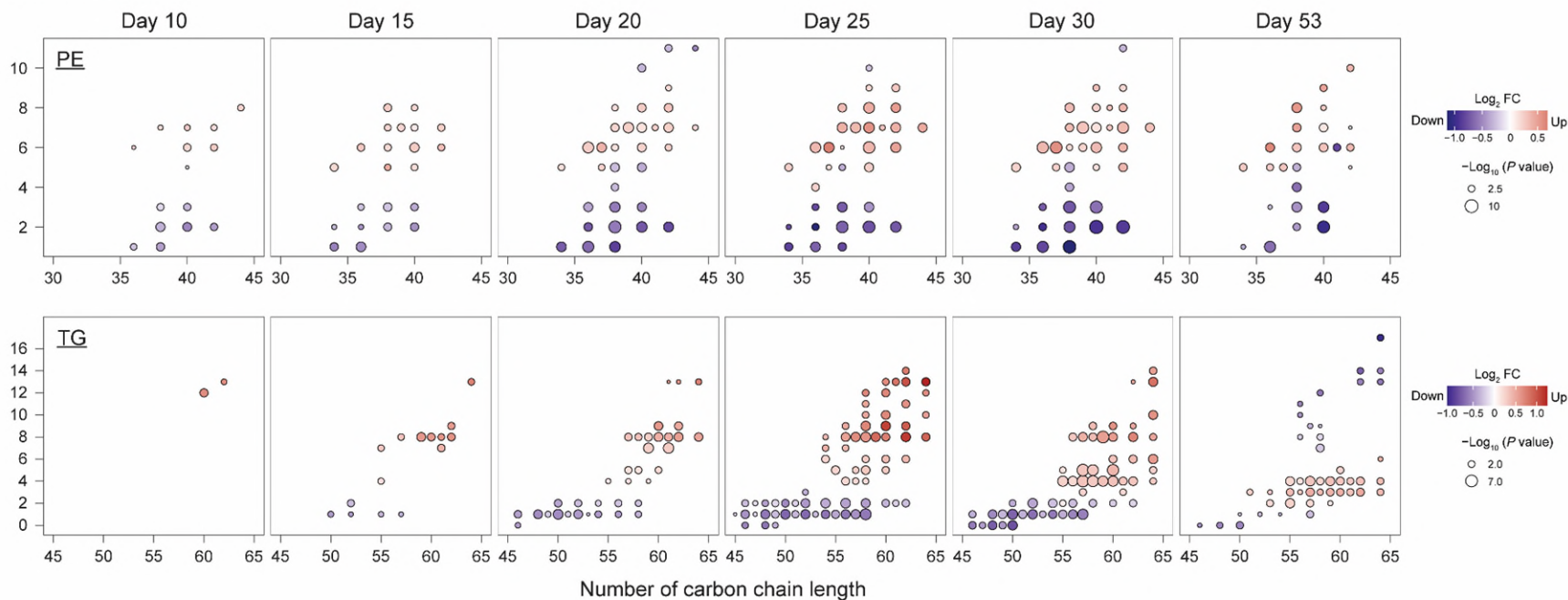
**Fig. S19.** Heatmap plot and hierarchical clustering (Euclidean distance and Ward procedure) of all identified lipids in liver of eight-week-old Arctic char. All data were log-transformed and Z-score scaled before analysis.



283

284 **Fig. S20.** Number of significantly altered glycerophospholipid (GP), glycerolipid (GL), or  
 285 sphingolipid (SP) species in liver of eight-week-old Arctic char by temperature shifts.  
 286 Significantly altered lipids were determined by one-way ANOVA followed by Fisher's LSD test  
 287 (FDR < 0.05).

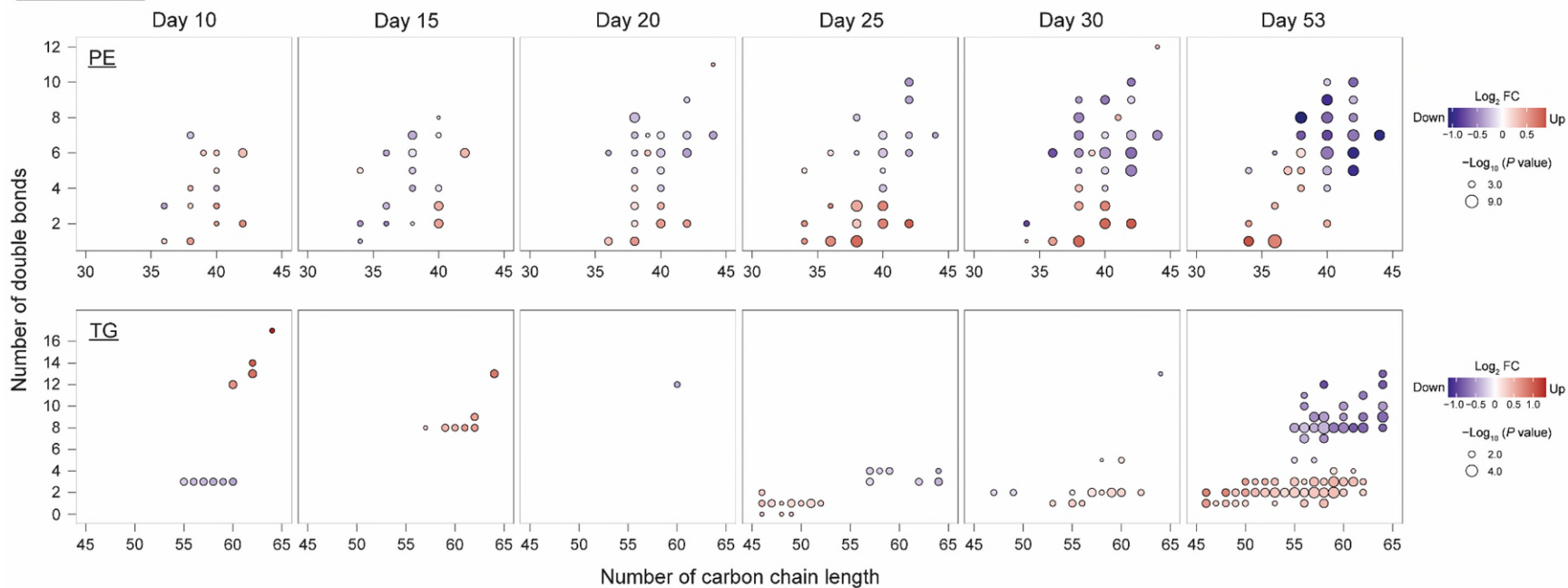
Cold vs control



288

289 **Fig. S21.** Changes in fatty acid composition of PE and TG species in liver of eight-week-old Arctic char during the course of stepwise  
290 temperature decreases. Dot color indicates the  $\log_2$ (fold change) relative to control. The dot size indicates the significance. FC: fold  
291 change.

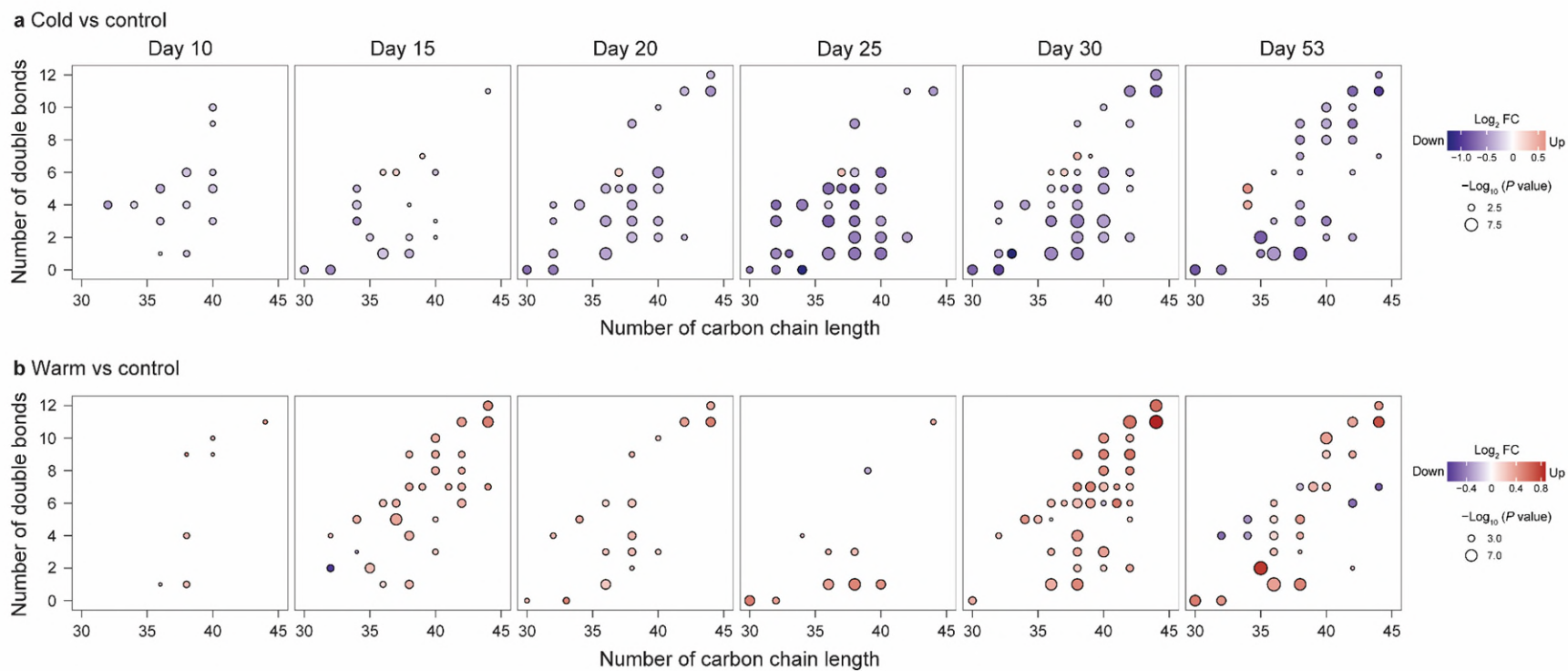
Warm vs control



292

293 **Fig. S22.** Changes in fatty acid composition of PE and TG species in liver of eight-week-old Arctic char during the course of stepwise  
294 temperature increases. Dot color indicates the  $\log_2$ (fold change) relative to control. The dot size indicates the significance. FC: fold  
295 change.

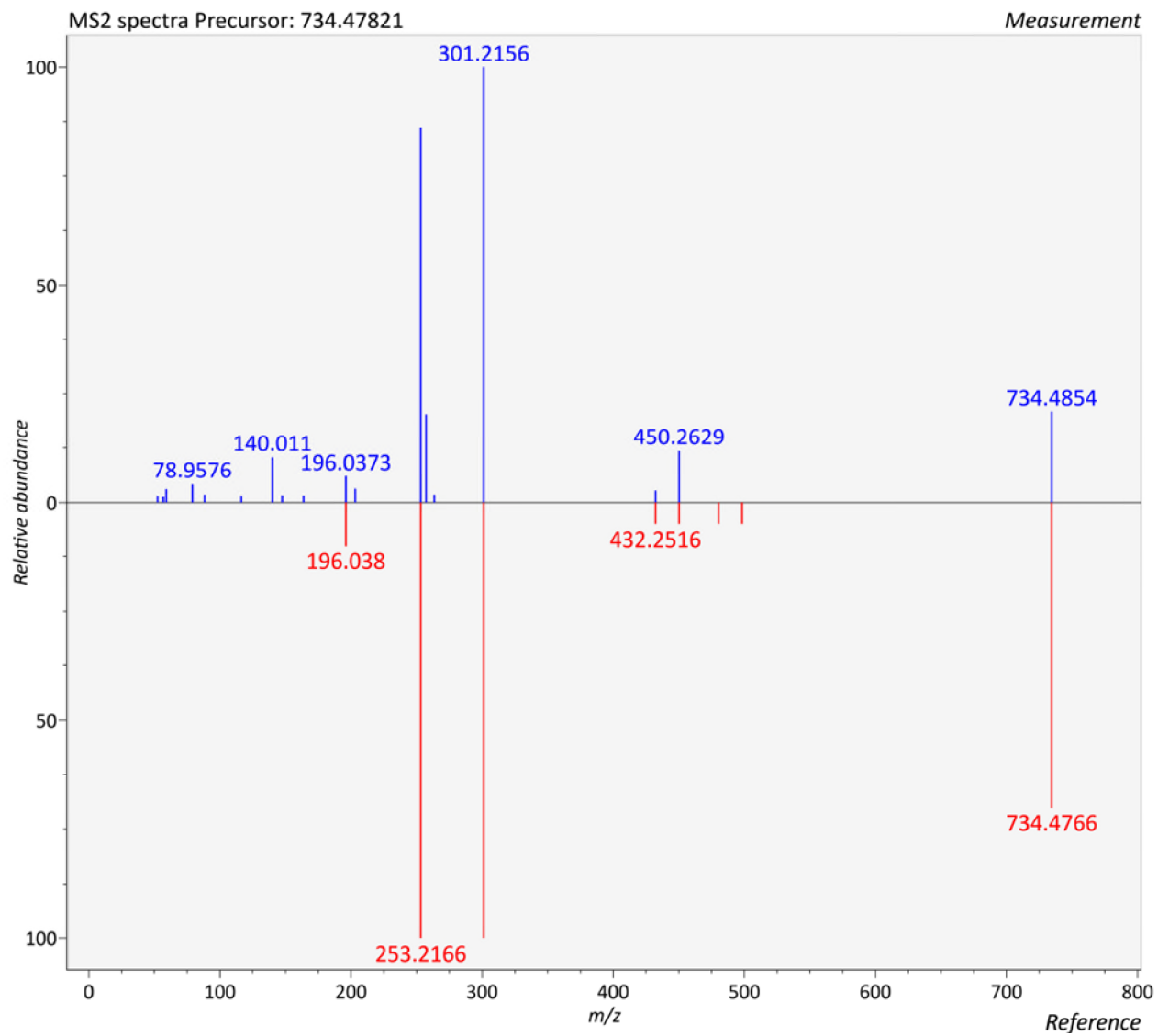




296

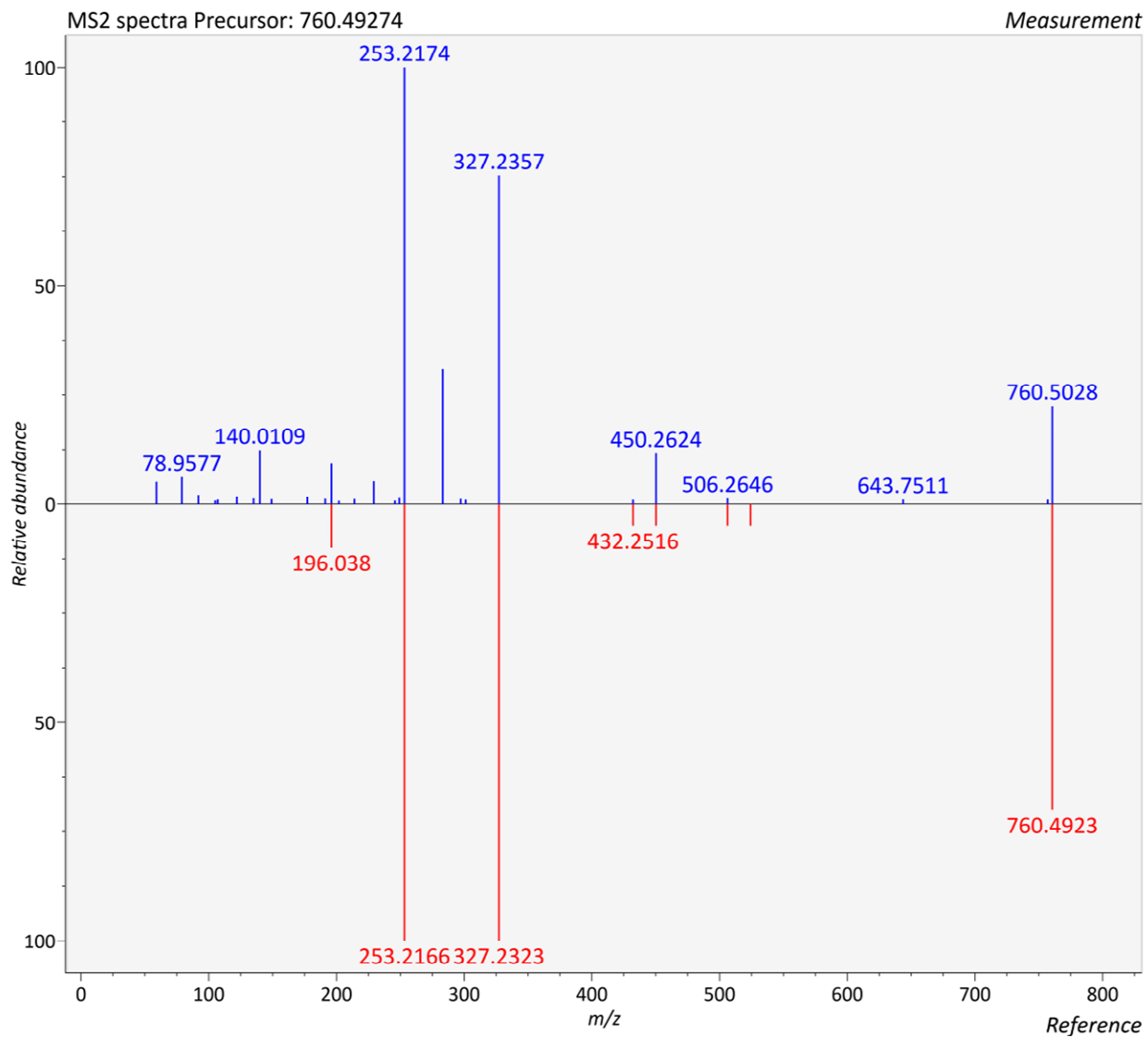
297 **Fig. S23.** Changes in fatty acid composition of PC species in liver of eight-week-old Arctic char during temperature shifts. Dot color  
298 indicates the log<sub>2</sub>(fold change) relative to control. The dot size indicates the significance. FC: fold change.





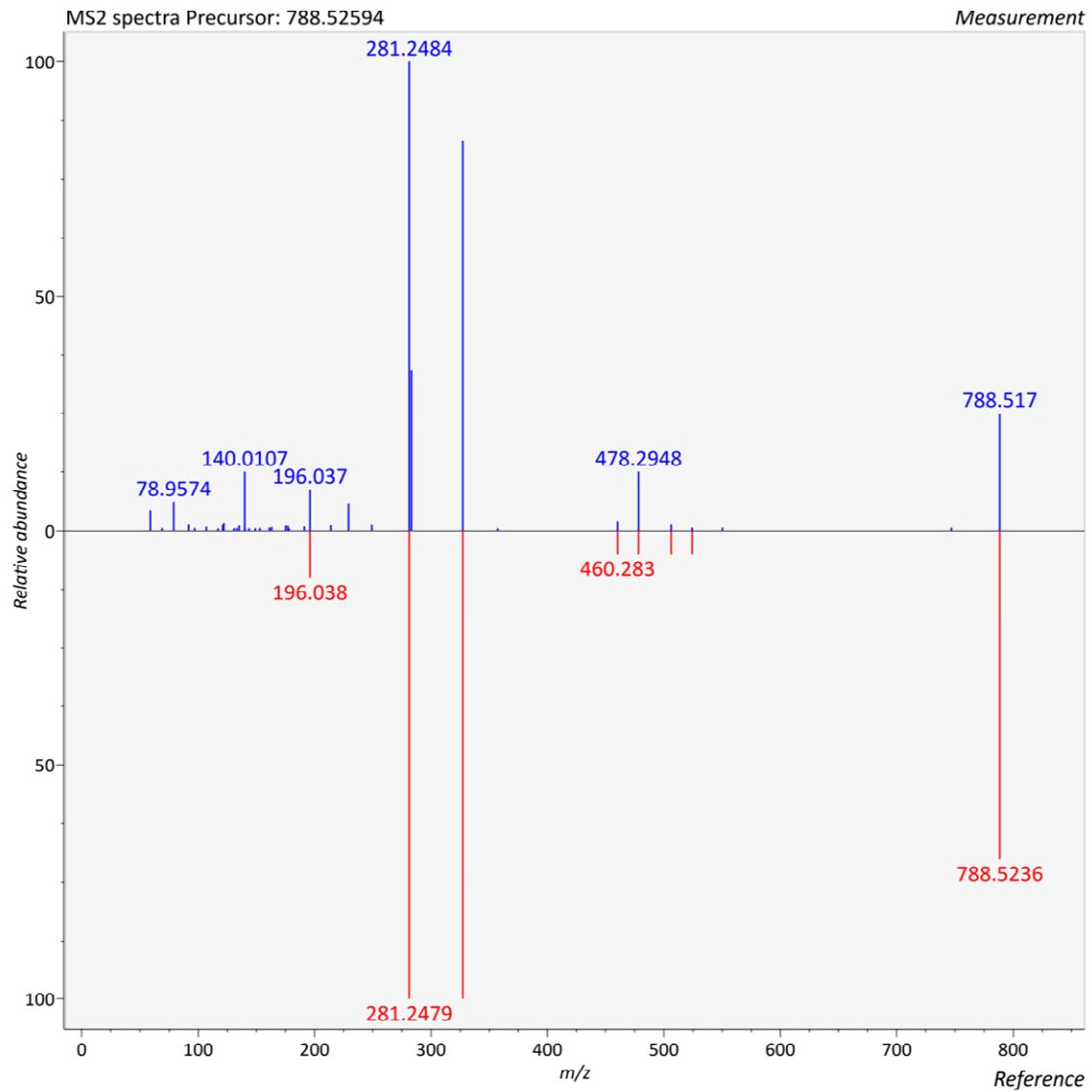
299

300 **Fig. S24.** Confirmation of PE 36:6|PE 16:1\_20:5 by MS2 matching.



301

302 **Fig. S25.** Confirmation of PE 38:7|PE 16:1\_22:6 by MS2 matching.



303

304 **Fig. S26.** Confirmation of PE 40:7|PE 18:1\_22:6 by MS2 matching.

305 **Table S1.** Analytical characteristics of the untargeted lipidomics method<sup>1</sup>

Lipid Standards	Exact Mass	RT (min)	Adduct Ion	Linearity		Recovery Rate (%)
				Concentration Range (µg/mL)	<i>R</i> <sup>2</sup>	
PC (15:0/18:1(d7))	752.6061	17.20	[M+H] <sup>+</sup>	0.05–10	0.998	80.98
lysoPC (18:1(d7))	528.3921	4.53	[M+H] <sup>+</sup>	0.01–10	0.998	89.52
PE (15:0/18:1(d7))	710.5591	17.59	[M+H] <sup>+</sup>	0.05–10	0.999	94.60
lysoPE (18:1(d7))	486.3451	4.75	[M+H] <sup>+</sup>	0.01–10	1.000	88.25
PG (15:0/18:1(d7))	741.5537	16.47	[M-H] <sup>+</sup>	0.05–10	0.999	79.90
TG (15:0/18:1(d7)/15:0)	811.7464	24.95	[M+NH <sub>4</sub> ] <sup>+</sup>	0.05–10	0.999	107.21
DG (15:0/18:1(d7))	587.5506	16.54	[M+NH <sub>4</sub> ] <sup>+</sup>	0.05–10	0.997	97.37
MG (18:1(d7))	363.3366	7.83	[M+H] <sup>+</sup>	1–10	0.999	113.50
CE (18:1(d7))	657.6441	26.33	[M+H] <sup>+</sup>	1–10	0.999	91.47
SM (d18:1/18:1(d9))	737.6397	16.36	[M+H] <sup>+</sup>	0.05–10	0.999	99.79
Cer (d18:1(d7)/15:0)	530.5404	17.07	[M+H] <sup>+</sup>	0.01–10	0.998	90.04

306 <sup>1</sup> Validation of the lipidomics method was performed in the presence of fish tissue matrix.

307 **References**

- 308 Calderón, C., Sanwald, C., Schlotterbeck, J., Drotleff, B., & Lämmerhofer, M. (2019).  
309 Comparison of simple monophasic versus classical biphasic extraction protocols for  
310 comprehensive UHPLC-MS/MS lipidomic analysis of HeLa cells. *Analytica chimica acta*,  
311 1048, 66–74. <https://doi.org/10.1016/j.aca.2018.10.035>
- 312 Sarafian, M. H., Gaudin, M., Lewis, M. R., Martin, F. P., Holmes, E., Nicholson, J. K., & Dumas,  
313 M. E. (2014). Objective set of criteria for optimization of sample preparation procedures for  
314 ultra-high throughput untargeted blood plasma lipid profiling by ultra performance liquid  
315 chromatography-mass spectrometry. *Analytical chemistry*, 86(12), 5766–5774.  
316 <https://doi.org/10.1021/ac500317c>
- 317 Food and Drug Administration. (2001). Guidance for industry: bioanalytical method validation.  
318 <http://www.fda.gov/cder/Guidance/4252fnl.pdf>.
- 319 Langfelder, P., & Horvath, S. (2008). WGCNA: an R package for weighted correlation network  
320 analysis. *BMC bioinformatics*, 9, 559. <https://doi.org/10.1186/1471-2105-9-559>
- 321 Benjamini, Y., & Hochberg, Y. (1995). Controlling the false discovery rate: a practical and  
322 powerful approach to multiple testing. *Journal of the Royal statistical society: series B*  
323 *(Methodological)*, 57(1), 289-300.
- 324 Shannon, P., Markiel, A., Ozier, O., Baliga, N. S., Wang, J. T., Ramage, D., Amin, N.,  
325 Schwikowski, B., & Ideker, T. (2003). Cytoscape: a software environment for integrated  
326 models of biomolecular interaction networks. *Genome research*, 13(11), 2498–2504.  
327 <https://doi.org/10.1101/gr.1239303>
- 328